ENGINEERING
LIBRARY

MAR 20 1950

JOURNAL OF THE AERONAUTICAL SCIENCES

VOLUME 17 MARCH, 1950 NUMBER 3

CONTENTS

Investigation of Lateral Dynamic Stability in the XB-47 Airplane..ROLAND J. WHITE 133

Steady Flow of Nonviscous Elastic Fluids in Axially Symmetric Channels.....
.....M. H. VAVRA 149

On a Family of Oblique Shock Curves.....EDWARD R. C. MILES 157

Inelastic Column Buckling.....TUNG-HUA LIN 159

The Pressure on a Slender Body of Nonuniform Cross-Sectional Shape in Axial Supersonic Flow.....ERNEST W. GRAHAM 173

Reply to Discussions of the Wright Brothers Lecture.....A. E. RUSSELL 176

Readers' Forum: "Station Functions in Flutter Analysis," by J. H. Greidanus and A. I. van de Vooren; "A Note on the Velocity of Sound," by M. V. Morkovin; "Further Remarks on the Velocity of Sound," by Morris Morduchow; "On the Compressibility Correction for Subsonic Unsteady Flow," by John W. Miles; "Upper and Lower Bounds on Variational Integral in Compressible Flow," by G. V. R. Rao; "Heat Addition to a Flowing Gas," by Roger Weatherston; "Potential Flow Around a Rotating Cylindrical Blade," by W. R. Sears; "A Note on the Evaluation of a Definite Integral," by Henry E. Fettis; "Lift-Curve Slope for Swept and Unswept Wings," by Innes Bouton; "Base Pressures at Supersonic Velocities," by Freeman K. Hill; "On the Surface Effects of a Compressible Laminar Boundary Layer," by Arthur N. Tifford; "On the Vorticity of the Flow Behind Curved Shock," by S. I. Pai; "Formulation of the Flutter Problem for Solution on an Electronic Analog Computer," by Eugene F. Baird and Henry J. Kelley; "Boundaries of Fluid Mechanics," by Keeve M. Siegel..178–192

Published by the

INSTITUTE OF THE AERONAUTICAL SCIENCES, INC.

JOURNAL OF THE AERONAUTICAL SCIENCES

Editor: HUGH L. DRYDEN, *Director, N.A.C.A.*

Associate Editor: ROBERT R. DEXTER *Associate Editor:* BERNEICE H. JARCK

The Institute of the Aeronautical Sciences publishes monthly the JOURNAL OF THE AERONAUTICAL SCIENCES AND THE AERONAUTICAL ENGINEERING REVIEW.

The JOURNAL OF THE AERONAUTICAL SCIENCES prints papers of scientific and technical interest to Institute members and subscribers. In general, it provides an opportunity for specialists to publish articles disclosing new knowledge and new applications in the field of the aeronautical sciences. The JOURNAL restricts itself to the aeronautical aspects of advances in science and engineering, and papers printed have either been submitted directly to the JOURNAL or have been previously presented at a meeting of the Institute.

The AERONAUTICAL ENGINEERING REVIEW keeps members and subscribers informed regarding the contents of new books and current periodicals in the field of aeronautics. It reviews new developments in the aircraft industry and reports on progress from house organs and catalogs published by aircraft and engine manufacturers and other companies engaged in aeronautical activities. It publishes papers on applied engineering and aircraft production. News of Institute activities is published in the REVIEW.

Statements and opinions expressed in the JOURNAL are to be understood as individual expressions of the authors and not those of the Institute.

SUBSCRIPTION RATES

Journal of the Aeronautical Sciences
Published Monthly

United States and Possessions		Foreign Countries Including Canada (American Currency Rate)	
1 Year	$12.00	1 Year	$13.00
Single Copies	1.50	Single Copies	1.50

Aeronautical Engineering Review
Published Monthly

United States and Possessions		Foreign Countries Including Canada (American Currency Rates)	
1 Year	$3.00	1 Year	$3.50
Single Copies	0.50	Single Copies	0.50

Notices of change of address should be sent to the Institute at least 30 days prior to actual change of address.

Manuscripts for publication, proofs, and all correspondence should be addressed to the Editorial Office of the JOURNAL.

Correspondence regarding subscriptions may be addressed to Publication Office, 20th and Northampton Sts., Easton, Pa., or to the Editorial Office of the JOURNAL OF THE AERONAUTICAL SCIENCES, 2 East 64th Street, New York 21, New York.

Copyright, 1950, by the Institute of the Aeronautical Sciences, Inc.

Entered as Second Class Matter at the Post Office, Easton, Pa., May 1, 1937. Acceptance for mailing at a special rate of Postage provided for in the Act of August 24, 1912. Authorized April 29, 1937.

JOURNAL OF THE AERONAUTICAL SCIENCES

VOLUME 17 MARCH, 1950 NUMBER 3

Investigation of Lateral Dynamic Stability in the XB-47 Airplane

ROLAND J. WHITE*

Boeing Airplane Company

ABSTRACT

This paper presents the method and analysis used to improve the lateral stability of the XB-47, which was a part of the U.S. Air Force development program on this airplane. Early flights indicated a tendency for the airplane to "Dutch Roll" at the lower indicated air speeds. Elimination of this flight condition has been accomplished by use of a servomechanism termed a "yaw damper," consisting of a yaw rate gyro pickup that operates the rudder to improve the airplane damping in yaw. The resulting flying qualities are believed to be considerably better than would be possible with other means of improving the dynamic stability. Problems encountered during the design and flight tests are discussed. A method of analysis based upon the airplane inverse frequency response characteristics has been used, from which the airplane stability has been obtained. This method has been extended to include the effect of airplane body side bending which influences the dynamic stability at higher indicated air speeds.

INTRODUCTION

THE LATERAL STABILITY of the XB-47 was investigated in the early design stage, using stability equations including the effect of the airplane product of inertia.[1] The analysis was based upon static stability coefficients obtained from wind-tunnel tests, along with calculated damping coefficients.

Early flight tests indicated that the calculations were generally correct but that the damping in yaw, particularly at low speeds and at altitude, was less than the pilots desired. The most important factor was that low damping could not be tolerated even though the periods were long. For example, during the landing approach the pilot's attention was required to prevent a Dutch Roll from occurring, which would be a handicap during blind landing approaches. The principal objection of the pilots to the poor damping stemmed from the rolling part of the motion. This was later confirmed by pilot checks on an airplane having poor directional damping but low dihedral effect, causing only a small rolling. While the rolling part of the motion is more apparent to the pilot, it should be noted that, even if rolling were not present, the yawing motion would still be poorly damped. This condition is characteristic of most all high-performance airplanes having high wing loadings, which results in a high "Relative Density Factor" $\mu = (W/g)/\rho Sb$, a term used in airplane stability analysis to express the ratio of the airplane mass to the mass of air enclosed in a volume equal to the wing area times a characteristic length of the airplane. It can be shown that the damping ratio is proportional to $\sqrt{1/\mu}$ when the airplane is considered as a simple vibrating system. Therefore, the number of cycles to damp to half amplitude is a function of μ. Since μ increases with altitude and wing loading, it should be expected that improvements to power plants and aerodynamics, permitting higher loadings and altitudes, should cause a decrease in damping, assuming that the general proportions of the airplane are not changed. Fig. 1 shows the relative density of a number of airplanes at their service ceiling, indicating the increase in μ that has taken place in recent years. Some means must be found to improve the damping on all future high-performance airplanes, since the damping is already marginal in many cases.

Following the early flight tests, during which a more clear understanding of the desired flying qualities was obtained, the stability was further analyzed to see which feature contributed to poor damping and to examine means of altering the general configuration to improve the damping to an acceptable condition. The dihedral effect resulting from the wing sweepback was first studied and found to reduce the damping somewhat, although the total magnitude of this effect was small compared to the desired increase in damping.

Presented at the Design Session, Annual Summer Meeting, I.A.S., Los Angeles, July 21–22, 1949.

* Aerodynamicist.

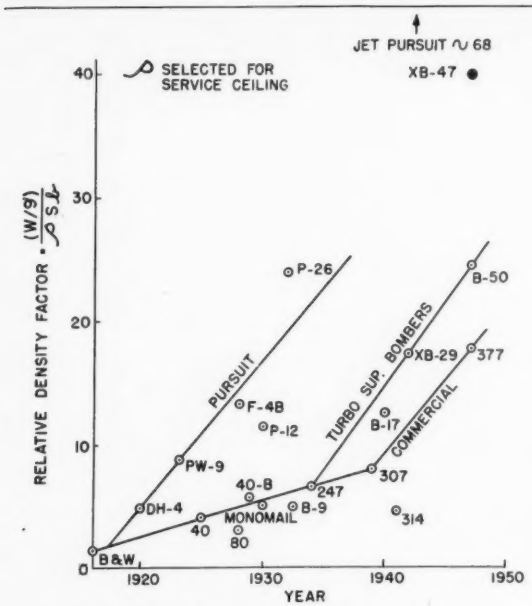

FIG. 1. Effect of time on relative density factor.

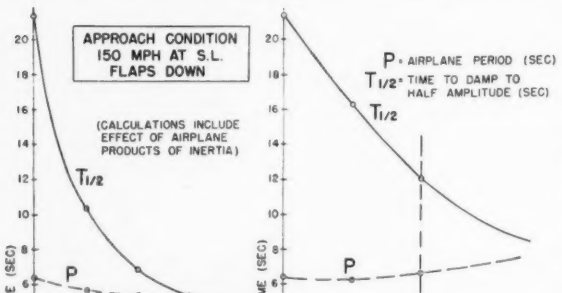
APPROACH CONDITION
150 MPH AT S.L.
FLAPS DOWN
(CALCULATIONS INCLUDE EFFECT OF AIRPLANE PRODUCTS OF INERTIA)
P = AIRPLANE PERIOD (SEC)
T1/2 = TIME TO DAMP TO HALF AMPLITUDE (SEC)
TIME (SEC)
PRESENT AIRPLANE
WING NACELLE CONTACTS GROUND AT σ = -4°
PERCENT INCREASE IN VERTICAL TAIL AREA
WING DIHEDRAL ANGLE (DEG)

FIG. 2. Effect of changes in tail area or wing dihedral on airplane stability.

It was also realized that if sufficient negative dihedral could have been obtained for the flaps-down approach condition, this would have given marginal static sideslip stability in the flaps-up condition at high speeds. Fig. 2 shows the effect of reducing the wing dihedral during the approach condition. Here, a large change was out of the question because of ground clearance. This same figure shows the effect of increasing the vertical tail area, indicating that a vertical tail of twice the present size would be necessary if damping to half amplitude in 1 cycle was desired.

While increasing the tail size increases the damping, it is problematical if any gain is made in the smooth-flying qualities when the vertical tail is increased above a certain size. This is because the excitation of the airplane due to side gusts will increase proportional to the increase in vertical tail size; hence, while the damping may be greater, so will the disturbances, resulting in a doubtful improvement in the airplane riding comfort. It is probable that the usual tail volume coefficients that satisfy the requirements for unsymmetrical power, static stability in sideslip, improved stalling qualities, etc., should determine the tail size, and some other means should be used if large increases in the damping are required to obtain the desired riding comfort.

Inasmuch as a rate gyro servomechanism was most easily assembled, consideration was given to improving the damping in the yaw axis.

The improvement of airplane stability by automatically moving a control surface in response to an airplane disturbance has been used in many instances. These devices range from springs, bob weights, and aerodynamic vanes to the present yaw damper or similar servomechanism devices—the latter being a more suitable, and a positive means, when power operated irreversible controls are used. The distinction between these devices and the normal autopilot is that they improve the airplane flying qualities so that the human pilot may more easily fly the airplane, whereas the normal autopilot adds direction sensing and has complete authority of the airplane flight path.

The use of a rate gyro to improve the damping in yaw was decided upon from practical installation considerations. This was initially thought to be a new idea, but later it was realized that this concept has been used at least in one known case.[2] The analysis in this paper will be limited to this type of control.

The method of analysis used has been useful in developing the yaw damper. Unfortunately, in several cases the analysis lagged the flight experience. However, the analysis has served to give a clear picture of the damper operation and was invaluable in making laboratory and flight-test changes.

DESCRIPTION OF YAW DAMPER

A general view of the XB-47 airplane is shown in Fig. 3. All control surfaces are power-operated and

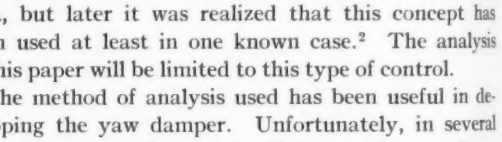

FIG. 3. General arrangement of XB-47.

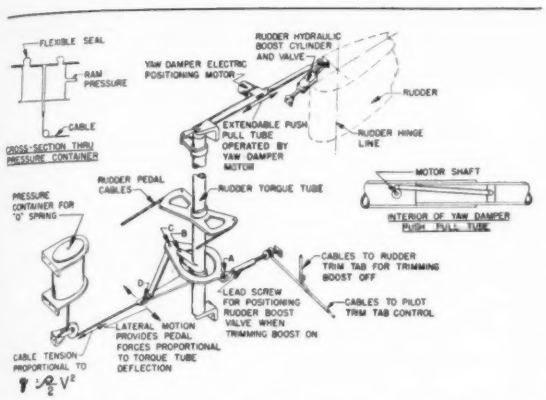
FLEXIBLE SEAL
RAM PRESSURE
CABLE
CROSS-SECTION THRU PRESSURE CONTAINER
YAW DAMPER ELECTRIC POSITIONING MOTOR
RUDDER HYDRAULIC BOOST CYLINDER AND VALVE
RUDDER
EXTENDABLE PUSH PULL TUBE OPERATED BY YAW DAMPER MOTOR
RUDDER HINGE LINE
MOTOR SHAFT
INTERIOR OF YAW DAMPER PUSH PULL TUBE
RUDDER PEDAL CABLES
RUDDER TORQUE TUBE
PRESSURE CONTAINER FOR "Q" SPRING
CABLES TO RUDDER TRIM TAB FOR TRIMMING BOOST OFF
LEAD SCREW FOR POSITIONING RUDDER BOOST VALVE WHEN TRIMMING BOOST ON
CABLES TO PILOT TRIM TAB CONTROL
LATERAL MOTION PROVIDES PEDAL FORCES PROPORTIONAL TO TORQUE TUBE DEFLECTION
CABLE TENSION PROPORTIONAL TO

FIG. 4. Schematic diagram of rudder system with yaw damper.

are irreversible for their normal operation with artificial pilot "feel." A sufficient amount of aerodynamic balance is provided for each control surface, so that control forces with the servo-off, while higher than desired for normal flying, are reasonable for emergency operation. As this paper is concerned with the rudder control system, a detailed description of this system is given.

A schematic diagram of the rudder controls located at the tail of the airplane is shown in Fig. 4. Their operation will be described first without consideration of the directional control damper. During "boost-on" operation, movement of the rudder pedal produces a rotation of the rudder torque tube, which is resisted by a torque at its lower end, developed by the artificial feel spring. The control arm at the upper end of the torque tube moves the push-pull tube to position the hydraulic boost control valve, which requires only a friction-resisting force of 3 to 5 lbs. In turn, the hydraulic boost cylinder moves the rudder until the follow-up link centers the boost valve at the desired rudder position. Pilot pedal forces are resisted at the lower end of the vertical torque tube by a force gradient, which is essentially linear with rudder deflection and proportional to the dynamic pressure. This is accomplished in the following manner: Point A of the torque-tube trim yolk remains fixed and movement of the torque tube rotates point B, causing point C also to rotate. This produces a sideward movement of point D. The artificial feel spring consists of a piston and fabric seal, providing a tension force in the cable attached at point D, which is located at the end of an arm that is free to rotate about the torque tube. Sideward movement of point D provides a force proportional to "q" and to the deflection of point D. When the pilot pedal force is released, point D centers itself and point C becomes essentially fixed. When it is desired to trim the rudder with "boost-on," movement of the trim control operates the jack screw to move point A. Here, the only resisting torque is that of the pedal control cables and the boost valve; hence, point B will move because the feel spring force keeps point C fixed. In this manner the boost valve is positioned, causing a change in the rudder position. During this operation parallel cables to the rudder trim tab (not shown) will tend to trim the rudder aerodynamically, so that, should the boost be turned off, the rudder will still remain closely in trim. When the boost is turned off, loss of hydraulic pressure relieves the air pressure in the "q" spring container and locks the boost follow-up motion so that the push-pull tube operates the rudder directly with no lost motion.

The directional control yaw damper has a rate gyro designed to develop an electrical signal voltage proportional to the rate of yaw of the airplane. This voltage then passes through a servo-amplifier to operate an electric push rod positioning motor. The motor operates the push-pull tube shown in Fig. 4 to extend or shorten it by an amount proportional to the electrical signal from the rate gyro. The push-pull tube at the torque-tube end is restrained from moving by the "q" spring; hence, the change in length positions the boost valve, causing the rudder to move. This push rod only operates the boost hydraulic valve; hence, the operation loads are small. The full extension and shortening of the push-pull tube is ± 0.40 in. and will produce a $\pm 5°$ of rudder movement. This has been found sufficient for the maximum oscillation amplitudes that the pilot would expect the airplane to damp with free controls. The operation of the rudder occurs without motion of the rudder pedals; hence, the pilot is not aware of the yaw damper operation, except in noting the more desirable flying qualities of the airplane. Since the yaw damper adds a differential signal to the

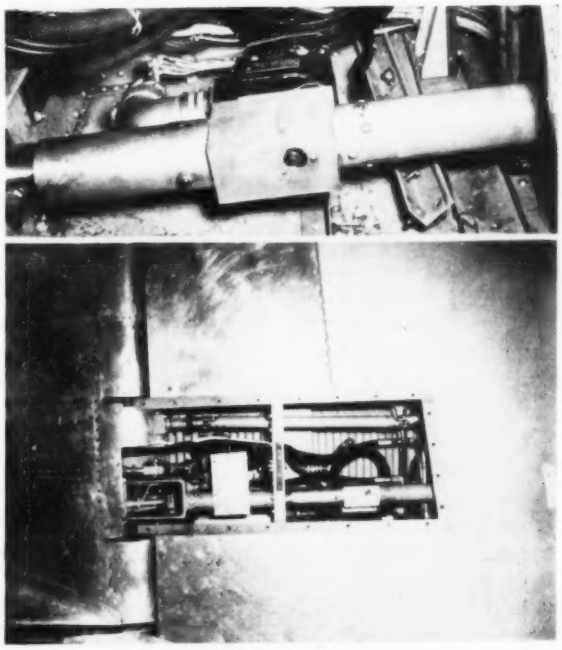

FIG. 5. Rudder boost push rod.

rudder, the pilot can overpower the yaw damper. An angular yaw velocity of the airplane will cause the gyro to precess about the transverse pivot axis, which is parallel to the lateral axis of the airplane, until the movement is balanced by springs restraining the motion. The deflection of the gyro gymbal develops a signal voltage in the yaw damper servo system, which acts to position the rudder.

The original yaw damper servo system was made up, for a brief time, out of surplus electrical parts. This was for the purpose of trying out the general idea, although it was anticipated that deficiencies in the response of the servo might occur. As a result of the flight and laboratory tests, various improvements were made to the system. Calculations in this paper are based on the yaw damper operating with the improved system. Fig. 5 shows a view of the rudder boost push rod and its installation in the vertical tail. The general operation of the rudder system may be visualized from the block diagram arrangement of Fig. 6, which shows how the yaw damper superimposes its motion with that of the pilot's pedal to operate the rudder.

Results

Flight-test graphic records of the airplane motion are shown in Figs. 7 and 8. Here the airplane is made to Dutch Roll with the damper-off showing the low damping. The pilot then turns the damper on and the Dutch Roll rapidly disappears. Fig. 7 represents the approach flight condition and Fig. 8 is typical of high-altitude flight.

The calculated periods and time to damp to half amplitude, along with several flight test check points, are shown in Fig. 9. These have been compared with the recent U.S. Air Force requirements, indicating that the airplane is unsatisfactory or marginal in several flight conditions without the yaw damper. Calculations with the yaw damper operating show an effective improvement. Flight results have indicated that higher damping is desirable; hence, in Fig. 9, a line marked "Desired by pilots" has been added. Fig. 10 is a stability diagram in which the damping in yaw and airplane static yaw stability form the variables. This figure shows how the yaw damper increases $C_{n_{\dot{\psi}}}$ to move the airplane point away from the oscillatory instability boundary, thereby improving both the Dutch Roll and spiral stability.

The magnitude of roll to yaw amplitude ratio is of interest and is shown in Fig. 11. Here the roll to yaw amplitude ratio changes because of different rudder input frequencies, which, of course, equals the airplane frequency. At the resonant frequency ω_R of both the high- and low-speed cases shown, the amplitude ratio is near 1.9. At higher frequencies, however, the roll effect becomes small. For this reason, the effect of roll may be neglected where higher frequencies are concerned, such as are encountered in certain types of hunting problems with automatic controls.

Flight-Test Experience

The first low-speed flight test with the yaw damper was extremely successful. Here the yaw damper removed the Dutch Roll tendency, and no hunting of the airplane was experienced. This flight record is shown in Fig. 7. In the following flight, the yaw damper rudder stops were set at $\delta_0 = \pm 3°$ instead of the previous setting of $\delta_0 = \pm 5°$. The 3° setting was found to reduce the effectiveness of the yaw damper; hence, the stops were reset to 5° and have been held there since.

One interesting aspect of the early flight tests was that a rheostat control was installed at the pilot's station to vary the sensitivity of the yaw damper. The sensitivity is defined as the amount of rudder movement produced by a steady unit rate of yaw. The pilot could vary this from 0.3 to 1.3 (degrees of rudder per degree per second yaw velocity). Invariably the pilot would report that the flying qualities were best when the sensitivity setting was maximum, giving maximum damping. It also appears that the pilot would like all airplane motions to appear "dead beat" to him. Actually, this requires only about 20 per cent of critical damping.

Initial flights were limited to an IAS = 200 m.p.h. until the damper operation was explored. When higher indicated air speeds were tried, a definite airplane hunting was experienced at a frequency greater than the natural airplane frequency. This was slightly noticeable and intermittent near IAS = 300 m.p.h. but became fully developed at IAS = 380 m.p.h. Calculations indicated that the servo system was not fast enough, causing the large phase losses to occur at too low a frequency, as will be shown later. The servo system was then improved with a faster motor that avoided the previous type of hunting. Another type of hunting then appeared at a frequency close to the airplane's natural frequency. This hunting motion was suspected as being due to the phase lags developed at extremely low yaw amplitudes, which is a common problem in the development of all servos. To improve this situation, the sensitivity of the internal electrical servo was increased, requiring additional complications to maintain stability of this part of the servo loop. This made the yaw damper more sensitive at low amplitudes and reduced the lag. Flight tests with this system showed that the system was improved to the point where it could be used satisfactorily in service. Examination of the phase lags throughout the complete system, including the hydraulic surface boost, is necessary before the system can be considered satisfactory at the smaller amplitudes of motion.

During the recent tests, a high-frequency hunting developed which was associated with body bending.

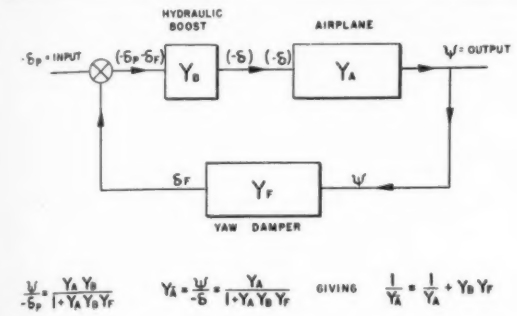

FIG. 6. Overall servomechanism block diagram of rudder system with yaw damper.

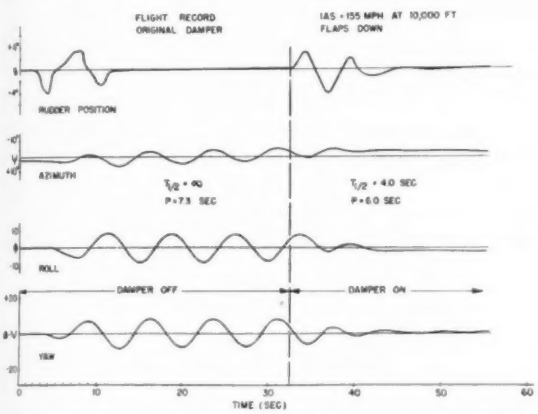

FIG. 7. Operation of yaw damper at approach condition.

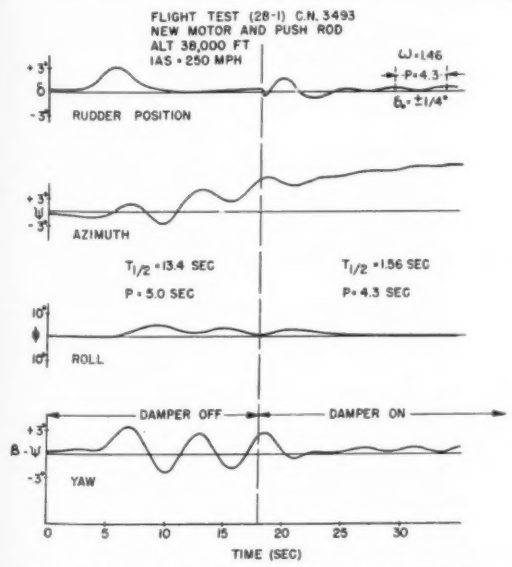

FIG. 8. Operation of yaw damper at high altitude.

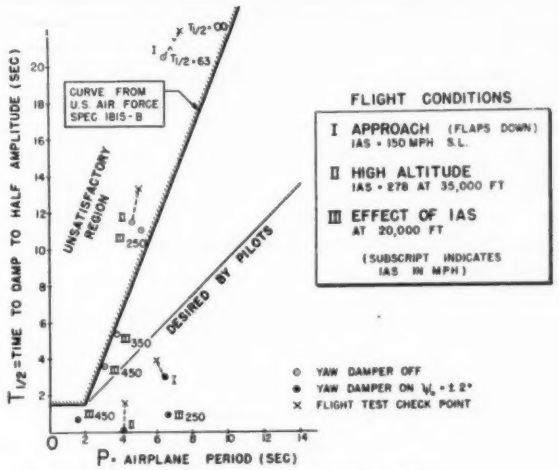
T1/2 = TIME TO DAMP TO HALF AMPLITUDE (SEC)
P = AIRPLANE PERIOD (SEC)
CURVE FROM U.S. AIR FORCE SPEC 1815-B
UNSATISFACTORY REGION
DESIRED BY PILOTS
T1/2 = ∞
T1/2 = 63
FLIGHT CONDITIONS
I APPROACH (FLAPS DOWN) IAS = 150 MPH S.L.
II HIGH ALTITUDE IAS = 278 AT 35,000 FT
III EFFECT OF IAS AT 20,000 FT
(SUBSCRIPT INDICATES IAS IN MPH)
YAW DAMPER OFF
YAW DAMPER ON φb = ± 2°
FLIGHT TEST CHECK POINT

FIG. 9. Summary of airplane stability.

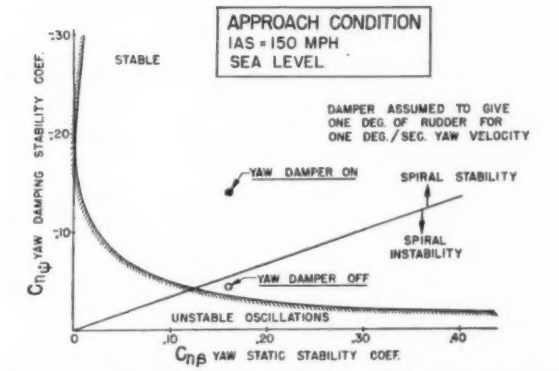

FIG. 10. Effect of airplane stability coefficients on stability boundaries.

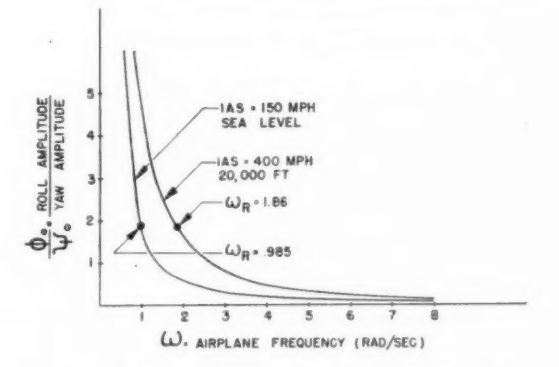

FIG. 11. Relation between yaw and roll amplitudes during a rudder motion frequency response.

This was corrected by moving the rate gyro near the airplane center of gravity. A technical discussion of this will be given later.

The pilots general acceptance of the yaw damper has been good. The fact that the yaw damper operates the rudder without transmitting its motion to the rudder pedals has been found to be favorable. During rapid rolls or entries into turns, the yaw damper has been beneficial. The only objectional features have been the airplane small hunting amplitudes and the increased pedal forces during the steady portion of the turns. Yaw damper modifications to eliminate the increased control forces during the turn will be discussed in a following section of this paper.

Method of Determining Airplane Stability from Frequency Response Calculations

The usual procedure for calculating airplane stability involves the solution of the airplane stability equations for the roots, which enables the period and time to damp to be evaluated. A similar procedure could be applied to the XB-47 airplane if an effective airplane damping coefficient due to the yaw damper were estimated. This method would not, however, conveniently predict any instability conditions that may exist for the yaw damper while in combination with the airplane; hence, it is of little use for design purposes. For this reason, the present analysis based upon a knowledge of the airplane and yaw damper steady-state frequency response characteristics has been used. By properly combining these frequency response curves, a method of estimating the period and time to damp of the airplane with or without the yaw damper is presented. The basic principle of the analysis has been based upon use of the inverse frequency response technique.[3]

(a) *Airplane Frequency Response*

The airplane frequency response will first be discussed by considering the airplane to have a single degree of freedom in yaw, as shown in Fig. 12a. Forcing the airplane to yaw in a positive direction at low frequencies requires the pilot to deflect the rudder in a negative direction according to the N.A.C.A. standard notation. For this reason a positive disturbance of the rudder will be considered as $-\delta$. By this simple expedient the N.A.C.A. standard notation can be used, and the resulting response curves will be recognizable to the servomechanism engineer. If the rudder is continuously oscillated in a sinusoidal manner at a given frequency ω and amplitude δ_0, the airplane will respond with a similar motion having the same frequency but, in general, a different yaw amplitude ψ_0. The airplane

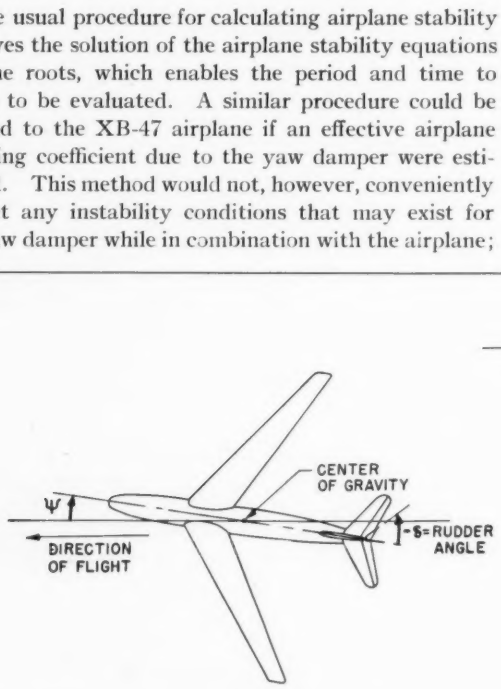

(a) AIRPLANE WITH POSITIVE YAW AND NEGATIVE DEFLECTED RUDDER

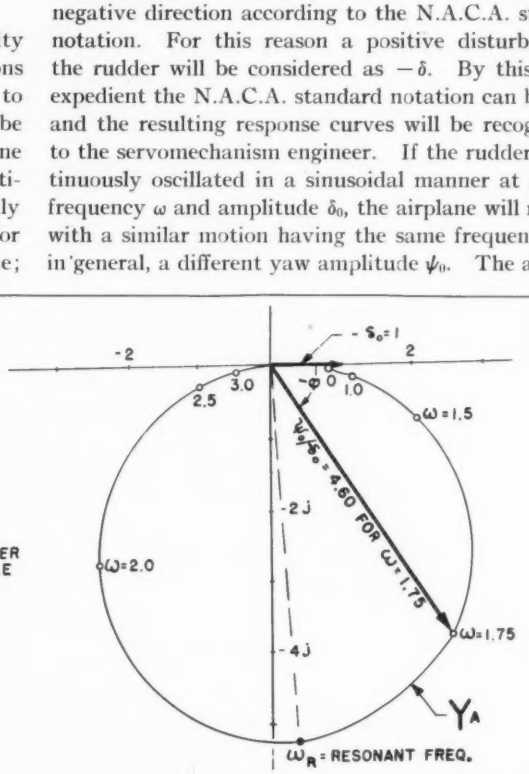

(c) POLAR PLOT OF AIRPLANE FREQ. RESPONSE

Φ = PHASE ANGLE = $(\frac{t_1}{P})\,2\pi$

ω = FREQUENCY = $\frac{2\pi}{P}$ (RAD/SEC)

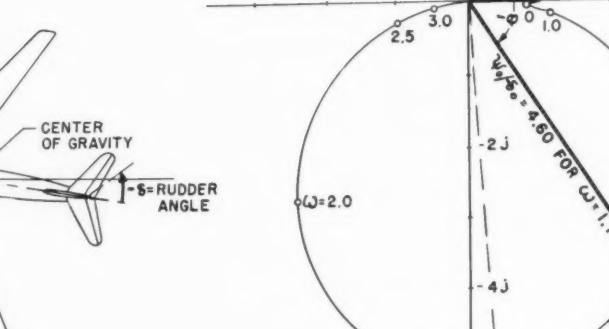

(b) TIME PLOT OF YAW RESPONSE FOR ω = 1.75

FIG. 12. Representation of airplane frequency response Y_A.

motion will lag the rudder motion in that the maximum yaw amplitude will occur after the rudder has experienced its maximum amplitude. The relation of the yaw motion with respect to the rudder motion may be represented by a pair of vectors, as shown in Fig. 12b. When this vector combination is rotated at the angular velocity ω for which they are drawn, their vertical components plotted against time provide a time-history plot of the airplane and rudder motion. Computing similar vectors for a series of frequencies will give a locus of the end points of the $\psi_0/-\delta_0$ vectors forming a polar representation of the airplane frequency response. In Fig. 12c, this locus is calculated from the equations of motion of the airplane given by the airplane transfer function Y_A considering a single degree of freedom. Equations for calculating Y_A for three degrees of freedom are given in Appendix A and were used in the actual stability calculations. The vector of maximum length of Fig. 12c corresponds to the resonant frequency of the airplane and is denoted as ω_R. At this frequency the pilot obtains the greatest amount of yaw for the least amount of rudder motion.

In the present analysis, it is more convenient to plot the airplane dynamic characteristic in terms of the amount of rudder amplitude and its phase relation necessary to sustain a continuous oscillation of the airplane. This is called the "airplane inverse frequency response" and is obtained by plotting the reciprocal of the length of each $\psi_0/-\delta_0$ vector using a negative value of the phase angle. Fig. 13 shows the Y_A plot of Fig. 12c converted into the airplane inverse transfer function denoted as $1/Y_A$. Here the resonant frequency vector becomes the minimum length vector in the plot. For the single degree of freedom considered, this plot has a parabolic shape. The next problem is to consider the yaw damper frequency response and to see how it may modify the present airplane inverse frequency response.

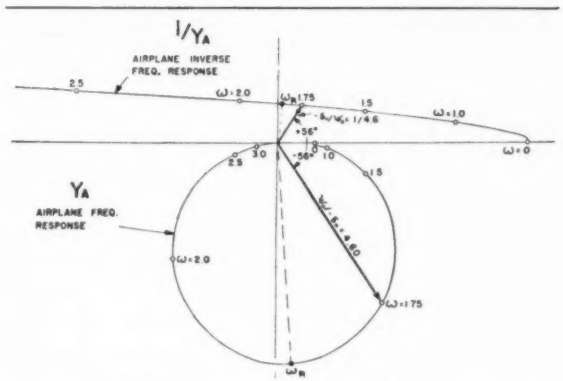

FIG. 13. Construction of airplane inverse frequency response $1/Y_A$.

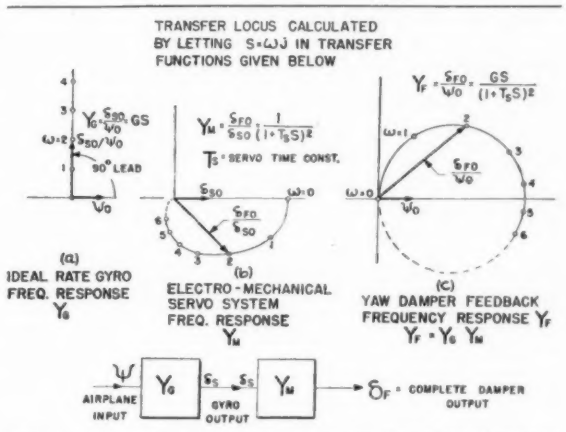
TRANSFER LOCUS CALCULATED BY LETTING S=ωJ IN TRANSFER FUNCTIONS GIVEN BELOW
T_S = SERVO TIME CONST.
(a) IDEAL RATE GYRO FREQ. RESPONSE Y_G
(b) ELECTRO-MECHANICAL SERVO SYSTEM FREQ. RESPONSE Y_M
(c) YAW DAMPER FEEDBACK FREQUENCY RESPONSE Y_F = Y_G Y_M
AIRPLANE INPUT
GYRO OUTPUT
COMPLETE DAMPER OUTPUT

FIG. 14. Basic components of yaw damper forming the feedback rudder response Y_F.

(b) *Yaw Damper Frequency Response*

The airplane yawing motion causes the rate gyro to produce an electrical signal that feeds into an electromechanical servomechanism to produce a rudder movement. At low frequencies a positive airplane yaw directs the yaw damper to produce a positive rudder angle or a $-(-\delta_F)$. The rate gyro will basically produce a 90° phase lead and a rudder displacement signal proportional to the yaw frequency. This gives a frequency response curve Y_G as shown in Fig. 14a. The resulting electrical signal then enters the electromechanical servo unit, which consists of an electro servo unit that operates the push-pull rod attached to the hydraulic boost, which in turn positions the rudder. For simplicity of this discussion, the frequency response of this combined unit is represented in Fig. 14b, where the transfer function Y_M is specified in a simple approximate manner. Here, the design variables are the sensitivity G and the servo time constant T_S. The frequency response of the rudder motion due to a yaw signal is then the vector product of $Y_G Y_M$ and is obtained by multiplying the respective vector lengths and adding their phase angles to form the feedback frequency response Y_F shown in Fig. 14c. This diagram represents the combined yaw damper and boost frequency characteristics, and for the assumptions made it is a circle.

The accurate estimation of Y_F from the design characteristics of the servomechanism is usually difficult because of the complicated and nonlinear characteristics of such devices. Therefore, the airplane manufacturer resorts to laboratory tests to measure the frequency response of existing automatic controls. This is done over the range of frequencies and amplitudes expected in flight. The results of typical laboratory tests will be shown later in this paper.

(c) *Combined Frequency Response of Airplane with Yaw Damper*

The yaw damper opposes any motion applied by the pilot to operate the rudder; hence, when the pilot ap-

plies a $(-\delta)$ rudder deflection to give the airplane a positive yaw, the damper supplies the rudder with a $-(-\delta_F) = \delta_F$ motion. As the frequency response Y_F of the yaw damper is the ratio of δ_F/ψ_0, it is possible to add each Y_F vector to the $1/Y_A$ vectors which represent the input motion $-\delta_0/\psi_0$. The resulting polar plot then becomes the overall inverse frequency response of the airplane with the yaw damper. This is merely a vector superposition of the two motions operating the rudder. The validity of this addition is given in Appendix C. Fig. 15 shows this vector addition, where the polar plot denoted as $1/Y_{\bar{A}}$ is the airplane inverse frequency response with the yaw damper operating.

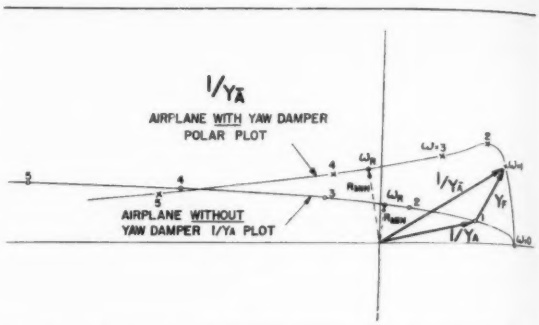

FIG. 15. Construction of inverse frequency yaw response of airplane with yaw damper.

(d) *Conditions for Airplane Instability*

Suppose next that, upon adding the Y_F vectors to the $1/Y_A$ vectors, the resulting $1/Y_{\bar{A}}$ curve passed through the origin. Then the reciprocal of the zero vector length at the frequency corresponding to the origin intersection would give an infinite airplane response in yaw, which is the condition that occurs for an undamped system when it is being excited at the resonant frequency. When the $1/Y_{\bar{A}}$ polar plot passes near the origin, the Y_F vector is opposite and almost equal to the $1/Y_A$ vector at some particular frequency. Under this condition the product of $Y_A Y_F$ approached 1.0 in magnitude, with the sum of the phase angles approaching 180, which corresponds to the Nyquist point frequently used in servomechanism analyses.[3, 4] When Y_F is greater than $1/Y_A$ for this condition, their product exceeds 1.0. This implies an instability according to the Nyquist theory in which $Y_A Y_F$ forms the loop transfer frequency response. It may therefore be concluded that the $1/Y_A$ polar plot should pass over the origin in a counterclockwise manner with increasing frequency, in order to avoid an unstable airplane oscillation. No attempt will be given here to explain the formal stability criterion, which is similar to that for the Nyquist diagram.

(e) *Calculation of Time to Damp from Combined Frequency Response*

Having established the condition for stability, it is of interest to determine, if possible, a way of predicting the amount of airplane oscillatory stability from these inverse frequency response curves. This is a complicated problem from the mathematical standpoint, especially when all three degrees of freedom are considered. If, however, the analysis is limited to the usual ranges of lateral stability coefficients of the airplane, a certain correlation is possible when this system is reduced to an equivalent one degree of freedom case. From the $1/Y_A$ curves generally encountered, the resonant frequency ω_R is practically identical to the airplane natural frequency, which is denoted here as ω_n. Also, if the damping is not too great, ω_R can be approximated by the undamped natural frequency ω_0 for purposes of estimating an effective static stability. The amount of damping should also be a function of the vector length R_{min}. If a damped oscillation is to occur, it should be expected to depend upon the airplane mass moment of inertia coefficient I_z, the airplane damping, and the airplane static stability. To obtain these quantities, the following assumptions have been made to present the airplane as having an equivalent single degree of freedom in yaw:

(1) The inertia will be taken as the calculated value of I_z.

(2) The damping will be assumed proportional to the ratio of the dynamic yaw response occurring at ω_R to the effective static yaw response.

(3) The airplane static stability giving the effective static yaw response can be obtained by determining an effective static yaw stability coefficient, $C_{n_{\bar{\beta}}}$, obtained by considering ω_R as an undamped natural frequency ω_0.

The third assumption is necessary when the three degree of freedom case is considered. Here the airplane has a zero static inverse yaw response due to the neutral directional stability. This type of stability is neutral for all airplanes and should not be confused with the normal spiral stability.

From assumptions (1) and (3), the undamped natural frequency is

$$\omega_0 \cong \omega_R \cong \sqrt{C_{n_{\bar{\beta}}}/I_z}$$

giving the effective static yaw stability as

$$C_{n_{\bar{\beta}}} = I_z \omega_R{}^2$$

The effective static yaw response then becomes

$$(\psi_0/-\delta_0)_{\text{static}} = -C_{n_\delta}/C_{n_{\bar{\beta}}}$$

since $\psi = -\beta$ for the one degree of freedom case. From the $1/Y_A$ curve the dynamic yaw response at ω_R is

$$(\psi_0/-\delta_0)_{\omega_R} = 1/R_{min}.$$

The ratio of these yaw responses will be called the dynamic resonant response ratio F and is

$$F = \frac{(\psi_0/-\delta_0)_{\omega_R}}{(\psi_0/-\delta_0)_{\text{static}}} = \frac{I_z\omega_R{}^2}{-C_{n_\delta}R_{min.}}$$

According to assumption (2), the damping should be a function of F. In order to verify this, a series of stability calculations have been made by varying several of the airplane stability coefficients over a wide range. Here, ω_R and $R_{min.}$ were obtained from $1/Y_A$ curves, and the corresponding stability equations were solved for the roots giving the natural frequency ω_n and the time to damp to half amplitude. In this case ω_R agreed closely with the calculated values of ω_n. Values of F were then plotted against the time to damp in periods, as shown in Fig. 16. In addition, a similar calculation was made for the yaw-damper using the simplified yaw damper analytical equations of Fig. 14 in conjunction with the airplane yaw response for a single degree of freedom. These results are also plotted in Fig. 16.

These calculated values are then compared with the theoretical F vs. $(T_{1/2}/P)$ curve calculated directly for a single degree of freedom. In this case the airplane equation of motion is

$$I_z\frac{d^2\psi}{dt^2} - C_{n_{\dot\psi}}\frac{d\psi}{dt} + C_{n_\beta}\psi = -C_{n_\delta}(-\delta)$$

when

$$\omega_0{}^2 = \frac{C_{n_\beta}}{I_z}, \quad \zeta = \frac{-C_{n_{\dot\psi}}}{2I_z\omega_0}, \quad k_\delta = \frac{-C_{n_\delta}}{C_{n_\beta}}$$

The differential equation of motion is

$$\frac{d^2\psi}{dt^2} + 2\zeta\omega_0\frac{d\psi}{dt} + \omega_0{}^2\psi = k_\delta\omega_0{}^2(-\delta)$$

where ζ = damping factor and k_δ = rudder effectiveness. For this case it can be shown that

$$\omega_n = \sqrt{1-\zeta^2}\,\omega_0, \quad \omega_R = \sqrt{1-2\zeta^2}\,\omega_0$$

giving

$$F = \frac{1-2\zeta^2}{2\zeta\sqrt{1-\zeta^2}}, \quad \frac{T_{1/2}}{P} = \frac{0.693}{2\pi}\frac{\sqrt{1-\zeta^2}}{\zeta}$$

The airplane is critically damped when $\zeta = \sqrt{1/2} = 0.707$. Any airplane that damps to half amplitude in a half cycle is well damped. Hence, this may be considered a practical maximum damping. Here, $\zeta \cong 0.20$, giving $\omega_n = 0.98$, $\omega_R = 0.96$, or $\omega_n/\omega_R = 1.02$.

This frequency comparison is made to show how close ω_R and ω_n agree for the single degree of freedom case. For design work with a yaw damper operating on the rudder, it is believed that the single degree of freedom curve shown, as obtained for a second order stability equation, may be used to obtain $(T_{1/2}/P)$ for all lateral stability cases and still be within the necessary engineering accuracy.

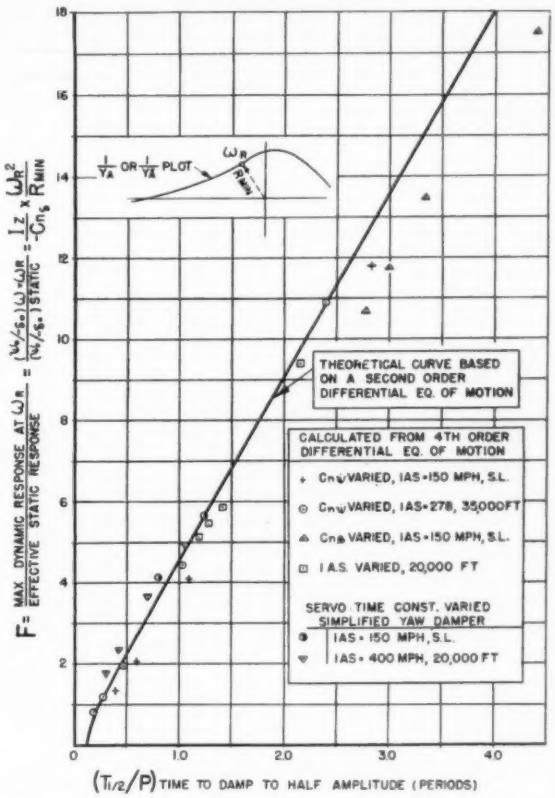
F= MAX. DYNAMIC RESPONSE AT ωn / EFFECTIVE STATIC RESPONSE = (ψ/δ0)ωn ωR²/(ψ/δ0) STATIC = Iz/-Cnδ x (ωR²/RMIN)
1/YA OR 1/YA PLOT
ωR
THEORETICAL CURVE BASED ON A SECOND ORDER DIFFERENTIAL EQ. OF MOTION
CALCULATED FROM 4TH ORDER DIFFERENTIAL EQ. OF MOTION
+ Cnψ VARIED, IAS=150 MPH, S.L.
⊙ Cnψ VARIED, IAS=278, 35,000FT
▲ Cnβ VARIED, IAS=150 MPH, S.L.
⊡ I.A.S. VARIED, 20,000 FT
SERVO TIME CONST. VARIED SIMPLIFIED YAW DAMPER
● IAS=150 MPH, S.L.
▼ IAS=400 MPH, 20,000 FT
(T1/2/P) TIME TO DAMP TO HALF AMPLITUDE (PERIODS)

FIG. 16. Correlation of resonant response ratio with time to damp.

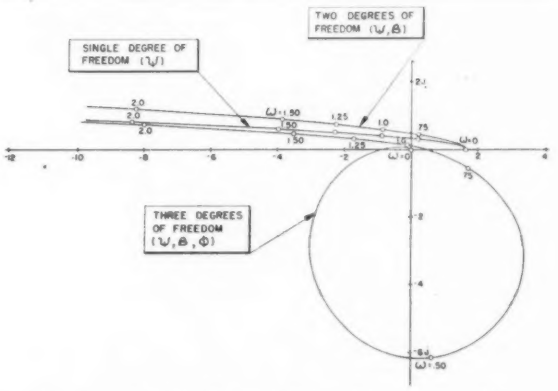

FIG. 17. Effect of different degrees of freedom on $1/Y_A$.

STABILITY CALCULATIONS FOR THE XB-47 AIRPLANE

The method of analysis of the previous section has been applied to the XB-47 airplane. Here, the $1/Y_A$ curves are calculated using equations of Appendix A, which considers three degrees of freedom of the airplane. These curves will then be combined with Y_F curves obtained from laboratory tests of the yaw damper.

It is of interest first to study the factors causing the $1/Y_A$ curves to change. Fig. 17 shows the change in

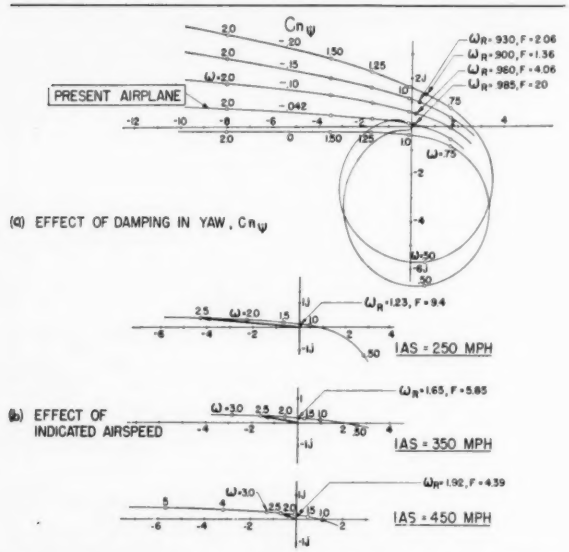

FIG. 18. Effect of air speed and damping on $1/Y_A$ for three degrees of freedom.

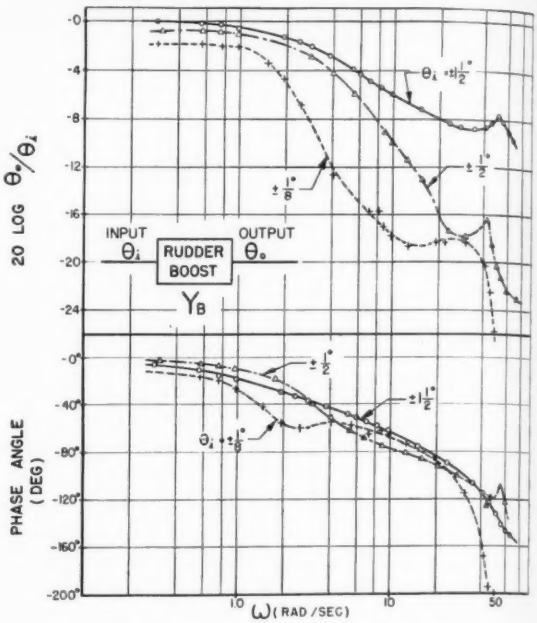

FIG. 21. Frequency response of rudder boost.

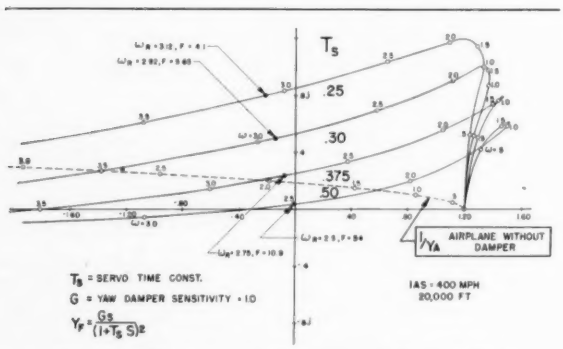

FIG. 19. Effect of servo time constant T_S on $1/Y_A$.

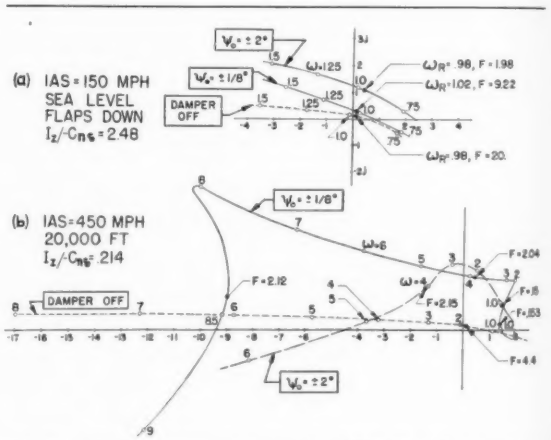

FIG. 22. Inverse frequency response of XB-47 with actual yaw damper.

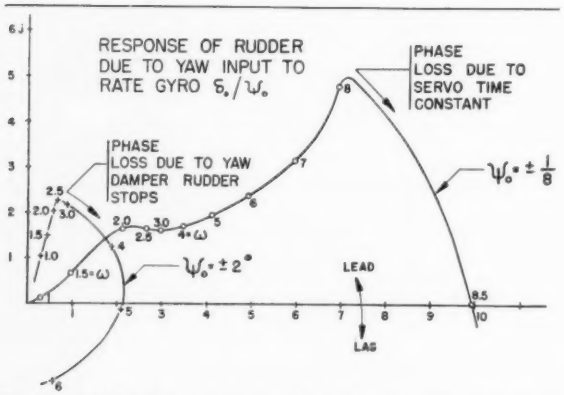
RESPONSE OF RUDDER DUE TO YAW INPUT TO RATE GYRO δ_r/ψ_o
PHASE LOSS DUE TO YAW DAMPER RUDDER STOPS
PHASE LOSS DUE TO SERVO TIME CONSTANT
$\psi_o = \pm 2°$
$\psi_o = \pm 1/8$
LEAD
LAG

FIG. 20. Y_F frequency response of actual yaw damper including rudder boost.

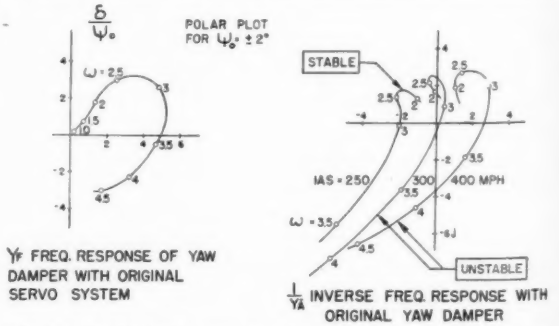

FIG. 23. Instability occurring for yaw damper system with original servo.

$1/Y_A$ due to different assumed degrees of airplane freedom. It can be seen that the effect of roll causes the $1/Y_A$ curve for the three degrees of freedom case to move nearer the origin, thus reducing the stability. The lower frequency points of this curve encircle the origin and approach zero frequency along the $\pm j$ axis depending upon the sign of the e_0 stability coefficient. The reason for this encirclement is the fact that at very low frequencies the forces due to roll are large compared to other forces present. This causes the change shown in the frequency response picture.

While the low-frequency results have not been important from the yaw damper design, they may be extremely important for autopilot design where the Y_F vector at zero frequency has no lead but a finite length. In this case the resulting $1/Y_{\bar{A}}$ vector at $\omega = 0$ will be over to the right of the diagram, which may cause the $1/Y_{\bar{A}}$ curve to pass under the origin at very low frequencies. This may result in an airplane long-period instability. Fig. 17 has been drawn for IAS = 150 m.p.h. When high air speeds are considered, the three degree of freedom curve can be approximated in a satisfactory manner for the higher frequencies by the single degree of freedom parabola as shown. Fig. 18a shows a series of $1/Y_A$ curves where the damping in yaw, $C_{n_{\dot{\psi}}}$, has been given different values. It may be noted here that, if $C_{n_{\dot{\psi}}}$ were increased by increasing the tail size, the curves of Fig. 18a would be shifted to the left because of the C_{n_β} change; hence, the resulting improvement would be small with regard to the airplane damping because of the increased resonant frequency. The yaw damper is designed basically to increase the $C_{n_{\dot{\psi}}}$ without changing the frequency. Calculated values of F are shown on these curves to indicate the nature of the airplane stability, which can readily be noted from Fig. 16. In Fig. 18b a series of $1/Y_A$ curves are drawn for different air speeds and show how the higher frequency points move nearer the origin as the air speed is increased. These curves also show an improvement in airplane stability at the higher indicated air speeds because $I_z/-C_{n_\delta}$ is reduced. The effect of the yaw damper servo time constant T_s, based on the damper frequency characteristics as defined in Fig. 14, is shown in Fig. 19. This figure has been drawn for IAS = 400 m.p.h. and shows how the airplane stability is decreased because of increasing T_s. Next, the actual yaw damper frequency response will be presented.

The yaw damper operates the push rod, which in turn operates the hydraulic boost. Both of these systems are nonlinear at the smaller amplitudes. In addition, large airplane disturbances will cause the yaw damper rudder stops to be encountered at $\delta = \pm 5$, which introduces a large amplitude nonlinear condition.

Because of these nonlinear characteristics, laboratory frequency response information for the entire yaw damper and boost combination is necessary. These data are shown in Fig. 20 for two typical amplitudes. The $\psi_0 = \pm 1/8°$ curve is representative of the low amplitude effects, which are important in studying airplane hunting. The $\psi_0 = \pm 2°$ curve will provide yaw damper characteristics used to calculate the airplane stability. These two polar plots represent the Y_F feedback frequency response which will be added according to Fig. 15 to obtain the $1/Y_{\bar{A}}$ curves. In Fig. 21 the frequency response of the rudder boost alone is shown. These effects are, of course, included in Fig. 20. The inverse frequency response curves with and without the yaw damper are shown in Fig. 22 for two representative conditions. The 150 m.p.h. case represents the case where the maximum yaw damper stability performance is required, while the 450 m.p.h. condition is critical in avoiding a possible hunting condition. These latter curves are of interest because of the large number of possible F values. Of all these F values, the critical one occurs on the $\psi_0 = 1/8°$ curve at $\omega_R = 8.4$, which shows the airplane to be stable from the hunting standpoint. Had a higher air speed been considered, this point would approach the origin causing an oscillatory instability. The values of $F = 0.15$ indicate a highly damped long period, while values of F near $\omega = 4$ are representative of the airplane stability with the damper operating.

The original servo system developed a lagging phase angle near $\omega = 3.5$ and, as a result, caused the airplane to hunt at the higher air speeds. Fig. 23 shows the original servo system frequency response, together with the corresponding $1/Y_{\bar{A}}$ curves, showing that hunting occurred near IAS = 300 m.p.h.

Effect of Body Side Bending on Location of Yaw Damper Rate Gyro

Recent flight tests resulted in an airplane hunting instability being developed at a higher frequency than had previously occurred ($\omega = 14$ rad. per sec.). Pilot observations associated this hunting with bending of the airplane body. The hunting condition was entirely corrected, however, when the rate gyro, which had been located near the tail, was moved forward nearer the airplane c.g. As a result, an analysis has been made to see whether this type of oscillation could be predicted. It was assumed that the body was hinged at an estimated hinge location and elastically restrained such as to provide a body bending frequency equal to that found from ground vibration tests. Appendix B contains the derived equations. Fig. 24 shows the $1/Y_A$ and $1/Y_{\bar{A}}$ curves calculated for IAS = 200, 300, and 400 m.p.h. for the rate gyro located in the tail. Here, the yaw damper frequency response Y_F was estimated by extrapolating the $\psi_0 = \pm 1/8°$ data to larger frequency values. These curves indicate a hunting near IAS = 300 m.p.h., with a frequency of $\omega_R = 17.5$ rad. per sec., although this is somewhat different

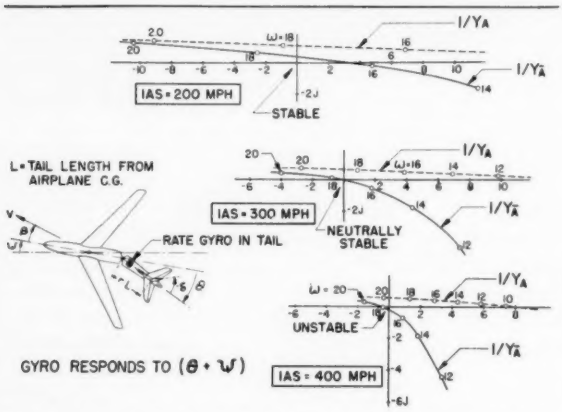

FIG. 24. Instability due to body bending for tail location of rate gyro.

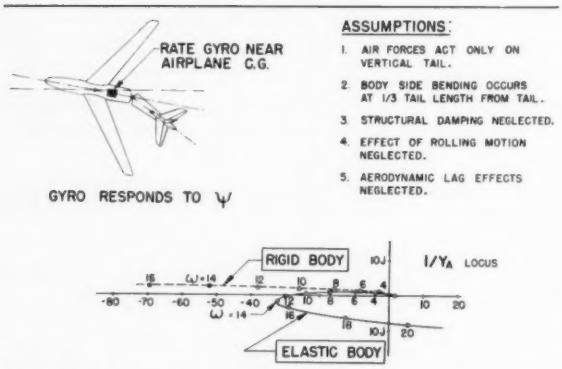
RATE GYRO NEAR AIRPLANE C.G.
GYRO RESPONDS TO Ψ
ASSUMPTIONS:
1. AIR FORCES ACT ONLY ON VERTICAL TAIL.
2. BODY SIDE BENDING OCCURS AT 1/3 TAIL LENGTH FROM TAIL.
3. STRUCTURAL DAMPING NEGLECTED.
4. EFFECT OF ROLLING MOTION NEGLECTED.
5. AERODYNAMIC LAG EFFECTS NEGLECTED.
RIGID BODY
ELASTIC BODY
1/YA LOCUS

FIG. 25. Effect of body side bending on airplane inverse frequency response $1/Y_A$.

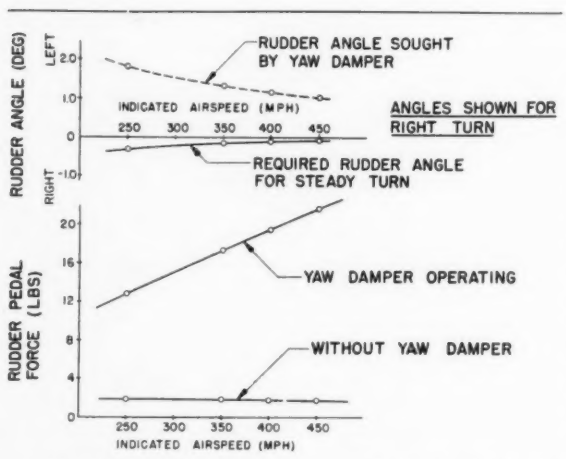

FIG. 26. Calculated rudder force and deflection during a 30° banked steady turn.

from the flight record that showed that hunting had occurred near IAS = 350 m.p.h. and at a frequency $\omega = 14$ rad. per sec. The agreement is believed to be reasonable in light of the data used and the simple assumptions made. A closer analysis would require a study of the actual amount of the θ motion picked up by the rate gyro.

Fig. 25 shows the inverse airplane frequency response $1/Y_A$ to be used when the gyro is located near the airplane c.g. Here, it can be seen that hunting cannot occur when the Y_F vectors are added to these curves, since the present yaw damper loses its lead near $\omega = 8$ rad. per sec. and its sensitivity is not great enough. Had the yaw damper and control surface boost been responsive such that the Y_F vector could lead until $\omega \cong 18$ rad. per sec., an airplane hunting could exist even for the gyro pickup near the airplane c.g. Here, the vectors, when added to the $1/Y_A$ vectors, could go on the opposite side and under the origin even if the sensitivity or gain ratio were small. In the light of these calculations, careful consideration of body bending should be made when high responsive autopilots are considered for elastic airplanes. It may be concluded that an optimum autopilot or airplane boost may not be the one having the fastest response.

Yaw Compensation During Steady Turning Flight

During a steady turn, the rate gyro deflects a constant amount due to the uniform angular velocity of the turn. This results in the rudder desiring to deflect to oppose the turn, which requires the pilot to apply an increased pedal force to properly position the rudder. The XB-47 has desirable turning characteristics when the damper is off, especially in smooth air where the Dutch Roll is not easily excited. The increase in the rudder pedal forces with the damper on has been objectionable to the pilots. These pedal forces have been calculated and are shown in Fig. 26. While the pedal forces are not especially high, they give the pilots a feeling of flying an airplane with a high amount of spiral stability, which is the actual case as indicated by the spiral stability boundary of Fig. 10.

The problem of reducing or eliminating these pedal forces requires a means of canceling the steady or constant signal of the rate gyro. The basic principle of doing this is to provide a device that has an equal and opposite static signal to match the static deflection signal produced by the rate gyro during a steady turn. This device should have a slow dynamic response, characterized by a large time constant, such that it will not impair the desirable dynamic gyro characteristics occurring near the resonant frequency of the airplane. This time constant should be short enough, however, so that after a steady turn is entered the pedal forces will be reduced in a reasonable time.

Two ways of accomplishing this will be briefly mentioned. The first method consists of including an R.C. (resistance capacity) electrical network in the yaw damper electrical system such that at very low frequencies a very small electrical signal is developed giving a negligible rudder movement.

A second method is to provide a slow responding electrical motor drive, which tends to make the electrical center of the gyro potentiometer follow the gyro signal. Here again, if the gyro is moving slowly or is positioned in a deflected position, as occurs in a turn, the resulting rudder signal will be small or zero. These methods are being studied, and either one should provide the necessary yaw compensation required during a steady airplane turn.

Conclusions

The present yaw damper has readily solved the lateral stability problem of the XB-47 airplane. The important design problem has not been one of basic operation of the yaw damper but rather of the proper detail design so as to avoid phase lags occurring at small amplitudes. There are undoubtedly other ways of operating the control surfaces to improve the lateral stability. Whether these methods can be used will depend upon how well any new type of damper operates at small amplitudes. It is believed that other methods should be investigated with the single aim of simplifying the yaw damper.

Further correlation of the present inverse frequency response method of analysis should be made to see whether the roots of the stability equation can be estimated in a similar manner for other airplane stability problems.

References

[1] Sternfield, L., *Some Considerations of the Lateral Stability of High-Speed Aircraft*, N.A.C.A. T.N. No. 1282, 1947.

[2] Morgan, M. B., *Control in Low Speed Flight*, Aeronautical Conference, London, 1947.

[3] Marcy, H. T., *Parallel Circuits in Servomechanisms*, A.I.E.E. Trans., August–September, 1946.

[4] Brown, G. S., and Campbell, D. P., *Principles of Servomechanisms*, John Wiley & Sons, Inc., New York, 1948.

[5] Zimmerman, C. H., *An Analysis of Lateral Stability in Power-off Flight with Charts for Design Use*," N.A.C.A. T.R. No. 589, 1937.

Appendix A

Calculation of Airplane Frequency Response in Yaw

Lateral equations for the airplane motion are given in reference 1. These equations and notations will be used with several modifications. It has been found for the XB-47 airplane that the product of inertia I_{xz} has a small influence on the airplane stability except at low speeds, where it is conservative to neglect these terms. For convenience, this term will be neglected. Also, the factor $2b\mu/v$ will be written as m_0, giving the following equations of motion:

$$\left.\begin{array}{lll} (m_0 s - C_{Y_\beta})\beta & (-C_L)\phi & (m_0 s)\psi = 0 \\ (-C_{l_\beta})\beta + (I_z s^2 - C_{l_{\dot\psi}} s)\phi & & (-C_{l_{\dot\psi}} s)\psi = 0 \\ (-C_{n_\beta})\beta & (-C_{n_{\dot\phi}} s)\phi + (I_z s^2 - C_{n_{\dot\psi}} s)\psi = & \\ & & -C_{n_\delta}(-\delta) \end{array}\right\} \quad (1a)$$

From wind-tunnel tests it was found that the effect of the rudder motion on roll and sideslip were small; hence, as shown in the above equations, the rudder motion is considered to affect the yaw only. Expanding the left side of Eq. (1) and substituting the root λ for the operator s gives the airplane stability equation

$$a_0\lambda^4 + b_0\lambda^3 + c_0\lambda^2 + d_0\lambda + e_0 = 0 \quad (2a)$$

where

$$\left.\begin{array}{rcl} a_0 &=& m_0 I_x I_z \\ b_0 &=& -(m_0 C_{l_{\dot\phi}} + C_{Y_\beta} I_z) I_z - m_0 I_x C_{n_{\dot\psi}} \\ c_0 &=& C_{Y_\beta} C_{l_{\dot\phi}} I_z + (m_0 C_{l_{\dot\phi}} + C_{Y_\beta} I_z) C_{n_{\dot\psi}} + \\ & & m_0 I_x C_{n_\beta} - m_0 C_{l_{\dot\psi}} C_{n_{\dot\phi}} \\ d_0 &=& -C_{Y_\beta} C_l C_{n_{\dot\psi}} + m_0 C_{l_\beta} C_{n_{\dot\phi}} - m_0 C_{l_{\dot\phi}} C_{n_\beta} - \\ & & C_L C_{l_\beta} I_z + C_{Y_\beta} C_{l_{\dot\psi}} C_{n_{\dot\phi}} \\ e_0 &=& -C_L(C_{l_{\dot\psi}} C_{n_\beta} - C_{l_\beta} C_{n_{\dot\psi}}) \end{array}\right\} \quad (3a)$$

The quartic stability Equation [Eq. (2)] has been most easily solved by the semigraphical method of Zimmerman,[5] permitting the airplane period and time to damp to half amplitude to be found.

In order to obtain the yaw response due to a rudder oscillation, Eq. (1) must be solved for the ratio $\psi/-\delta$. This solution gives Y_A and, written in determinant form, becomes

$$Y_A = \frac{\psi}{-\delta} = \frac{\begin{vmatrix} (m_0 s - C_{Y_\beta}), & -C_L, & 0 \\ -C_{l_\beta}, & (I_z s^2 - C_{l_{\dot\phi}} s), & 0 \\ -C_{n_\beta}, & -C_{n_{\dot\phi}} s, & -C_{n_\delta} \end{vmatrix}}{\begin{vmatrix} (m_0 s - C_{Y_\beta}), & -C_L, & m_0 s \\ -C_{l_\beta}, & (I_z s^2 - C_{l_{\dot\phi}} s), & -C_{l_{\dot\psi}} s \\ -C_{n_\beta}, & -C_{n_{\dot\phi}} s, & (I_z s^2 - C_{n_{\dot\psi}} s) \end{vmatrix}} \quad (4a)$$

Expanding these determinants in terms of the operator s gives

$$Y_A = \frac{a_1 s^3 + b_1 s^2 + c_1 s + d_1}{s(a_0 s^4 + b_0 s^3 + c_0 s^2 + d_0 s + e_0)} \tag{5a}$$

where

$$\left.\begin{aligned} a_1 &= -C_{n_\delta} m_0 I_z \\ b_1 &= C_{n_\delta}(m_0 C_{l_{\dot\phi}} + C_{Y_\beta} I_z) \\ c_1 &= -C_{n_\delta} C_{Y_\beta} C_{l_{\dot\phi}} \\ d_1 &= C_{n_\delta} C_L C_{l_\beta} \end{aligned}\right\} \tag{6a}$$

The frequency response is found by letting $s = \omega j$ and evaluating the resulting complex function for various values of ω. When this is done,

$$Y_A = \frac{\psi_0}{-\delta_0} = \frac{X_1 + Y_1 j}{X_2 + Y_2 j} \tag{7a}$$

where

$$\left.\begin{aligned} X_1 &= d_1 - b_1\omega^2, \quad Y_1 = c_1\omega - a_1\omega^3 \\ X_2 &= -d_0\omega^2 + b_0\omega^4, \quad Y_2 = e_0\omega - c_0\omega^3 + a_0\omega^5 \end{aligned}\right\} \tag{8a}$$

For each frequency the vector length is

$$Y_A = |\psi_0/-\delta_0| = X_1 \cos\varphi_2 / X_2 \cos\varphi_1 \tag{9a}$$

with a phase angle

$$\varphi = \varphi_1 - \varphi_2 \tag{10a}$$

where $\tan\varphi_1 = Y_1/X_1$ and $\tan\varphi_2 = Y_2/X_2$.

Stability coefficients for the XB-47 airplane, together with the resulting frequency response coefficients, are given in Table 1. The resulting calculations have been used on Figs. 17, 18, 22, and 23.

Appendix B

Effect of Body Side Bending on Airplane Frequency Response

The effect of body side bending will alter the angle of attack of the vertical tail. During this type of motion, aerodynamic loads on the airplane wing and body will be small compared to those developed on the vertical tail. For this reason the mass forces on the airplane body and wing will be considered, but only the aerodynamic forces acting on the vertical tail will be used. It will also be assumed that the airplane can sideslip and yaw but that no roll occurs. As has been pointed out previously, this is a valid assumption at the higher frequencies. The representation of the body bending is made by assuming an effective body hinge pivot point for the aft body angular motion θ, as shown in Fig. 24. The after part of the body is assumed to be restrained from moving by an elastic restraint proportional to θ. The corresponding spring constant K_θ has been evaluated using the calculated weight of the entire empennage, and the measured frequency has been obtained from ground tests.

Table 1
Airplane Stability Coefficients

Flight Condition	IAS = 150, Sea Level, Flaps Down	IAS = 278, 35,000 Ft., Flaps Up	IAS = 400, 20,000 Ft., Flaps Up
V (m.p.h.)	150	500	550
W (lbs.)	125,000	125,000	125,000
C_L	1.5	0.443	0.214
$m_0 = 2b\mu/V$	10.4	10.1	5.36
I_x	0.107	0.0311	0.0172
I_z	0.248	0.072	0.0346
$C_{l_{\dot\phi}}$	−0.1095	−0.0316	−0.0289
$C_{l_{\dot\psi}}$	0.0765	0.0107	0.0062
$C_{n_{\dot\phi}}$	−0.0274	−0.00198	0
$C_{n_{\dot\psi}}$	−0.0422	−0.0112	−0.0101
C_{l_β}	−0.225	−0.140	−0.140
C_{n_β}	0.16	0.12	0.12
C_{Y_β}	−0.78	−0.61	−0.61
a_0	0.276	0.0226	0.003185
b_0	0.350	0.02788	0.006618
c_0	0.2726	0.0431	0.01258
d_0	0.335	0.0458	0.01979
e_0	−0.00412	0.000127	0.000143
a_1	0.1113	0.0314	0.0092
b_1	0.1222	0.0338	0.01653
c_1	0.00854	0.00193	0.00173
d_1	0.03375	0.0062	0.0030

b = 116 ft. S = 1,428 sq.ft.

Referring to Fig. 24, the equations of motion become:

Side Force

$$a_t S_t q\left(\beta - \theta - \frac{Lr}{V}\dot\theta - \frac{L}{V}\psi - k_\delta\delta\right) - \frac{W_t}{g} rL\ddot\theta + \frac{W}{g} V\dot\beta + \frac{W}{g} V\dot\psi = 0 \tag{1b}$$

Yawing Moment

$$a_t S_t Lq\left(\beta - \theta - \frac{Lr}{V}\dot\theta - \frac{L}{V}\psi - k_\delta\delta\right) - \frac{W_t}{g} L^2 r\ddot\theta - \frac{W}{g} K_z^2\ddot\psi = 0 \tag{2b}$$

Body Bending

$$a_t S_t qLr\left(\beta - \theta - \frac{Lr}{V}\dot\theta - \frac{L}{V}\psi - k_\delta\delta\right) - \frac{W_t}{g} L^2 r^2\ddot\theta - \frac{W_t}{g} L^2 r\ddot\psi + \frac{W_t}{g} LrV\dot\beta + \frac{W_t}{g} LrV\dot\psi - K_\theta\theta = 0 \tag{3b}$$

where

a_t = slope of vertical tail lift curve (C_L per rad.)
S_t = vertical tail area, sq.ft.

L = tail length
W = gross weight of entire airplane, lbs.
W_t = weight of empennage, lbs.
K_z = radius of gyration of complete airplane
K_θ = body spring constant, ft.lbs. per rad.

These equations will be written in a nondimensional form for convenience of solution. Basing all lengths in terms of half wing spans, the following notation is defined:

$$\begin{aligned}
\mu &= 2(W/g)/\rho Sb \\
\mu_t &= 2(W_t/g)/\rho Sb \\
k_z &= 2K_z/b \\
C_{n_\beta} &= a_t(S_t/S)(L/b) \\
C_{Y_\beta} &= -a_t(S_t/S) \\
m &= C_{Y_\beta}/2\mu \\
E &= K_\theta/qSbr \\
l &= (2L/b) \\
k_\delta &= -C_{n_\delta}/C_{n_\beta} \\
D\theta &= (2V/b)\dot{\theta}, \quad D^2\theta = (2V/b)^2\ddot{\theta} \\
D\theta &= (b/2V)\dot{\theta}
\end{aligned}$$

Substituting the above notation in the equations of motion and rearranging,

$$[D\beta - m\beta] + [(1 + ml)D\psi] + \left[-\frac{\mu_t}{\mu} lrD^2\theta + mlrD\theta + m\theta\right] = mk_\delta(-\delta) \quad (4b)$$

$$[-C_{n_\beta}\beta] + [\mu k_z^2 D^2\psi + C_{n_\beta} lD\psi] + [\mu_t l^2 rD^2\theta + C_{n_\beta} lrD\theta + C_{n_\beta}\theta] = C_{n_\beta}k_\delta(-\delta) \quad (5b)$$

$$[-\mu_t lD\beta - C_{n_\beta}\beta] + [\mu_t l^2 D^2\psi + (C_{n_\beta} - \mu_t)lD\psi] + [\mu_t l^2 rD^2\theta + C_{n_\beta} lrD\theta + (E + C_{n_\beta})\theta] = C_{n_\beta}k_\delta(-\delta) \quad (6b)$$

Based on the above equations, the stability equation becomes:

$$a_0'\lambda^4 + b_0'\lambda^3 + c_0'\lambda^2 + d_0'\lambda + e_0' = 0 \quad (7b)$$

where

$$\left.\begin{aligned}
a_0' &= \mu_t k_z^2 l^2 r(\mu - \mu_t) - \mu_t^2 l^4 r \\
b_0' &= C_{n_\beta} lr[k_z^2(\mu - \mu_t) - \mu_t l^2] \\
c_0' &= C_{n_\beta}\left[\mu k_z^2 - \mu_t l^2\left(1 + \frac{\mu_t}{\mu} r\right)\right] + ml\mu_t(\mu k_z^2 - \mu_t l^2 r) + \mu k_z^2 E \\
d_0' &= C_{n_\beta} lE - m\mu k_z^2 E \\
e_0' &= C_{n_\beta} E
\end{aligned}\right\} \quad (8b)$$

Eqs. (7) and (8) permit the periods and time to damp to be calculated using the following equations:

$$\left.\begin{aligned}
&\lambda = \bar{a} + \bar{\omega}j, \quad \omega = (2V/b)\bar{\omega} \\
&P = (2\pi/\bar{\omega})(b/2V), \quad T_{1/2} = (-0.693/\bar{a})(b/2V)
\end{aligned}\right\} \quad (9b)$$

Equations giving the inverse frequency response can be calculated by the procedure given in Appendix A. Here,

$$\frac{1}{Y_A} = \frac{-\delta_0}{\psi_0} = \frac{[e_0' - c_0'\bar{\omega}^2 + a_0'\bar{\omega}^4] + [d_0'\bar{\omega} - b_0'\bar{\omega}^3]j}{c_1'} \quad (10b)$$

where $c_1' = k_\delta C_{n_\beta} E$.

The body bending inverse response is

$$\frac{-\delta_0}{\theta_0} = \frac{[e_0' - c_0'\bar{\omega}^2 + a_0'\bar{\omega}^4] + [d_0'\bar{\omega} - b_0'\bar{\omega}^3]j}{-a_2'\bar{\omega}^2} \quad (11b)$$

where

$$a_2' = \mu k_z^2 k_\delta(m\mu_t l + C_{n_\beta}) - \mu_t C_{n_\beta} k_\delta l^2$$

It is desired to calculate the effect of locating the yaw damper gyro in the tail where the gyro pickup is $(\theta + \psi)$; hence, the airplane inverse frequency response to be used for the gyro in the tail is

$$\left(\frac{1}{Y_A}\right)_{\text{tail}} = \frac{-\delta_0}{(\theta_0 + \psi_0)} = \frac{[e_0' - c_0'\bar{\omega}^2 + a_0'\bar{\omega}^4] + [d_0'\bar{\omega} - b_0'\bar{\omega}^3]j}{[c_1' - a_2'\bar{\omega}^2]} \quad (12b)$$

Eq. (10) is used to calculate the $1/Y_A$ curves of Fig. 25 and Eq. (12) gives the $1/Y_A$ curve for the rate gyro located in the tail portion of the airplane as used in Fig. 24.

Typical coefficients for the XB-47 airplane for IAS = 400 m.p.h. at 20,000 ft. are given below:

W = 125,000 lbs.		W_t = 8,477	
b = 116 ft.		r = 0.333	
S = 1,428 sq.ft.		ω_0 = 138 cycles per min. = 14.4 rad. per sec.	
ρ = 0.001265		S_t = 227 sq.ft.	
K_z = 24.6 ft.		$(b/2V)$ = 0.072	
L = 46 ft.		l = 0.792	

Then

μ = 37.0		m = −0.00762	
u_t = 2.51		$K_\theta = \omega_0^2(rL)^2(W_t/g)$ = 12.8×10^6	
C_{Y_β} = −0.564		E = 0.568	
C_{n_β} = 0.223		k_z^2 = 0.181	
k_δ = 0.625			

giving

a_0' = 2.448	a_2' = 0.6044
b_0' = 0.2747	c_1' = 0.0734
c_0' = 4.937	
d_0' = 0.1293	
e_0' = 0.1267	

(*Continued on next page*)

Appendix C

Servomechanism Derivation of Inverse Transfer Method

In this appendix the method of obtaining $1/Y_{\bar{A}}$ from the servomechanism standpoint will be analyzed. Fig. 6 is a block diagram of the airplane rudder system with hydraulic boost and yaw damper.

The only physical input to this system is through the pilot's pedal motion $(-\delta_P)$. The output motion is the yaw ψ. The feedback signal δ_F opposes the pilot pedal motion; hence, the rudder boost output $-\delta$ for the closed loop is

$$-\delta = Y_B(-\delta_F - \delta_P) \tag{1c}$$

The various transfer functions may be expressed as follows:

$\psi = Y_A(-\delta)$ airplane transfer function
$-\delta = Y_B(-\delta_P)$ rudder boost (no feedback included)
$\delta_F = Y_F(\psi)$ feedback transfer function

When these relations are substituted in Eq. (1c) for the closed loop circuit, the output ψ due to the input $-\delta$ may be written as

$$\frac{\text{output}}{\text{input}} = \frac{\psi}{-\delta_P} = \frac{Y_A Y_B}{1 + Y_A Y_B Y_F} \tag{2c}$$

It is desired, however, to consider the rudder motion as the input and to modify this by the response of the feedback to form $1/Y_{\bar{A}}$. As the rudder can only be operated through the boost, a signal must be applied to the rudder pedal to produce the reference input $-\delta$ considering the feedback δ_F absent. This input pedal motion is $-\delta_P = -\delta/Y_B$; then the yaw response with the feedback operating becomes

$$\psi/-\delta = Y_{\bar{A}} = Y_A/(1 + Y_A Y_B Y_F) \tag{3c}$$

or the inverse airplane frequency response with yaw damper operating is

$$1/Y_{\bar{A}} = (1/Y_A) + Y_B Y_F \tag{4c}$$

In the analysis considered in this report, the hydraulic boost transfer function Y_B has been included with the feedback response, and the product $Y_B Y_F$ has been used as Y_F.

Steady Flow of Nonviscous Elastic Fluids in Axially Symmetric Channels

M. H. VAVRA*

United States Naval Postgraduate School

SUMMARY

Subject matter is the axially symmetric steady flow of a nonviscous elastic fluid, with constant total energy, between two arbitrary coaxial surfaces of revolution. By means of orthogonal, curvilinear coordinates, a transformation of the Eulerian equation of motion is obtained which permits the determination of the meridional velocities for arbitrary distributions of the tangential velocity components. Based on this relation, an iteration method is described which serves to calculate arbitrary three-dimensional flow fields.

An application of the theory to an irrotational flow in an inlet channel for a centrifugal compressor wheel shows the importance of determining the flow ahead of rotating wheels in order to evaluate the correct inlet conditions for the impeller.

Rotational motion gives flow patterns that are entirely different from those of irrotational motions. Depending on the vorticity and the shape of the channel contours, there exist definite relations between the meridional and the tangential velocity components to make possible a stable motion that follows the channel surfaces without separation.

The method is particularly suited to determine pressure gradients in curved diffusors and inlet ducts of compressors and turbines in order to estimate the possibility of flow separation.

SYMBOLS

E	= total energy per unit mass
M	= mass flow per unit time
P	= $\int dp/\rho$
V	= magnitude of velocity
V_1	= magnitude of tangential velocity
V_2	= magnitude of meridional velocity
a_0	= velocity of sound at stagnation
h_1, h_2, h_3	= variable parameters of the system of coordinates
n	= distance along normals to the meridian lines
p	= static pressure
p_0	= stagnation pressure
r	= distance from axis of symmetry
R	= radius of curvature of meridian
u_1, u_2, u_3	= orthogonal coordinates
$\bar{V}$	= velocity vector
$\bar{fe}$	= vector of external force per unit mass
$\bar{i}, \bar{e}_2, \bar{e}_3$	= unit vectors in directions u_1, u_2, u_3, respectively
$\bar{j}$	= unit vector in direction of the axis of symmetry
$\bar{r}$	= radius vector
ψ	= potential of $\bar{fe}$
Ω_1	= scalar, component of $\nabla \times \bar{V}$ in direction u_1
Ω_2	= scalar, component of $\nabla \times \bar{V}$ in direction u_2
$\gamma = c_p/c_v$	= ratio of specific heats at constant pressure and constant volume
θ	= angle of surface u_1 = constant with fixed plane, containing the axis of symmetry
ρ	= mass density
ρ_0	= mass density at stagnation

Subscripts

1 = tangential direction
2 = meridional direction
3 = direction of normal

Received February 1, 1949. Revised and received July 15, 1949.

* Professor, Department of Aeronautics.

INTRODUCTION

A NONVISCOUS ELASTIC FLUID is made to undergo a steady motion in an axially symmetric channel which is formed by the rotation around an axis of the curves C_0 and C_i of Fig. 1. The channel is fixed in space and does not contain blades to guide the flow. The total energy of each fluid particle is the same and no heat exchange shall take place between the fluid and the channel contours. The meridian line m of Fig. 1, rotated around the axis, produces a surface of revolution to which the flow velocities shall be tangent. The curves, perpendicular to the meridians, are called normals.

DERIVATION OF FLOW RELATIONS

Equation of Motion

The Eulerian equation of motion for steady flow is from reference 1, page 62,

$$\bar{V} \cdot \nabla \bar{V} = \bar{fe} - (1/\rho)\nabla p \tag{1}$$

or

$$\bar{V} \cdot \nabla \bar{V} = -\nabla(P + \psi) \tag{2}$$

since the only forces acting upon the mass particles are those due to gravity. They have a potential; hence,

$$\bar{fe} = -\nabla\psi \tag{3}$$

With $P = \int dp/\rho$, there is

$$(1/\rho)\nabla p = \nabla P \tag{4}$$

If V denotes the magnitude of $\bar{V}$, Eq. (2) may be expressed by

$$\bar{V} \times \nabla \times \bar{V} = \nabla[(V^2/2) + P + \psi] = \nabla E \tag{5}$$

E represents the total energy per unit mass, consisting of the kinetic energy, the enthalpy, and the geopotential energy. Since the total energy is constant at all stations in the flow, there is $\nabla E = 0$, which implies that the flow must either be irrotational or that the curl $\bar{V}$ must be parallel to the velocity vector $\bar{V}$ at all stations in the flow.[2]

From Eq. (5), for $\nabla E = 0$, and Eq. (2)

$$\bar{V} \cdot \nabla \bar{V} = \nabla(V^2/2) \tag{6}$$

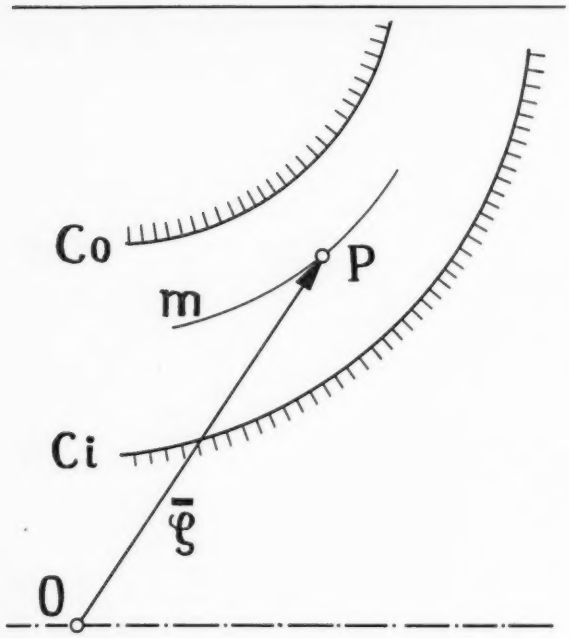

FIG. 1. Meridional contours of axially symmetric channel with arbitrary station P on meridian m.

Eq. (6) describes the motion of a fluid particle in a flow which has constant total energy. Moreover, the flow must be steady, and, similar to the assumptions made for the derivation of the Eulerian equation, the variables and their derivatives must be single-valued, finite and continuous functions in the flow field under consideration. Therefore, Eq. (6) cannot be applied to a region in which there exists a shock front. It is, however, applicable for elastic fluids independent of whether the flow is rotational or irrotational.

Orthogonal Coordinates

An arbitrary station in the flow region—say, the point P of Fig. 1—shall be located by the three mutually perpendicular, coordinate surfaces u_1 = constant, u_2 = constant, and u_3 = constant, as shown in Fig. 2. The coordinate surface u_3 = constant is the surface of revolution, obtained by rotating the meridian m around the axis of symmetry. The surface u_2 = constant is a surface of revolution with a generatrix perpendicular to the meridian lines. Fig. 3 shows that the coordinate surface u_1 = constant is a plane containing the axis with $u_1 = \theta$ = constant.

Let $\bar{\xi}$ be the radius vector of the point P from a fixed origin 0 on the axis. A neighboring point to P shall be located at the terminus of $\bar{\xi} + d\bar{\xi}$. Thus,

$$d\bar{\xi} = \frac{\partial \bar{\xi}}{\partial u_1} du_1 + \frac{\partial \bar{\xi}}{\partial u_2} du_2 + \frac{\partial \bar{\xi}}{\partial u_3} du_3 \tag{7}$$

or with the variable parameters h_1, h_2, h_3

$$d\bar{\xi} = \bar{\imath}_1 h_1 du_1 + \bar{\imath}_2 h_2 du_2 + \bar{\imath}_3 h_3 du_3 \tag{8}$$

$\bar{\imath}_1, \bar{\imath}_2, \bar{\imath}_3$ are the unit vectors tangent to the coordinates u_1, u_2, u_3. They form a right-handed system, as shown in Figs. 2 and 3. From these figures, there are, since $u_1 = \theta$,

$$h_1 = \overline{PP_1}/du_1 = rd\theta/d\theta = r \tag{9}$$

$$h_2 = \overline{PP_2}/du_2 = ds/du_2 \tag{10}$$

$$h_3 = \overline{PP_3}/du_3 = dn/du_3 \tag{11}$$

Equation of Motion in Orthogonal Coordinates

There are

$$\bar{V} = \bar{\imath}_1 V_1 + \bar{\imath}_2 V_2 \tag{12}$$

$$V^2 = V_1^2 + V_2^2 \tag{13}$$

All partial derivatives of scalar values, with respect to u_1, are equal to zero because of the axial symmetry of the flow. With the operator ∇ from reference 1, page 15,

$$\bar{V} \cdot \nabla \bar{V} = \frac{V_1^2}{h_1}\frac{\partial \bar{\imath}_1}{\partial u_1} + \frac{V_1 V_2}{h_1}\frac{\partial \bar{\imath}_2}{\partial u_1} + \frac{V_1 V_2}{h_2}\frac{\partial \bar{\imath}_1}{\partial u_2} + \frac{V_2^2}{h_2}\frac{\partial \bar{\imath}_2}{\partial u_2} + \bar{\imath}_1 \frac{V_2}{h_2}\frac{\partial V_1}{\partial u_2} + \bar{\imath}_2 \frac{1}{h_2}\frac{\partial (V_2^2/2)}{\partial u_2} \tag{14}$$

and

$$\nabla\left(\frac{V^2}{2}\right) = \frac{\bar{\imath}_2}{h_2}\frac{\partial (V_1^2/2)}{\partial u_2} + \frac{\bar{\imath}_2}{h_2}\frac{\partial (V_2^2/2)}{\partial u_2} + \frac{\bar{\imath}_3}{h_3}\frac{\partial (V_1^2/2)}{\partial u_3} + \frac{\bar{\imath}_3}{h_3}\frac{\partial (V_2^2/2)}{\partial u_3} \tag{15}$$

The changes of the unit vectors in direction of the coordinates can easily be determined. For instance, the increase of $\bar{\imath}_1$ from u_1 to $u_1 + du_1$ equals

$$d\bar{\imath}_1 = (\partial \bar{\imath}_1/\partial u_1) du_1 \tag{16}$$

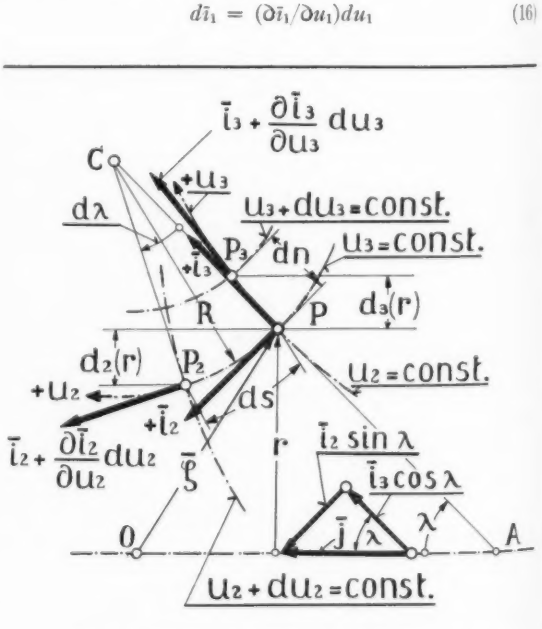

FIG. 2. Orthogonal coordinates in meridian plane.

From Fig. 3

$$d\bar{i}_1 = \bar{j}d\theta \times \bar{i}_1 \tag{17}$$

since the unit vector $\bar{i}_1$ is rotated around the axis of symmetry by an angle $d\theta$. The unit vector $\bar{j}$ is parallel to the axis of symmetry, with the direction shown in Fig. 2. There is $\bar{j} = \bar{i}_2 \sin\lambda + \bar{i}_3 \cos\lambda$, and

$$d\bar{i}_1 = d\theta(\sin\lambda\, \bar{i}_2 \times \bar{i}_1 + \cos\lambda\, \bar{i}_3 \times \bar{i}_1) \tag{18}$$

From Eqs. (16) and (18), since $du_1 = d\theta$,

$$\partial\bar{i}_1/\partial u_1 = -\bar{i}_3 \sin\lambda + \bar{i}_2 \cos\lambda \tag{19}$$

Similarly,

$$\partial\bar{i}_2/\partial u_2 = \bar{i}_3\,(d\lambda/du_2) \tag{20}$$

$$\partial\bar{i}_1/\partial u_2 = 0 \tag{21}$$

$$\partial\bar{i}_2/\partial u_1 = -\bar{i}_1 \cos\lambda \tag{22}$$

With the variable parameters of Eqs. (9) to (11) and writing $[\partial(\ )/\partial u_2]\, du_2 = d_2(\ )$, $[\partial(\ )/\partial u_3]\, du_3 = d_3(\ )$, Eq. (6) becomes

$$\bar{i}_1 V_2\left[-\frac{V_1}{r}\cos\lambda + \frac{d_2(V_1)}{ds}\right] + \bar{i}_2 V_1\left[\frac{V_1}{r}\cos\lambda - \frac{d_2(V_1)}{ds}\right] + \bar{i}_3\left[-\frac{V_1^2}{r}\sin\lambda + V_2^2\frac{d\lambda}{ds} - \frac{d_3(V_1^2/2)}{dn} - \frac{d_3(V_2^2/2)}{dn}\right] = 0 \tag{23}$$

The differential $d_2(\ )$ represents the increase of a scalar from u_2 to $u_2 + du_2$ or along ds in Fig. 2. Hence, $d_2(\ )/ds$ equals the rate of change of the scalar with respect to the meridian lines or $+u_2$. Similarly, $d_3(\ )/dn$ is the rate of change of a scalar with respect to the normals to the meridian lines or $+u_3$.

From Fig. 2,

$$d\lambda/ds = -1/R \tag{24}$$

The minus sign is introduced to make a distinction between convex and concave shapes of the meridian lines. A radius vector, with its origin at the center of curvature C and its terminus at the point of reference at the meridian, is introduced. The radius of curvature R at a particular point on a meridian line is defined as a positive value if the aforementioned radius vector points in direction of $+\bar{i}_3$ and vice versa. Hence, R in Fig. 2 is a negative radius of curvature.

Eq. (23), with Eq. (24), establishes the following relations:

$$(V_1/r)\cos\lambda = d_2(V_1)/ds \tag{25}$$

$$2\frac{V_1^2}{r}\sin\lambda + \frac{d_3(V_1^2)}{dn} + 2\frac{V_2^2}{R} + \frac{d_3(V_2^2)}{dn} = 0 \tag{26}$$

Eqs. (25) and (26) are the equations of motion in directions of the meridians and the normals, respectively, which can easily be integrated.

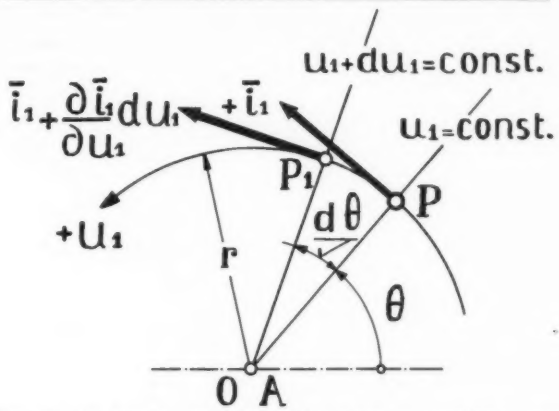

FIG. 3. Orthogonal coordinates in plane perpendicular to the axis of symmetry seen from the origin 0 toward A of Fig. 2.

Integration of the Equations of Motion

From Fig. 2,

$$ds\cos\lambda = -d_2(r) \tag{27}$$

Eq. (25), with Eq. (27),

$$rd_2(V_1) + V_1 d_2(r) = d_2(V_1 r) = 0 \tag{28}$$

Eq. (28) states that the angular momentum per unit mass remains constant along u_2 or on a surface of revolution produced by the rotation of a particular meridian m around the axis of symmetry. This relation is obvious, since no external moment is exerted upon the fluid particles. From Fig. 2,

$$\sin\lambda = d_3(r)/dn \tag{29}$$

Hence, Eq. (26) may be expressed as

$$\frac{d_3(V_2^2)}{dn} + \frac{2}{R}V_2^2 + 2\frac{V_1}{r}\frac{d_3(V_1 r)}{dn} = 0 \tag{30}$$

This linear differential equation of the first order for V_2^2, with variable coefficients and the variable n, has the general solution[4]

$$V_2^2 = e^{-\int(2/R)dn}\left[C - \int 2\frac{V_1}{r}\frac{d_3(V_1 r)}{dn}e^{+\int(2/R)dn}\,dn\right] \tag{31}$$

Therefore, it is possible to determine the distribution of the meridional velocity component V_2 along the normals if r, R, and V_1 are known. C is a constant of integration.

Eq. (31) can be modified by introducing the vorticity vector $\nabla \times \bar{V}$ of the flow. From reference 1, pages 14 and 16, there is for the variable parameters of Eqs. (9) to (11),

$$\nabla \times \bar{V} = \bar{i}_1\Omega_1 + \bar{i}_2\Omega_2 \tag{32}$$

with

$$\Omega_1 = \frac{V_1}{V_2}\frac{1}{r}\frac{d_3(V_1 r)}{dn} \tag{33}$$

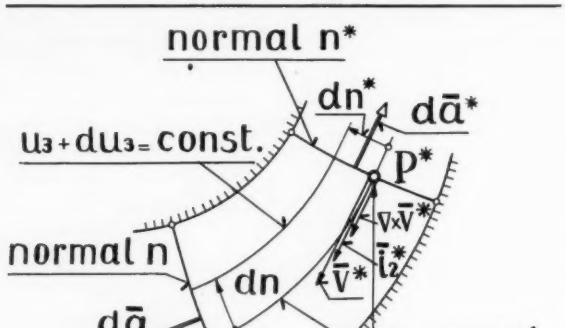

FIG. 4.

and

$$\Omega_2 = (1/r)[d_3(V_1 r)/dn] \tag{34}$$

The curl of $\bar{V}$ has no component in direction of the normals, and, since $\Omega_1/\Omega_2 = V_1/V_2$, it can be seen that the vector $\nabla \times \bar{V}$ is always parallel with the velocity vector $\bar{V}$.

Irrotational motion exists if either $V_1 = 0$ or $d_3(V_1 r)/dn = 0$. In the first case, the flow has no tangential velocity components. The other case represents a flow for which the product $V_1 r$ is constant along the normals, or, since $V_1 r$ is constant anyway along the meridians, a free-vortex flow with $V_1 r$ = constant at all stations in the flow. The meridional component Ω_2 of $\nabla \times \bar{V}$ may be substituted into Eq. (31).

Distribution of the Meridian Velocity V_2 Along the Normals

For particular channel contours, there shall be known the meridian lines (or surfaces u_3 = constant) and the normals to the meridians (or surfaces u_2 = constant). As shown in Fig. 4, the vorticity shall be given at one particular normal n^*. The vector $\nabla \times \bar{V}$ at station P on an arbitrary normal n can be determined from $\nabla \times \bar{V}^*$ at the point P^* on the normal n^*, and on the same surface u_3 = constant as the point P. Applying Gauss' divergence theorem (reference 1, page 20) for $\nabla \times \bar{V}$ to a region bounded by the surfaces u_3 = constant, $u_3 + du_3$ = constant, and the surfaces u_2 = constant at the normals n and n^*, gives

$$\int\int_{(S)} \nabla \times \bar{V} \cdot d\bar{a} = \int\int\int_{(R)} \nabla \cdot \nabla \times \bar{V} dv = 0 \tag{35}$$

since $\nabla \cdot \nabla \times \bar{V} = 0$. The vector $d\bar{a}$ in the surface integral is a normal surface vector of an element of area and is considered positive if it points away from the bounded region. With Eq. (32) and

$$\nabla \times \bar{V}^* = \bar{\imath}_1^* \Omega_1^* + \bar{\imath}_2^* \Omega_2^* \tag{36}$$

Eq. (35) gives, with the notations of Fig. 4,

$$d\bar{a} \cdot \nabla \times \bar{V} + d\bar{a}^* \cdot \nabla \times \bar{V}^* = 0$$

or, in scalar form,

$$\Omega_2 = (r^*/r)\,(dn^*/dn)\,\Omega_2^* \tag{37}$$

Hence, it is sufficient to know the vorticity along a particular normal n^* and the shape of the meridian lines to obtain the vorticity at arbitrary stations in the flow field.

From Eq. (28),

$$V_1 = V_1^*(r^*/r) \tag{38}$$

V_1^* is the tangential velocity component on the normal n^* at the point on the same surface u_3 = constant as the station where the velocity V_1 exists.

The velocity V_2 shall be determined at the station P of Fig. 5. Meridian lines and normals are known. Moreover, V_1^* and, consequently, Ω_2^* are given along the particular normal n^*. Let Q be a moving point on the normal n between the surfaces u_{3i} = constant and u_3 = constant. To P and Q correspond the points P^* and Q^* on the normal n^*. The integrations of Eq. (31) shall be carried out in direction $+\bar{\imath}_3$. Thus, the constant of integration of Eq. (31) is

$$C = (V_{2i})^2$$

namely, the square of the meridian velocity on the normal at the surface u_{3i} = constant. Using the symbols of Fig. 5, Eq. (31) becomes, with Eqs. (34) and (38),

$$V_2^2 = A^2(V_{2i}^2 - B^2) \tag{39}$$

wherein

$$A^2 = e^{-2\int_{n=0}^{n} dn/R} \tag{40}$$

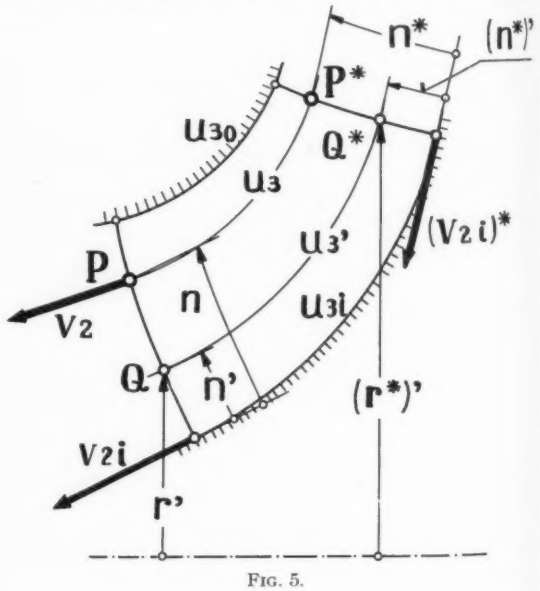

FIG. 5.

$$B^2 = 2\int_{n^*=0}^{n^*}\left[V_1^{*\prime}\Omega_2^{*\prime}\frac{(r^{*\prime})^2}{(r')^2}e^{2\int_{n=0}^{n'}dn/R}\right]dn^* \quad (41)$$

$V_1^{*\prime}$, $\Omega_2^{*\prime}$, $r^{*\prime}$, n^* are values corresponding to the point Q^* on the normal n^*, whereas r' and n' correspond to station Q on the normal n. The first integral in Eq. (41) can always be evaluated along the normal n^* from u_{3i} = constant to u_3 = constant, independent of the normal where the point P is located. However, the integrals constituting the powers of the basis e must be solved for the particular normal n on which P is situated.

Eq. (39) holds for flow fields that satisfy the same conditions as those necessary for the use of Eq. (6). It is interesting to note that neither the density of the fluid nor the potential of the gravity forces appears in Eq. (39). For a given pattern of the meridian lines and the distribution of the tangential velocity components along one particular normal, Eq. (39) makes possible the evaluation of the meridional velocity at all stations in the flow, provided that the velocities V_{2i} along the inner contour are known.

For irrotational flows—i.e., for free-vortex flows or for $V_1 = 0$—there is $\Omega_2 = 0$, and, from Eq. (39),

$$V_2/V_{2i} = e^{-\int_{n=0}^{n} dn/R} \quad (42)$$

This relation has been derived by G. Fluegel in 1914.[3] Another particular solution is obtained from Eq. (43) if, besides $\Omega_2 = 0$, the centers of curvature of all meridian lines passing across a normal coincide. In this case, the normal is a straight line, and

$$dn = dR$$

or [see reference 6, Eq. (329), page 291]

$$V_2R = V_{2i}R_i = \text{constant} \quad (43)$$

R_i is the radius of curvature of the inner contour of the channel. For the aforementioned conditions, not only the angular momentum of V_1 with respect to the axis of symmetry is constant but also the angular momentum of V_2 with respect to the center of curvature.

The velocities V_{2i} can be determined with the equation of continuity. The mass flow across a normal is

$$M = 2\pi\int_0^n \rho r V_2 dn \quad (44)$$

and with Eq. (39)

$$V_{2i} = \frac{M/2\pi}{\int_0^n \rho r A\sqrt{1-(B/V_{2i})^2}dn} \quad (45)$$

For an incompressible fluid there is $\rho = \rho_0 = \text{constant}$. For an isentropic process of a perfect gas, neglecting geopotential energy differences,[5]

$$\frac{\rho}{\rho_0} = \left[1 - \frac{\gamma-1}{2}\left(\frac{V_1^2}{a_0^2} + \frac{V_2^2}{a_0^2}\right)\right]^{1/(\gamma-1)} \quad (46)$$

Eqs. (45) and (46) show that the velocity V_{2i} can only be determined directly if $B = 0$ and $\rho = \rho_0$—i.e., for an irrotational flow of an incompressible fluid. For a general case, a value of V_{2i} must be chosen to determine V_2 and ρ from Eqs. (39) and (46), respectively. Thereafter, the chosen V_{2i} has to be checked by means of Eq. (45).

Calculating Procedure

An iteration method must be used to determine the flow field in a given channel, since the meridian lines of the flow must be known before the above relations can be used. First, an approximate picture of the meridian lines must be established, and it is useful to apply methods that are indicated on pages 136 and 291 of reference 6. However, in most cases it is possible to anticipate the ratios V_2/V_{2i} along the normals from the curvatures of the boundaries and the component Ω_2 of the curl vector by properly interpreting Eq. (39). The meridian lines of this first approximation are preferably drawn in such a manner that equal mass flow exists between two neighboring surfaces u_3 = constant. Further, the radii of curvature of these meridians have to be determined along different normals. If graphical methods are used, this procedure has to be carried out with great accuracy to obtain consistent results.

From the flow conditions at the normal n^*, it is then possible to determine the values of A and B, with Eqs. (40) and (41), for the first approximation of the flow lines. Subsequently, the values V_{2i} of the meridian velocities at the inner contour must be chosen for the different normals.

Eq. (45) is used to determine whether the value of V_{2i}, necessary for the given mass flow through the channel, equals the initially chosen value of V_{2i}. The assumed magnitude of V_{2i} must be changed until this agreement is obtained. With these data it becomes possible to determine the points of intersection of the meridian lines with the assumed normal for equal mass flow between surfaces u_3 = constant.

This procedure, carried out for different normals, gives a new set of flow lines which will probably differ from the first approximation. The new flow lines will then be used as the second approximation with which the afore-described procedure has to be repeated. In this manner successive approximations have to be carried out until the assumed flow net coincides with the calculated one.

Numerical Example of an Irrotational Flow†

Fig. 6 shows an inlet channel ahead of a centrifugal compressor wheel with a weight flow of 35 lbs. of air per sec. Stagnation pressure and temperature of the

† The calculations of this example and the mathematical analysis of the channel contours were carried out by Lt. Gerald M. Monroe, U.S.N., now Graduate Student, California Institute of Technology.

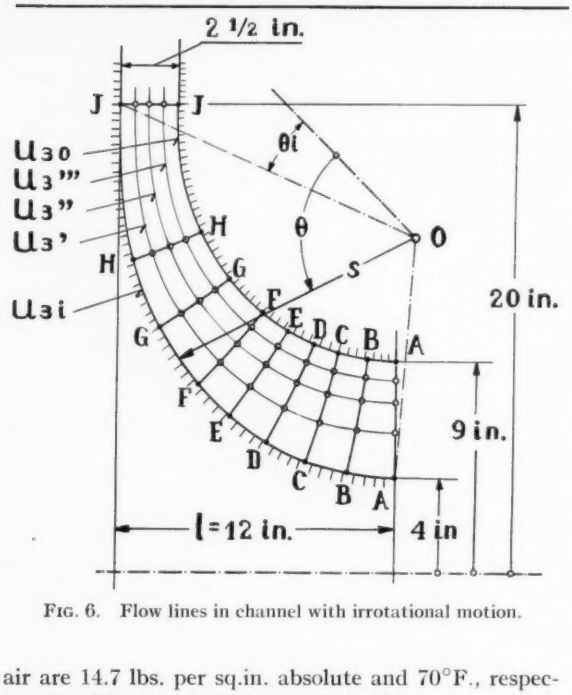

FIG. 6. Flow lines in channel with irrotational motion.

air are 14.7 lbs. per sq.in. absolute and 70°F., respectively. The impeller inlet is situated at station A-A. Ahead of station J-J the channel consists of two walls, perpendicular to the axis, between which there is arranged a number of guide vanes, equally spaced along a coaxial circle, to produce constant tangential velocity components along station J-J. The curvatures of the channel contours are zero at station J-J and gradually increase to a maximum at station A-A. Such contours may be expressed by equations of the form (see Fig. 6)

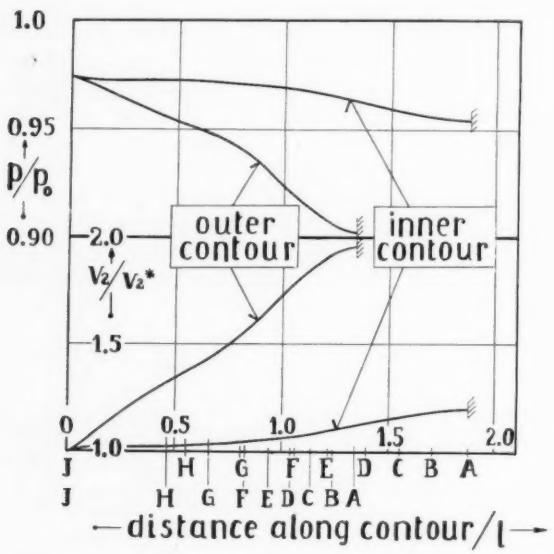

FIG. 7. Velocities and pressures along the contours of the channel of Fig. 6 for irrotational motion.

$$s = b\theta^{-k}$$

From the two points at stations A and J, it is possible to determine the fixed origins 0 and the angles θ_i, where the curves have zero curvature. For the inner contour or the surface u_{3i} = constant, there is

$$s = (11.84)\ \theta^{-(0.1675)} \text{ with } \theta_i = 21.4°$$

For the outer contour

$$s = (9.27)\ \theta^{-(0.0402)} \text{ with } \theta_i = 11.4°$$

From these equations, the radii of curvature of the contours can be calculated.

$V_1 r$ is constant at all stations and equals 46.6 sq.ft. per sec. Preliminary calculations showed that ρ/ρ_0 from Eq. (46) varies less than 3 per cent between J-J and A-A. Therefore, constant density was assumed along particular normals, and the respective ratios ρ/ρ_0 were determined from the mean values at each normal.

For the first approximation of the meridian lines, it was assumed that the curvatures of the meridians at station A-A change linearly from $1/R$ = (0.0932) in.$^{-1}$ at r = 4 in. to $1/R$ = (0.1097) at r = 9 in. At station J-J the meridian lines are parallel and equally spaced for equal mass flow between them, since $R = \infty$. With Eqs. (42) and (44) it is possible to determine the points of intersection of the meridians with the normal at A-A for equal mass flow between them. The first approximation of the flow net shall consist of meridian lines that satisfy the relation $s = b\theta^{-k}$ between the two known points at A-A and J-J, respectively, with zero curvature at J-J. By drawing the normals with the calculated slopes and using Eq. (42) with the determined radii of curvature the ratios V_2/V_{2i} along the different normals are given. Consequently, the points of intersection of the second approximation of the meridian lines with the initial normals can be established, again for equal mass flow between surfaces u_3 = constant. These points are marked by the small circles in Fig. 6. It can be seen that they practically coincide with the corresponding points of the first approximation. Thus, no repetition of the calculating procedure seems warranted.

In Fig. 7 are plotted the pressure ratios p/p_0 along the inner and outer contours of the channel. p_0 is the stagnation pressure of the fluid. The pressure gradient at the outer contour reaches values that are about four times the maximum pressure gradient at the inner contour of the channel. Fig. 7 also shows the velocity ratios V_2/V_2^* along the contours. The constant meridian velocity V_2^* at station J-J equals 218 ft. per sec. At A-A, the ratios V_2/V_2^* are (1.95) and (1.19) at the outer and inner contour, respectively, so that V_2 at station A-A changes from 260.5 ft. per sec. at the radius r = 4 in. to 426 ft. per sec. at r = 9 in. Fig. 8 illustrates the velocity distributions at stations A-A, E-E, and J-J of Fig. 6, together with the flow angles

α, measured between the actual velocities and the circumferential direction.

In Fig. 9 are shown the angles α at station A-A, together with the flow angles β, relative to an impeller rotating at 6,000 r.p.m. The angles α and β are usually determined for constant meridional velocity at the impeller inlet.[7] In Fig. 9, $\alpha_{av.}$ and $\beta_{av.}$ are angles calculated with a constant velocity V_2 of 345 ft. per sec. It can be seen that the actual relative flow angles differ from $\beta_{av.}$ by about 8° at the inner radius and by about 6° at the outer radius. Fig. 6 of reference 7 illustrates the considerable influence of the angles β upon the efficiency of centrifugal compressor wheels, and it seems necessary that proper attention is paid to the actual velocity distributions at the impeller inlet. The "angles of attack," proposed in reference 7, are of the order of magnitude of the difference between $\beta_{av.}$ and β of Fig. 9, although the present inlet channel has extremely small curvatures. Usual designs, having small axial extensions and bigger curvatures, will produce considerably larger differences between the actual angles β and the ones calculated with constant meridional velocity.

Inlet ducts, similar to the one of Fig. 6, produce meridian velocities at station A-A which increase with increasing radius. Especially with channels having small axial extensions, the actual Mach Number of the relative flow at the outer diameter of the impeller inlet will be considerably higher than the one calculated with an assumed constant meridian velocity. This fact might explain the phenomenon that "choking" effects are sometimes experienced with compressor wheels having apparent local Mach Numbers that are well below unity.

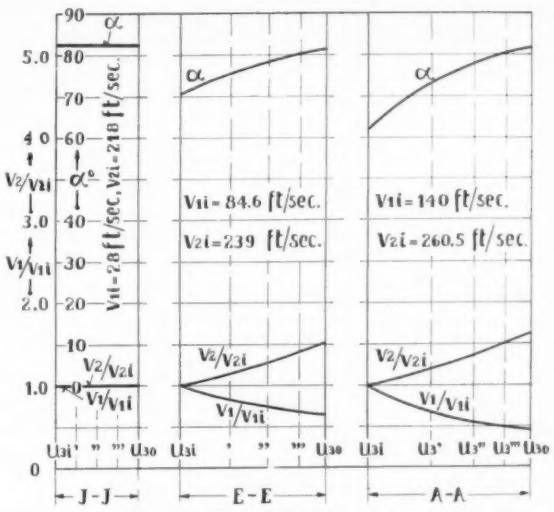

FIG. 8. Velocity distribution and flow angles, at the normals J-J, E-E, and A-A of the channel of Fig. 6, for irrotational motion.

NUMERICAL EXAMPLE OF A ROTATIONAL FLOW

The channel of Fig. 6 shall be used to produce a flow at station A-A which has tangential components V_1 that are proportional to the radius r. With c as an arbitrary constant, there is $V_1 = cr$, and from Eq. (34) with $dn = dr$

$$\Omega_2 = 2c$$

The meridional component of the vorticity vector at station A-A is therefore constant and equal to the curl of a flow which rotates around the axis in the same manner as a solid body. Station A-A will be used as the normal n^* along which the integrations of Eq. (41) are carried out.

The meridian lines of the first approximation are supposed to have horizontal tangents at station A-A and vertical tangents at J-J of Fig. 6. The meridian lines at J-J will have certain curvatures that, however, are small since the contours are straight lines, and the integrals of Eq. (40) will very nearly equal unity. Moreover, the assumption is made that the curvatures along A-A change in the same manner as those of the calculated meridian lines of the foregoing example.

With a weight flow of 14 lbs. of air per sec. of the channel and the same air conditions as in the previous example, the density changes may be ignored. A and B along station A-A can be determined with Eqs. (40) and (41). With a trial-and-error procedure it will then be possible to evaluate the velocity V_{2i} from

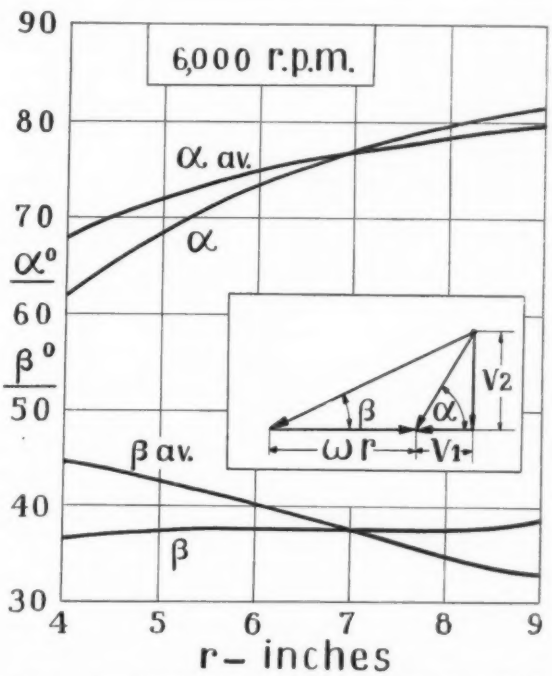

FIG. 9. Actual flow angles α and β for calculated velocity distribution at station A-A of Fig. 6, for irrotational motion and an impeller at 6,000 r.p.m., and angles $\alpha_{av.}$ and $\beta_{av.}$ for constant meridian velocity.

Eq. (45) and, hence, also V_2 with Eq. (39). For a chosen value of $V_1 = (127.32)r$ (V_1 in ft. per sec., r in ft.) at station A-A, there was $V_{2i} = 125$ ft. per sec. Thus, the points of intersection of different meridians with station A-A can be established. Eq. (41) can now be solved for station J-J, with r^* and dn^* from station A-A. Trial-and-error methods, with chosen values of V_{2i}, introduced in Eq. (45), give the points of intersection at this station along which the radius r is constant and R equals infinity by assumption.

The first approximation of the flow net shall be again a set of meridian lines between the two known points at stations A-A and J-J satisfying the relation $s = b\theta^{-k}$. With the radii r and R of these flow lines, it is possible to establish a second approximation in the manner outlined before. Also in this example, a good coincidence between these two flow nets was reached, making further approximations unnecessary.

Fig. 10 shows the velocity profiles and the flow angles α at stations A-A and J-J of Fig. 6, as well as along a normal almost at the same position as E-E in Fig. 6. The meridional velocities V_2 are practically constant along the three stations, in spite of the varying radii of curvature. Contrary to the first example, the angles α are decreasing from the inner to the outer contour of the channel.

A peculiar condition can be seen from Eq. (39), since V_2 equals zero if $V_{2i} = B$ and, if B is larger than V_{2i}, the values of V_2 are imaginary. This indicates that no equilibrium of the forces acting upon a flow particle is possible. Since Ω_2 and, consequently, the value of B from Eq. (41) depends on the distribution of the tangential velocity component along the normals, it is not possible to choose the magnitude of V_1 arbitrarily for a given massflow through the channel. To each mass flow and a given vorticity at a particular station, there corresponds a maximum value of V_1, for which the meridional velocity component becomes zero at one or more stations in the flow. Conversely, for a given V_1 distribution, there exists a minimum mass flow that produces the same effect. In the present case, the maximum values of B exist at the outer contour. There are:

at A-A: $B = 94.2$ ft. per sec. $V_{2i} = 125$ ft. per sec.

at E-E: $B = 76.6$ ft. per sec. $V_{2i} = 108.7$ ft. per sec.

at J-J: $B = 42.7$ ft. per sec. $V_{2i} = 90.4$ ft. per sec.

Hence, with the same tangential velocity components, it is only possible to reduce the flow rate from its assumed value of 14 lbs. per sec. to about (14) (94.2)/125 = 10.5 lbs. per sec., for a reduction to zero of the meridian velocity at the outer contour at station A-A. At E-E and J-J, the smallest possible flow rates would be 9.95 and 6.65 lbs. per sec., respectively. Therefore, conditions at A-A limit the minimum flow rate. For still smaller mass flows the flow will be unstable, since

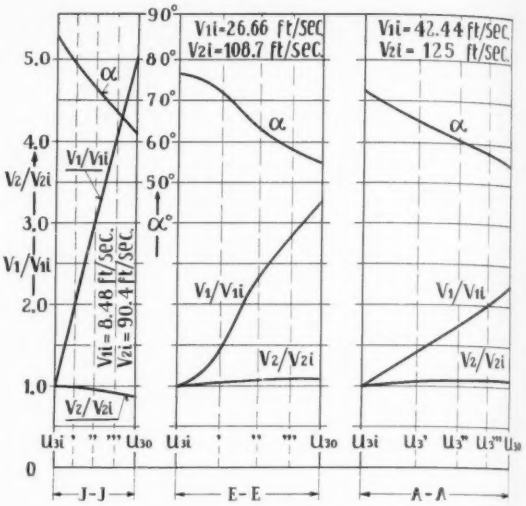

FIG. 10. Velocity distribution and flow angles at the normals J-J, E-E, and A-A of the channel of Fig. 6, for rotational motion with constant vorticity at station A-A.

the velocities will not be able to produce the forces necessary for the equilibrium of the mass particles. The flow would separate from the outer contour of the channel, thereby increasing the meridional velocity components until equilibrium becomes again possible.

For free-vortex flows, no such limiting conditions exist, since B always equals zero, and the tangential components can be increased arbitrarily. In actual irrotational flows, however, where the relation $V_1 r$ = constant does not hold within the boundary layers, there seems to exist the possibility of a minimum flow rate, below which the flow might become unstable. Such a phenomenon could be the reason for flow separations that are different from those due to pressure gradients at the boundaries.

General Remarks

Considerable calculating work and numerous graphical integrations are required to carry out the proposed method. Especially for channels having large changes of the curvatures of the contours, hence, where it is not possible to select a reasonably close first approximation, a number of successive trials will be necessary. However, it was found that the results converge rapidly for flows at low Mach Numbers. Supersonic flow in axially symmetric channels could be treated with the method set forth, provided no shock fronts exist, which will roughly be the case if the meridian velocities are subsonic for supersonic total velocities. However, it is possible that the method converges but slowly, or not at all, if the first approximation of the meridian lines differs too much from the actual flow net.

Despite these limitations, the method will give interesting results for many applications, such as diffusors

(*Continued on page 172*)

On a Family of Oblique Shock Curves

EDWARD R. C. MILES*

Institute for Cooperative Research, The Johns Hopkins University

SUMMARY

The curves $M \sin \sigma$ = constant, where M is the free-stream Mach Number and σ is the shock angle, are level curves for the principal pressure, density, and temperature ratios across an oblique shock. If these curves are adjoined to the family of shock polars, dynamic relations, as well as the kinematic relations associated with the shock polar, are exhibited graphically. It has been customary to obtain these curves by interpolation. In this note, a simple analytic representation is derived.

INTRODUCTION

IT IS KNOWN that the principal ratios of state variables behind and in front of an oblique shock are functions of $M \sin \sigma$, where M is the free-stream Mach Number and σ is the shock angle.[1, 2] Thus, with $\gamma = 1.400$,

$$\bar{p}/p = (7M^2 \sin^2 \sigma - 1)/6$$

$$\bar{\rho}/\rho = 6M^2 \sin^2 \sigma/(5 + M^2 \sin^2 \sigma)$$

$$\frac{\bar{T}}{T} = \frac{(7M^2 \sin^2 \sigma - 1)(M^2 \sin^2 \sigma + 5)}{36M^2 \sin^2 \sigma}$$

$$\frac{\bar{p}_0}{p_0} = \left(\frac{6M^2 \sin^2 \sigma}{M^2 \sin^2 \sigma + 5}\right)^{7/2} \left(\frac{6}{7M^2 \sin^2 \sigma - 1}\right)^{5/2}$$

In these equations, p, ρ, T, and p_0 denote, respectively, free-stream static pressure, density, temperature, and stagnation pressure. A dash over a letter indicates that the quantity is evaluated immediately behind the shock wave.

The curves $M \sin \sigma$ = constant are important as being level curves for the ratios given above. If this family of curves is drawn on the same axes with the family of shock polars, the resulting diagram is of considerable value for the graphical calculation of dynamic, as well as kinematic quantities related to oblique shocks. The pressure, density, and temperature ratios as functions of $M \sin \sigma$ for $\gamma = 1.400$ are shown in Table 1. The level values of $M \sin \sigma$ are to be preferred, for example, to those of the throttle factor $\bar{p}_0/p_0$. The simple physical interpretation of $M \sin \sigma$ is a further advantage.

It seems not to have been observed that the curves $M \sin \sigma$ = constant are susceptible of a simple parametric representation by means of rational functions. The curves of the family may therefore be plotted rapidly with an arbitrarily high degree of accuracy. For simplicity, the derivation is given for $\gamma = 1.400$; the general case requires only formal changes.

Received April 26, 1949.

* Research Mathematician.

CURVES OF CONSTANT M SIN σ

Consider the equation

$$M \sin \sigma = C \tag{1}$$

where

$$\tan \sigma = (M^* - x)/y \tag{2}$$

where x and y are the rectangular coordinates of the velocity behind the shock wave and M, taken in the x direction, is the quotient of the free-stream velocity by the critical velocity. Then,[3]

$$y^2 = \frac{(M^* - x)^2(M^*x - 1)}{1 + (5/6)M^{*2} - M^*x} \tag{3}$$

This set of equations is completed by the identity

$$M^2 = 5M^{*2}/(6 - M^{*2}) \tag{4}$$

TABLE 1

Pressure, Density, and Temperature Ratios as Functions of $M \sin \sigma$

$\gamma = 1.400$

$M \sin \sigma$	$\bar{p}/p$	$\bar{\rho}/\rho$	$\bar{p}_0/p_0$	$\bar{T}/T$
1.0	1.0000	1.0000	1.000	1.0000
1.1	1.2450	1.1691	0.999	1.0649
1.2	1.5133	1.3416	0.993	1.1280
1.3	1.8050	1.5157	0.979	1.1909
1.4	2.1200	1.6896	0.958	1.2547
1.5	2.4583	1.8621	0.930	1.3202
1.6	2.8200	2.0317	0.895	1.3880
1.7	3.2050	2.1976	0.856	1.4583
1.8	3.6133	2.3592	0.813	1.5316
1.9	4.0450	2.5157	0.767	1.6079
2.0	4.5000	2.6667	0.721	1.6875
2.1	4.9783	2.8119	0.674	1.7705
2.2	5.4800	2.9512	0.628	1.8569
2.3	6.0050	3.0846	0.583	1.9468
2.4	6.5533	3.2119	0.540	2.0403
2.5	7.1250	3.3333	0.499	2.1375
2.6	7.7200	3.4490	0.460	2.2383
2.7	8.3383	3.5590	0.424	2.3429
2.8	8.9800	3.6636	0.390	2.4512
2.9	9.6450	3.7629	0.358	2.5632
3.0	10.3333	3.8571	0.328	2.6790
3.1	11.0450	3.9466	0.301	2.7986
3.2	11.7800	4.0315	0.276	2.9221
3.3	12.5383	4.1120	0.253	3.0494
3.4	13.3200	4.1884	0.2322	3.1803
3.5	14.1250	4.2609	0.2130	3.3150
3.6	14.9533	4.3296	0.1954	3.4538
3.7	15.8050	4.3949	0.1792	3.5963
3.8	16.6800	4.4568	0.1645	3.7427
3.9	17.5783	4.5156	0.1510	3.8927
4.0	18.5000	4.5714	0.1388	4.0469
4.1	19.4450	4.6245	0.1275	4.2048
4.2	20.4133	4.6749	0.1173	4.3666
4.3	21.4050	4.7229	0.1080	4.5322
4.4	22.4200	4.7685	0.0995	4.7017
4.5	23.4583	4.8119	0.0917	4.8750
4.6	24.5200	4.8532	0.0846	5.0524
4.7	25.6050	4.8926	0.0781	5.2334
4.8	26.7133	4.9301	0.0721	5.4184
4.9	27.8450	4.9659	0.0697	5.6073
5.0	29.0000	5.0000	0.0617	5.8000

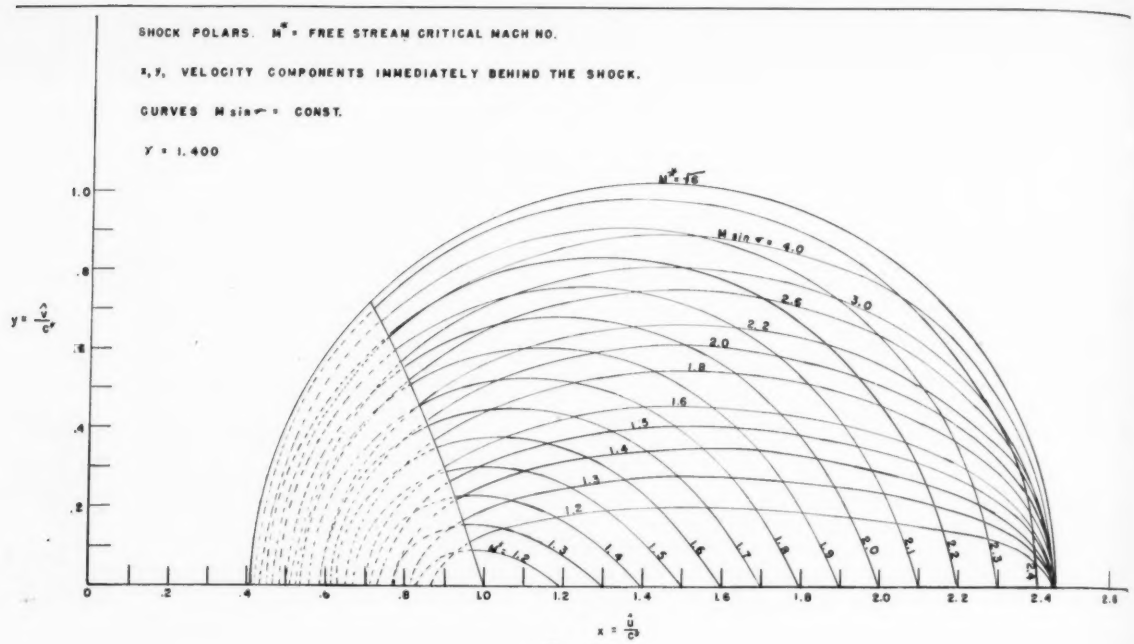

FIG. 1.

If M and σ are eliminated from these equations, there remain the pair of equations

$$(C^2 + 5)M^{*2} - 6M^*x - 6(C^2 - 1) = 0 \qquad (5)$$

$$C^2y^2(6 - M^{*2}) = (M^* - x)^2 \times [(C^2 + 5)M^{*2} - 6\,C^2] \qquad (6)$$

These might be taken as parametric equations of the required curves, but one can do better. In Eq. (5), place $M^*x = t$, from which

$$M^{*2} = 6(t + C^2 - 1)/(C^2 + 5)$$

and, since $x^2 = t^2/M^{*2}$,

$$x^2 = (C^2 + 5)t^2/6(t + C^2 - 1) \qquad (7)$$

These substitutions are made in Eq. (6), which thereupon reduces to

$$y^2 = \frac{(C^2 - 1)^2\,(6 - t)(t - 1)}{6C^2(t + C^2 - 1)} \qquad (8)$$

Eqs. (7) and (8) constitute the parametric representation of the required curves. While the parameter t may be eliminated, the resulting rectangular form is a rather unwieldy fourth degree equation.

Some obvious properties of the curves may be noted. In the construction of a curve, only the positive values of x, of course, are of significance. All the curves are symmetric with respect to the x-axis. All have the x intercept $\sqrt{6}$, which corresponds to $t = 6$. The other x intercept, corresponding to $t = 1$, is $\sqrt{C^2 + 5}/C\sqrt{6}$. The latter intercept is a maximum—namely, 1—when $C = 1$, and it decreases toward $1/\sqrt{6}$ as $C \to \infty$.

The family of curves fills up a circle. In fact, if $C \to \infty$, the parametric equations become

$$x = t/\sqrt{6}, \quad y^2 = (6 - t)(t - 1)/6$$

The rectangular equation is

$$x^2 + y^2 - (7x/\sqrt{6}) + 1 = 0$$

which will be recognized as the boundary circle of the family of shock polars. This is the only curve of the family $M \sin \sigma = C$ which has an axis of symmetry parallel to the y-axis.

The shock polars, and the curves $M \sin \sigma =$ constant are shown in Fig. 1. In engineering applications, it has been found desirable, for graphical estimates, to have both the family of shock polars and the family of curves $M \sin \sigma =$ constant referred to a system of polar coordinates. The velocity magnitude immediately behind the shock, as well as the deflection angle, may thereby be read directly.

REFERENCES

[1] Schubert, F., *Contribution to the Theory of the Steady Compression Shock*, Z. angew. Math. Mech. 23, pp. 129–138, British R.T.P., 1943.

[2] Crocco, L., *Singolarita della corrente gassosa iperacustica nell'intorno di una prora a diedro*, L'Aerotecnica XVII, pp. 519-536, 1937.

[3] Sauer, R., *Gasdynamik;* J. W. Edwards, p. 70, 1945.

Inelastic Column Buckling*

TUNG-HUA LIN†

Bureau of Aircraft Industry, China

SUMMARY

In this paper the buckling of a pin-ended column with small initial curvature in the plastic range is investigated. The initial curvature is unavoidable in actual columns because of eccentricity and nonhomogeneity of materials. A method of calculating the deflection of a column with known small initial deflection up to the maximum load is shown, and an illustrative example is given. From the load-deflection curve, the maximum load is obtained. The effect of reversal of strain on the middle part of the column on the convex side, when the load and deflection are big as described by Shanley,[1, 2] and the effect of variation of tangent modulus of elasticity across the section are analyzed. The load at which this reversal of strain starts and the method of calculating the extent of the reversal of strain on the cross section are shown. The theoretical analysis given in this paper shows the different factors affecting maximum load and the mechanism of column failure. The method of computing the deflection curve at each load is shown so that the shortening of the column can be found. This may be required for analyzing an indeterminate structure with inelastic columns as members.

The mechanism of the start of deflection of a perfect column without initial curvature is explained, and the proposed method for calculating the load-deflection curve can also be applied to a perfect column and its maximum load can be determined.

INTRODUCTION

THE FAILING LOAD of columns has been discussed by many authors. Within the elastic range, Euler's equation applies very well. For a column with initial curvature, the increase of deflection with load is shown in Southwell's[3, 4] well-known method for predicting critical load from the load-deflection test of the particular column with small initial curvature. This shows clearly how the column behaves under various loads in the elastic range.

For the critical load of a perfect column in the inelastic range, two well-known formulas have been proposed. One is the tangent modulus equation $P_{cr.} = \pi^2 E_t I/L^2$ known as the Engesser theory. The other is the double or reduced modulus formula $P_{cr.} = \pi^2 E_r I/L^2$ known as the Considère-Engesser theory or Kármán theory.[5] E_t is the tangent modulus at that load and E_r is the reduced modulus shown in reference 5. The reduced modulus theory is based on the assumption that after the column reaches the critical uniform stress, it bends and the strain on one side increases giving change of stress according to the tangent modulus while the strain on the other side decreases giving change of stress according to the elastic modulus. The reduced modulus formula had been generally considered to be the true theoretical solution for perfect columns until Shanley raised the point that the column may bend simultaneously with increasing axial loading as shown in his papers, "The Column Paradox"[8] and "Inelastic Column Theory."[1] He reached the conclusion that the maximum load of a perfect column will be somewhere between the tangent modulus load and reduced modulus load. There is some range from the tangent modulus load to the reduced modulus load, so it is desirable to have a method of calculating the maximum load more definitely.

In this paper a complete analysis of an inelastic column with known small initial curvature is given and an illustrative example is worked out. A method is proposed for calculating the deflection curve of an inelastic column up to the failing load so as to obtain the maximum load and to show how the column behaves under different loads. This method can also be applied to a perfect column with no initial curvature, so the load-deflection curve of a perfect column and its maximum load can be obtained.

THEORETICAL ANALYSIS

The basic assumptions used for the following analysis are as follows: (1) Plane before loading remains plane after loading. (2) The fibers of the column act as if they were separate fibers and follow the same stress-strain curve as in simple compression and tension tests.

The symbols used are listed below. The modified section referred to in the following is the section derived from the geometrical section of the column by multiplying the width of the geometrical section b by E_t/E, the ratio of the tangent modulus at this point to the elastic modulus. This ratio varies across the section. The width of the modified section b' equals bE_t/E. The neutral axis of the modified section passes through its centroid. E_t changes back to E in the region where the compressive strain decreases. This will be discussed in more detail under the section on "Reversal of Strain."

LIST OF SYMBOLS

P = applied load
I = moment of inertia of column cross section
I' = moment of inertia of the modified section about its neutral axis
A = cross-sectional area of the column
A' = area of the modified section
ρ = radius of gyration of column cross section

Received May 9, 1949.

* The author is greatly indebted to Sir Richard Southwell and Prof. J. F. Baker, of Cambridge University, for their most kind criticisms and suggestions.

† Technical Mission in England, S.M., A.F.R.Ae.S., M.I.A.S.

ρ' = radius of gyration of the modified cross section
h = depth of column section
h_1 = distance from the neutral axis of modified section to outside fiber on the concave side
h_2 = distance from the neutral axis of modified section to outside fiber on the convex side
b = width of column section
b' = width of the modified section
L = column length
E = Young's modulus (slope of stress-strain curve in elastic range)
E_t = tangent modulus (local slope of stress-strain curve)
y = deflection of the column geometrical axis from the line of thrust
y_0 = initial deflection of the column geometrical axis from the line of thrust
x = distance along the line of thrust measured from one end of the column
δ = deflection of the column at center
$\bar{\delta}$ = initial deflection of the column at center
$\delta' = \delta - \bar{\delta}$
$P_{cr.1} = \pi^2 E I_1'/L^2$
$P_{cr.}$ = critical load of the column. It is the load at which the column starts to increase deflection without increasing load, i.e., $dy/dP = \infty$. Within elastic limit $P_{cr.1} = P_{cr.}$
M = moment
η = distance from the neutral axis of the modified section
σ = stress
σ' = average stress P/A
$\sigma_{cr.1}' = P_{cr.1}/A$
e = strain
η_1 = distance from the neutral axis of the modified section to where $de/dP = 0$

Since no actual column is absolutely straight and homogeneous, an initial deflection is used to represent the initial curvature. For a perfect column, it can be equated to zero in the following equations.

In the elastic range for small deflection, from the condition of equilibrium,

$$EI\left(\frac{d^2y}{dx^2} - \frac{d^2y_0}{dx^2}\right) + Py = 0 \tag{1}$$

Let

$$y = \sum \delta_n \sin \frac{n\pi x}{L} \tag{2}$$

$$y_0 = \sum \bar{\delta}_n \sin \frac{n\pi x}{L} \tag{3}$$

Substitute Eqs. (2) and (3) in Eq. (1),

$$-\sum \frac{n^2\pi^2}{L^2}\delta_n \sin\frac{n\pi x}{L} + \sum \frac{n^2\pi^2}{L^2}\bar{\delta}_n \sin\frac{n\pi x}{L} + \frac{P}{EI}\sum \delta_n \sin\frac{n\pi x}{L} = 0$$

Multiply by $\sin \frac{n\pi x}{L}\,dx$ and integrate from $x = 0$ to $x = L$; all the terms, except $m = n$, vanish.

$$-\delta_n \frac{n^2\pi^2}{L^2} + \bar{\delta}_n \frac{n^2\pi^2}{L^2} + \delta_n \frac{P}{EI} = 0 \tag{4}$$

$$\delta_n\left(\frac{P}{EI} = \frac{n^2\pi^2}{L^2}\right) + \bar{\delta}_n \frac{n^2\pi^2}{L^2} = 0$$

$$\delta_n = \frac{\bar{\delta}_n}{1 - [P/(n^2\pi^2 EI)/L^2]} \tag{5}$$

$$P_{cr.} = \pi^2 EI/L^2$$

$$\delta_n = \frac{\bar{\delta}_n}{1 - (P/n^2 P_{cr.})} \tag{6}$$

$$\delta_n' = \delta_n - \bar{\delta}_n = \left(\frac{1}{1 - (P/n^2 P_{cr.})} - 1\right)\bar{\delta}_n$$

$$\delta_n' \doteq \frac{\bar{\delta}_n P}{n^2 P_{cr.} - P} = \frac{\bar{\delta}_n}{(n^2 P_{cr.}/P) - 1}$$

$$\delta_1' = \frac{\bar{\delta}_1}{(P_{cr.}/P) - 1} \tag{7}$$

As P approaches $P_{cr.}$, $\bar{\delta}_1$ is much more amplified than the amplitudes of other harmonics.

$$\delta' = \sum \delta_n' \cong \delta_1' = \frac{\bar{\delta}_1}{(P_{cr.}/P) - 1} \tag{8}$$

This shows the relation of the increase of deflection with load in the elastic range.

When the column is loaded beyond the elastic limit, the flexural rigidities of the different sections of the column vary with the load. At a particular section of the column under a given load and moment, from the condition of equilibrium,

$$P = \int \sigma\, dA \tag{9}$$

$$M = \int \sigma\eta\, dA \tag{10}$$

For a small increment of load ΔP and a small increment of moment ΔM, from Eqs. (9) and (10),

$$\Delta P = \int \Delta\sigma\, dA \tag{11}$$

$$\Delta M = \int \Delta\sigma\eta\, dA \tag{12}$$

$$\Delta\sigma = E_t \Delta e \tag{13}$$

From the assumption that planes before loading remain planes after loading,

$$e = e_0 + K\eta \tag{14}$$

where K is a constant.

Assume the value of E_t as constant in the interval from P to $P + \Delta P$ and from M to $M + \Delta M$. The smaller the value of ΔP and ΔM, the more accurate will be the result. With E_t remaining the same, there is no change in the modified section within the interval.

$$\Delta e = \Delta e_0 + \eta \Delta K \tag{15}$$

From Eqs. (11), (15), and (12)

$$\Delta P = \int E_t(\Delta e_0 + \eta \Delta K) b d\eta \tag{16}$$

$$\Delta M = \int E_t(\Delta e_0 + \eta \Delta K) b \eta d\eta \tag{17}$$

By definition of the neutral axis of the modified section

$$\int E_t b \eta d\eta = 0 \tag{18}$$

$$\int E_t b d\eta = EA' \tag{19}$$

$$\int E_t b \eta^2 d\eta = EI' \tag{20}$$

From Eqs. (16) to (20),

$$\Delta P = EA' \Delta e_0 \tag{21}$$

$$\Delta M = EI' \Delta K \tag{22}$$

From Eqs. (15), (21), and (22)

$$\Delta e = \frac{\Delta P}{EA'} + \frac{\Delta M}{EI'} \eta \tag{23}$$

When the increment of load and moment approach zero, the increments Δe, ΔP, and ΔM are replaced by differentials de, dP, and dM.

$$de = \frac{dP}{EA'} + \frac{dM}{EI'} \eta \tag{24}$$

$$d\sigma = \frac{E_t dP}{EA'} + \frac{E_t dM}{EI'} \eta \tag{25}$$

Let the column load P be increased to $P + \Delta P$ and the deflection y be increased to $y + \Delta y$. From the condition of equilibrium, $\Delta M = (P + \Delta P)(y + \Delta y) - Py$

$$\Delta M = -EI' \Delta(d^2y/dx^2) = (P + \Delta P)\Delta y + \Delta P y \tag{26}$$

$$\Delta \frac{d^2y}{dx^2} + \frac{P + \Delta P}{EI'} \Delta y + \frac{\Delta P}{EI'} y = 0 \tag{27}$$

$$\frac{d^2 \Delta y}{dx^2} + \frac{P + \Delta P}{EI'} \Delta y + \frac{\Delta P}{EI'} y = 0 \tag{28}$$

Effect of Eccentricity

Due to the fact that with deflection the strain, and hence the tangent modulus across the section, varies from the concave to the convex side, the neutral axis of the modified section does not coincide with the geometrical axis and changes with load. But the increment of load still applies at the geometrical axis and hence will have an eccentricity x_0 on the modified section. This eccentricity increases rapidly as reversal of strain occurs. So in the last term in Eqs. (26) to (28), y should be measured from the neutral axis of the modified section. But y was taken as the perpendicular distance from the line of thrust to the geometrical axis, so an eccentricity x_0 should be added to y in the last term in Eqs. (26) and (28) and these equations become

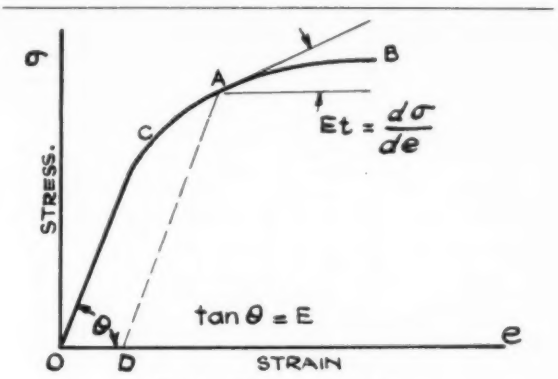

FIG. 1. Stress-strain curve.

$$\Delta M = (P + \Delta P)\Delta y + \Delta P(y + x_0) = EI' \Delta K \tag{29}$$

$$\frac{d^2 \Delta y}{dx^2} + \frac{P + \Delta P}{EI'} \Delta y + \frac{\Delta P}{EI'} (y + x_0) = 0 \tag{30}$$

Integrate Eq. (30) and let the lower limit be $x = L/2$:

$$\frac{d\Delta y}{dx} = -\int_{L/2}^{x} \frac{P + \Delta P}{EI'} \Delta y \, dx - \int_{L/2}^{x} \frac{\Delta P}{EI'} (y + x_0) dx + C \tag{31}$$

At $x = L/2$, $d\Delta y/dx = 0$, so $C = 0$.

$$\Delta y = -\int_{L/2}^{x}\int_{L/2}^{x} \frac{P + \Delta P}{EI'} \Delta y \, dx \, dx - \int_{L/2}^{x}\int_{L/2}^{x} \frac{\Delta P}{EI'} (y + x_0) dx \, dx + C_1 \tag{32}$$

At $x = L/2$, $\Delta y = \Delta\delta$, so $C_1 = \Delta\delta$.

$$\Delta\delta - \Delta y = \int_{L/2}^{x}\int_{L/2}^{x} \frac{P + \Delta P}{EI'} \Delta y \, dx \, dx + \int_{L/2}^{x}\int_{L/2}^{x} \frac{\Delta P}{EI'} (y + x_0) dx \, dx \tag{33}$$

The above integrals are the moment of the area under the curves of $(P + \Delta P)\Delta y/EI'$ and $\Delta P(y + x_0)/EI'$ between $x = L/2$ and $x = x$ about the section $x = x$. The Δy curve can be calculated by assuming $\Delta\delta$ and finding Δy by starting from the center section $x = L/2$. If the Δy at $x = L$ equals zero the assumed $\Delta\delta$ is correct, otherwise $\Delta\delta$ should be modified until this condition is satisfied. For further increment of load, the new EI' at different sections should be calculated and the above process repeated.

Reversal of Strain

A typical compressive stress-strain curve is shown in Fig. 1. When the strain is increased from zero, the stress follows the curve $OCAB$. If the strain is increased up to A and then reduced, the stress-strain curve will not follow A to C, but A to D which has the same

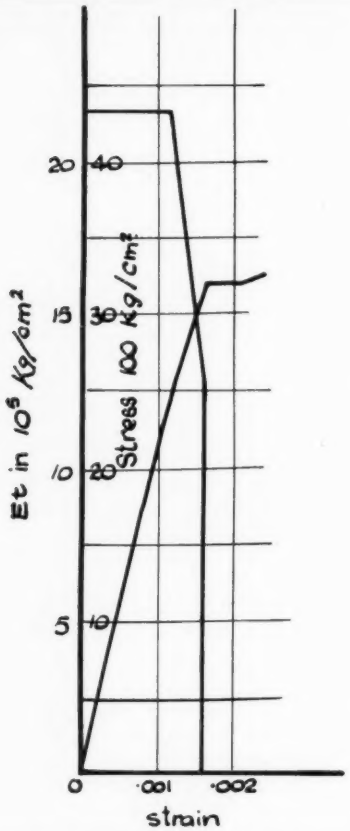

FIG. 2. Stress-strain curve for mild steel for composition (from reference 7).

slope giving Young's modulus of elasticity E. So beyond the proportional limit, if the compressive strain of a portion of the section decreases with the increase of load, E would occur instead of E_t. So where $de/dP > 0$, E_t would occur, and where $de/dP < 0$, E would occur.

Now let us consider the distribution of strain across the section when the stress is beyond the proportional limit.

$$\Delta e = \frac{\Delta P}{EA'} + \frac{\Delta M}{EI'}\eta \tag{24}$$

$$\Delta M = (P + \Delta P)\Delta y + (y + x_0)\Delta P \tag{29}$$

From the above two equations

$$\Delta e = \frac{\Delta P}{EA'} + \frac{(P + \Delta P)\Delta y + (y + x_0)\Delta P}{EI'}\eta \tag{34}$$

$$\frac{\Delta e}{\Delta P} = \frac{1}{EA'} + \frac{P(\Delta y/\Delta P) + y + \Delta y + x_0}{EI'}\eta \tag{35}$$

When $\Delta e/\Delta P = 0$,

$$\frac{1}{A'} = -\frac{P(\Delta y/\Delta P) + y + \Delta y + x_0}{I'}\eta_1$$

$$\eta_1 = -\frac{\rho'^2}{P(\Delta y/\Delta P) + y + \Delta y + x_0} \tag{36}$$

As the value of ΔP approaches zero, Δy approaches zero and $\Delta y/\Delta P = dy/dP$, then Eq. (36) becomes

$$\eta_1 = -\frac{\rho'^2}{P(dy/dP) + y + x_0} \tag{37}$$

η_1 is the point on the convex side, beyond which the compressive strain decreases and E_t changes back to E. When η_1 is greater than h_2, there is no region of reversal of strain. Up to $\eta_1 = h_2$, the tangent modulus is effective across the whole section. Further load and deflection would introduce a double modulus, by which is meant that Young's modulus E extends over a portion of the section from the convex side and the tangent modulus covers the remaining portion. As load and deflection increase, there will be an increase of the region where Young's modulus is valid. The modified section at different stages of loading is illustrated in Fig. 3, which is based on the linear variation of E_t with e that occurs in a region beyond the proportional limit (as shown in Fig. 2) for most engineering materials. For regions in which this linearity does not hold, the modified section should be based on the actual variation of

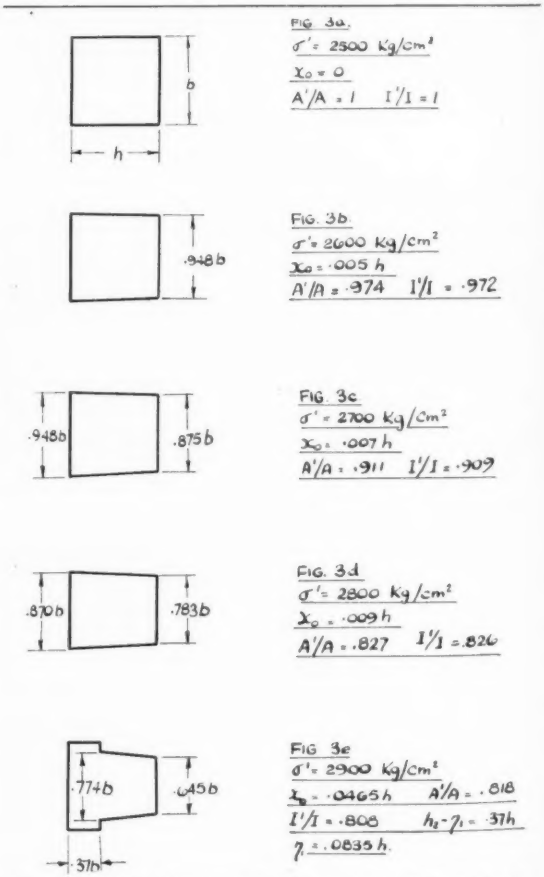

FIG. 3. Modified sections of mid-section at different loads.

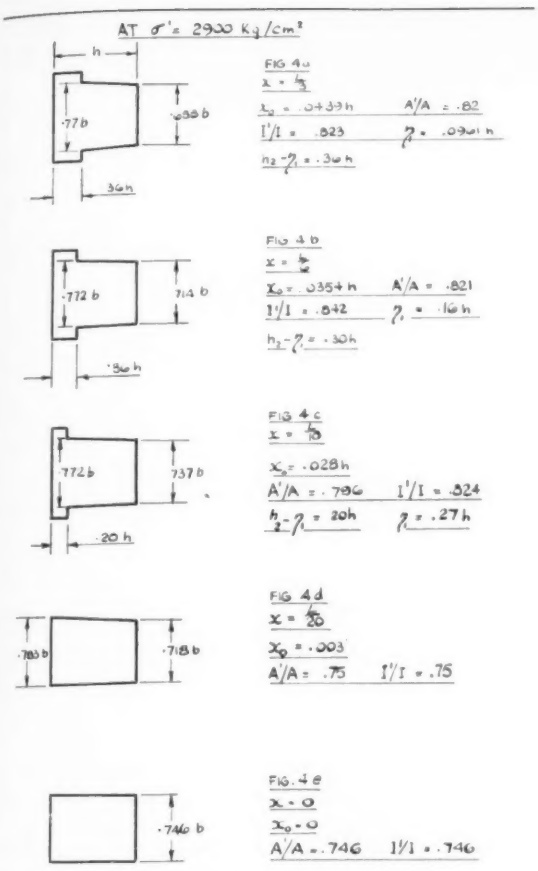

FIG. 4. Modified sections at different sections of column.

E_t with e. The reversal of strain would affect both the value of I' and the position of neutral axis.

With given form of section, stress-strain curve of the material and the known initial deflection (the initial deflection may be found from Southwell's[3, 4] test in elastic range), the load-deflection curve may be obtained by Eq. (7) until the extreme fiber stress on the concave side is equal to the elastic limit of the material. Then for subsequent increase of load, get the first approximate curve of the increment of deflection Δy as if the column were of constant EI' equal to that at center section. From Eq. (30)

$$\frac{d^2\Delta y}{dx^2} + \frac{(P + \Delta P)}{EI'}\Delta y + \frac{\Delta P}{EI'}(y + x_0) = 0 \quad (30)$$

Let

$$\Delta y = \sum \Delta\delta_n \sin\frac{n\pi x}{L}, \quad y = \sum \delta_n \sin\frac{n\pi x}{L}, \quad x_0 = \sum a_n \sin\frac{n\pi x}{L}$$

$$\frac{d^2\Delta y}{dx^2} = -\sum \frac{n^2\pi^2}{L^2}\Delta\delta_n \sin\frac{n\pi x}{L}$$

Substitute the above in Eq. (30)

$$-\sum \frac{n^2\pi^2}{L^2}\Delta\delta_n \sin\frac{n\pi x}{L} + \frac{P + \Delta P}{EI'}\sum \Delta\delta_n \sin\frac{n\pi x}{L} + \frac{\Delta P}{EI'}\left(\sum \delta_n \sin\frac{n\pi x}{L} + \sum a_n \sin\frac{n\pi x}{L}\right) = 0$$

I' at different sections is assumed equal to I_1' at center section throughout the following analysis. Multiply the above equation by $\sin(m\pi x/L)dx$ and integrate from the limit of $x = 0$ to $x = L$. All the terms $m \neq n$ vanish and the terms $m = n$ give the following equations:

$$-\frac{n^2\pi^2}{L^2}\Delta\delta_n + \frac{P + \Delta P}{EI_1'}\Delta\delta_n + \frac{\Delta P}{EI_1'}(\delta_n + a_n) = 0$$

$$\left[-\frac{n^2\pi^2 EI'}{L^2} + (P + \Delta P)\right]\Delta\delta_n + \Delta P(\delta_n + a_n) = 0 \quad (38)$$

Substitute $P_{cr.1}$ for $\pi^2 EI_1'/L^2$,

$$(n^2 P_{cr.1} - P - \Delta P)\Delta\delta_n = \Delta P(\delta_n + a_n)$$

$$\frac{\Delta\delta_n}{\Delta P} = \frac{\delta_n + a_n}{n^2 P_{cr.1} - P - \Delta P} \quad (39)$$

$$\frac{\Delta\delta}{\Delta P} = \sum \frac{\Delta\delta_n}{\Delta P} = \sum \frac{\delta_n + a_n}{n^2_{cr.1} - P - \Delta P}$$

As in the elastic case, the increase of first harmonic is much more than the other harmonics as P approaches $P_{cr.1}$, so the increments of other harmonics are neglected.

$$\frac{\Delta\delta}{\Delta P} = \sum \frac{\delta_n + a_n}{n^2 P_{cr.1} - P - \Delta P} \cong \frac{\delta_1 + a_1}{n^2 P_{cr.1} - P - \Delta P}$$

As stated above, the I' at different sections are assumed to be equal to I_1' at center section. It is further assumed that the amplitude of the first harmonic

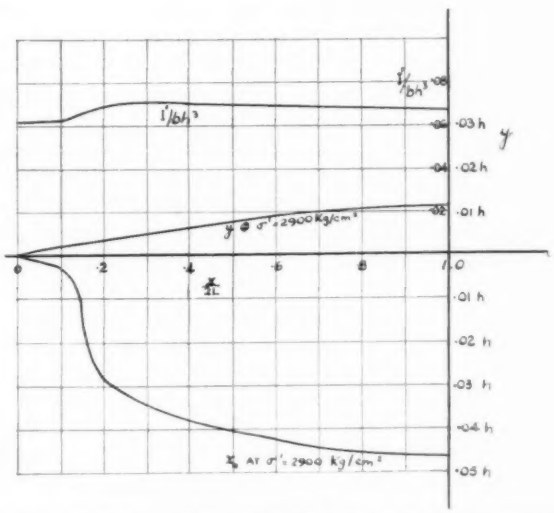

FIG. 5. Deflection and eccentricity of modified sections along length of column.

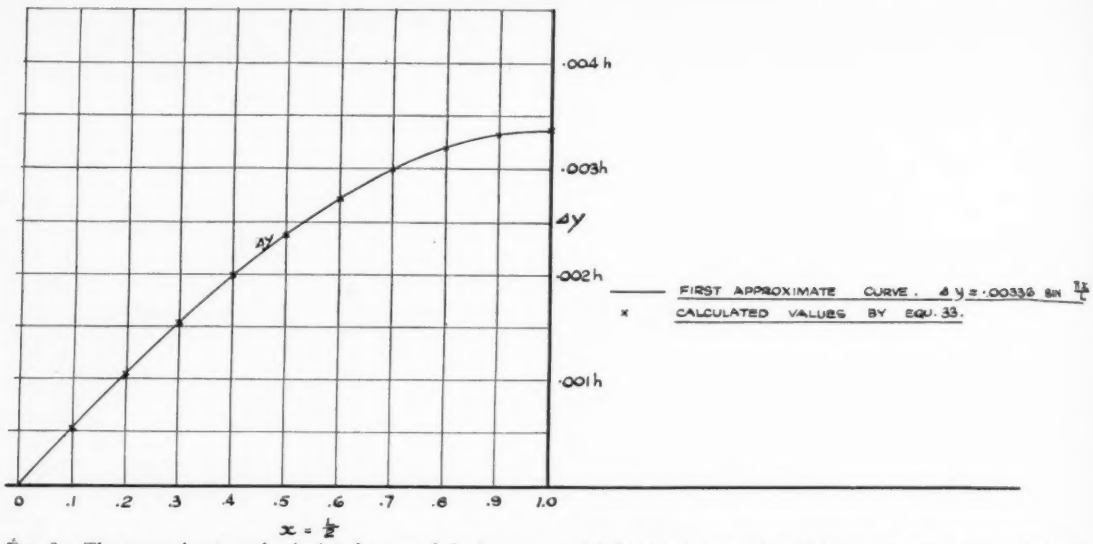

FIG. 6. The approximate and calculated curve of the increment of deflection due to $4\sigma' = 10$ kg. per sq.cm. at $\sigma' = 2{,}900$ kg. per sq.cm.

of eccentricity a_1 and that of the deflection curve δ_1 are equal to their values x_0 and δ at the center, respectively.

$$\frac{\Delta\delta}{\Delta P} = \frac{\delta + x_0}{P_{cr\cdot_1} - P - \Delta P} \tag{40}$$

As ΔP approaches zero, $\Delta\delta/\Delta P = d\delta/dP$.

$$\frac{d\delta}{dP} = \frac{(\delta + x_0)}{(P_{cr\cdot_1} - P)} \tag{41}$$

From Eq. (37), at $x = L/2$

$$\eta_1 = \frac{-\rho'^2}{P(d\delta/dP) + \delta + x_0}$$

From the above equation and Eq. (41)

$$\eta_1 = \frac{-\rho'^2}{(\delta + x_0)[(P/P_{cr\cdot_1} - P) + 1]}$$

$$\eta_1 = \frac{-\rho'^2}{(\delta + x_0)[(P_{cr\cdot_1}/P_{cr\cdot_1} - P)]} \tag{42}$$

From Eq. (42) and the relation $P_{cr\cdot_1} = \pi^2 EI_1'/L^2$, the modified section at $x = L/2$ for the first approximation can be determined and so the values of A_1', I_1', and $d\delta/dP$ at the center section are obtained. With the above assumptions, the curve of the increment of deflection for the first approximation is first harmonic.

$$\Delta y = \Delta\delta \sin(\pi x/L)$$

$$\Delta y/\Delta P = (\Delta\delta/\Delta P) \sin(\pi x/L)$$

$$dy/dP = (d\delta/dP) \sin(\pi x/L)$$

With this dy/dP value put in Eq. (37), η_1 is found for different sections. If $\eta_1 > h_2$ there is no reversal of strain. If $\eta_1 < h_2$ reversal of strain occurs in the region $\eta > \eta_1$ to $\eta = h_2$. If the deviation of I' at various sections from I_1' is negligible, no revision of the increment deflection is necessary. If the deviation is not negligible, apply Eq. (33) and by the moment area method, obtain the increment deflection curve due to the increased bending moment. If this curve deviates negligibly from the first approximate curve, the first approximate curve is considered to be accurate enough. If not, the increment deflection curve obtained from the bending moment is used as an assumed second approximation and the process is repeated until the curve obtained from the increased bending moment agrees closely with the assumed curve. After the Δy is obtained in this way, the increment of strain across the section can be obtained by finding Δe_0 from Eq. (21). Where there is no reversal of strain across the section and the E_t vs. e curve is linear, e_0 can be taken from the stress-strain curve corresponding to the average stress of the section P/A. From Eq. (29)

$$\Delta K = \frac{(P + \Delta P)\Delta y + (y + x_0)\Delta P}{EI'}$$

where ΔK equals $\Delta(e_1 - e_2)/h$. Then from the strain distribution, the new EI' can be computed. Then add the further increment of load, and repeat the process until the increase of deflection becomes very large indicating that the buckling load is being approached. This method involves the assumption that in the interval from P to $P + \Delta P$, EI' remains constant at the value corresponding to P. The error in this assumption diminishes as ΔP decreases. ΔP taken should be small where E_t varies sharply with strain e. The convergence of the above successive approximation method is shown in Appendix (II).

For an actual column, the value of E_t decreases almost linearly with strain beyond the proportional limit as shown in Fig. 2. The value of I' actually varies little from the ends to the center of the column before the

reversal of strain occurs. For a first approximation, assume EI' to be constant and equal to EI_1' at the center of the column. For a steel column of rectangular section [calculated in Appendix (I)], the difference between the value of E_tI at the ends and EI_1' at the center is about 1 per cent before the occurrence of the reversal of strain, so the above first approximation curve is close enough for the calculation of the increment of deflection until the reversal of strain occurs. After the reversal of strain occurs, the increment of deflection is calculated by the moment area method based on Eq. (33). For those sections with reversal of strain, Eq. (21) should be used for the increment of axial strain e_0.

The load-deflection curve of a steel column of rectangular section, of slenderness ratio of 75 and with initial deflection of $0.001h$ in Kármán's test,[5] is calculated by the above method and shown in Appendix (I). The calculated curve agrees very well with tested values.

For a column of small L/ρ, as load increases, EI remains constant up to the proportional limit. Beyond the proportional limit, EI decreases due to the reduction of EI to E_tI ($E_t < E$). Then with increase of deflection, a portion of the cross section has negative de/dP at the convex side and double modulus occurs. For the portion $\eta > \eta_1$, E_t changes back to E, but on the rest of the section, E_t still exists and decreases according to the stress-strain curve of the material. Generally as the reversal of strain occurs, the effective moment of inertia and eccentricity increase. This increase of eccentricity increases deflection as load increases. Eventually the deflection increases indefinitely for a definite increase of load and the maximum load is reached.

A perfect column will remain straight up to the tangent modulus load. If there is no slight disturbance, the column may remain straight even beyond the tangent modulus load. A slight disturbance is assumed to be present all the time. This slight disturbance is here represented by an infinitesimal deflection $\delta = \epsilon \cong 0$. When this $\delta = \epsilon$ is very small, EI' may be taken as constant along the column equal to E_tI. From Eqs. (41) and (42)

$$d\delta/dP = (\delta + x_0/P_{cr\cdot_1} - P) \tag{41}$$

$$\eta_1 = \frac{-\rho'^2}{(\delta + x_0)(P_{cr\cdot}/P_{cr\cdot} - P)} \tag{42}$$

At $\delta = \epsilon \cong 0$, $x_0 = 0$

$$d\delta/dP = (\epsilon/P_{cr\cdot} - P)$$

$$\eta_1 = \frac{-\rho'^2}{\epsilon(P_{cr\cdot}/P_{cr\cdot} - P)}$$

Here $P_{cr\cdot} = \pi^2E_tI/L^2$. When $P_{cr\cdot} - P$ approaches the magnitude of ϵ, $d\delta/dP$ increases to a finite value. Let $P_{cr\cdot} - P = n\epsilon$, where n is a finite number.

$$d\delta/dP = 1/n$$

$$\eta_1 = \frac{-n\rho'^2}{P_{cr\cdot}} = \frac{-n\rho'^2}{(\pi^2EA'\rho'^2/L^2)}$$

$$\eta_1 = -nL^2/\pi^2EA' \tag{43}$$

Equate η_1 to $-h_2$.

$$h_2 = nL^2/\pi^2EA'$$

$$n = \frac{P_{cr\cdot} - P}{\epsilon} = \frac{\pi^2EA'h_2}{L^2} = \frac{\pi^2E_tAh_2}{L^2} \tag{44}$$

As P approaches $P_{cr\cdot}$, at first, n is big and $\eta_1 > h_2$ until the ratio $(P_{cr\cdot} - P)/\epsilon$ reaches the value shown in Eq. (44); then $\eta_1 = h_2$. Further decrease of n occurs as P approaches nearer to $P_{cr\cdot}$ and η_1 will be less than h_2 and double modulus occurs. Where reversal of strain occurs, the tangent modulus is changed back to elastic modulus, so I' and $P_{cr\cdot}$ increase in value and the eccentricity of the modified section increases rapidly to finite value. Then δ increases with additional load according to Eq. (41), mainly because of x_0. When δ increases to a finite value, the variation of tangent modulus across the section will also increase eccentricity of the modified section. η_1 decreases according to Eq. (42) and the eccentricity of the modified section increases. So the deflection increases with further additional load. With increase of deflection, the compressive strain on the concave side increases more than at the neutral axis of the modified section. The tangent modulus on the concave side decreases more than that at the neutral axis. (For all engineering materials the tangent modulus decreases with strain beyond elastic limit.) This decrease of tangent modulus will have the effect of reducing the moment of inertia of the modified section and hence the critical load. The combined effect of the reversal of strain, the decrease of tangent modulus at the neutral axis and the further decrease of the tangent modulus on the concave side will give a critical load at each value of load. Deflection starts at no reversal of strain $\eta_1 > h_2$ and not at $\eta_1 = 0$ as in the reduced modulus theory. This explains why deflection starts at the tangent modulus load and not at the reduced modulus load for a perfect column with no initial curvature. With further increment of load and deflection, η_1 decreases and approaches zero at critical load, while the compressive strain increases more on the concave side than at the neutral axis. Since the tangent modulus decreases with compressive strain beyond the proportional limit, the decrease of tangent modulus is more on the concave side than at the neutral axis of the modified section. The EI' of the modified section is thus less than E_tI in the reduced modulus theory. Hence the reduced modulus load is not reached. Taking into consideration the effect that η_1 decreases gradually from h_2 and $P_{cr\cdot}$ and x_0 increase with the decrease of η_1, the increment of deflection with load beyond the tangent modulus load can be found in the same way as for the column with initial curvature, as explained previously.

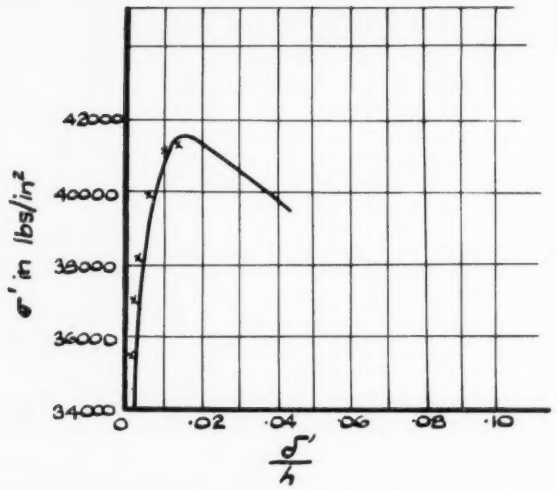

FIG. 7. Load-deflection curve for steel column $L/P = 75$. Curve from test in reference 7. x calculated value. Initial deflection $\bar{\delta}$ $0.001h$.

With load-deflection curve computed, the maximum load can be obtained quite closely.

The critical load would depend on EI' along the whole length of the column. For an actual column with small initial curvature, when the load increases near the critical load, the deflection increases and the denominator of the right side of Eq. (37), especially the term dy/dP, increases and η_1 decreases, approaching zero at critical load. This decrease of η_1 increases EI' of the modified sections. On the other hand, with increasing deflection, the compressive strain increases more on the concave side than at the neutral axis. So the tangent modulus decreases with the distance from the neutral axis on the concave side. This causes the tangent modulus on the concave side to be less than the tangent modulus at tangent modulus load. The excess of the effect caused by reversal of strain over the effect caused by the decrease of tangent modulus on the concave side at the maximum load, increases the maximum load above the tangent modulus load.

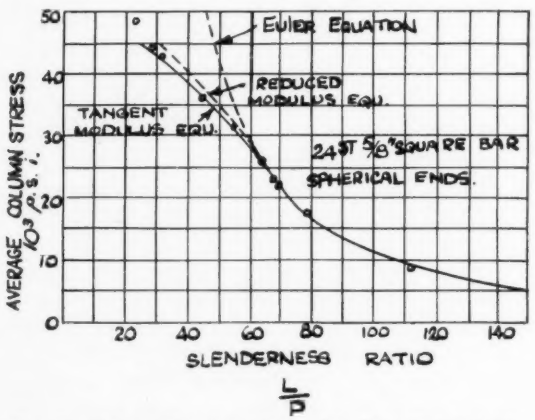

FIG. 8. Column theories and test data (Van Den Brook), reference 1.

For very short columns of 24ST, the rate of the decrease of tangent modulus with increase of strain near the critical load is much less, so the effect of the decrease of tangent modulus on the concave side on EI' is much less. The tangent modulus at the neutral axis is quite near to the tangent modulus on the concave side in the reduced modulus theory. And in very short columns, the tangent modulus does not vary much with the distance from the neutral axis and would be quite close to the value at neutral axis and to the tangent modulus value of the reduced modulus theory. The difference in value of the tangent modulus and elastic modulus increases with the critical stress, so for short columns with high critical stress, the effect of reversal of strain is more prominent. Hence, the maximum load would deviate more from the tangent modulus load. Test points of the very short columns, therefore, often lie closer to the reduced than to the tangent modulus curve as shown in Fig. 8 and other similar tests.

APPENDIX (I)—CALCULATION OF LOAD-DEFLECTION CURVE OF A STEEL COLUMN

In the following, the load-deflection curve of a steel column tested by Kármán,[5] of rectangular section with initial deflection of $0.001h$ at the center and slenderness ratio L/ρ of 75, is calculated based on the method shown. The following data are taken from reference 5. The stress-strain curve of the material is taken from Fig. 6 of the reference. The tangent modulus is calculated from the stress-strain curve and plotted in Fig. 2.

$$L/\rho = 75, \qquad E = 2{,}170{,}000 \text{ kg. per sq. cm.}$$
$$\bar{\delta} = 0.001h$$

At $\sigma' = 34{,}000$ lbs. per sq.in. or 2,400 kg. per sq. cm., $\delta' = 0.0016h$. For this deflection and load, the column is in the elastic range. So Eq. (8) is used to find $\bar{\delta}_1$.

$$\delta' = \frac{\bar{\delta}_1}{(P_{cr.}/P) - 1}$$

$$P_{cr.} = A\sigma_{cr.}', \qquad P = A\sigma'$$

$$\delta' = \frac{\delta_1}{(\sigma_{cr.}'/\sigma') - 1} \tag{45}$$

$$\sigma_{cr.}' = \frac{\pi^2 EI}{L^2 A} = \frac{\pi^2 E}{(L/\rho)^2} \tag{46}$$

$$= \frac{\pi^2 \times 2{,}170{,}000}{75^2} = 3{,}810 \text{ kg. per sq.cm.}$$

At $\sigma' = 2{,}400$, $\delta'/h = 0.0016$. From Eq. (45)

$$0.0016h = \frac{\bar{\delta}_1}{(3{,}810/2{,}400) - 1}$$

$$\bar{\delta}_1/h = 0.000938$$

The first harmonic is much more amplified than other harmonics, so the deflected curve, at $\sigma' = 2{,}400$ kg.

TABLE 1

Calculation of Load-Deflection Curve of a Steel Column of Slenderness Ratio $L/\rho = 75$ with Initial Deflection of $0.001h$

			1	2	3	4	5	6	7
(1)	σ'	kg. per sq.cm.	2,400	2,500	2,600	2,700	2,800	2,900	2,910
(2)	σ'	lbs. per sq.in.	34,100	35,500	36,900	38,300	39,700	41,200	41,300
(3)	e_0	from Fig. 2	0.00110	0.00115	0.00121	0.00126	0.00133	0.00142	....
(4)	$E_{t_0}/10^6$, kg. per sq.cm.	from Fig. 2	2.17	2.17	2.13	2.00	1.83	1.60	....
(5)	δ'/h	$(5)_{n+1} = (5)_n + (21)_n$ (n denotes column number)	0.00160*	0.00180	0.00203	0.00283	0.00496	0.01024	0.01360†
(6)	$e_1 - e_2$	$\frac{(5)}{47.6}$	0.000034	0.000038	0.0000428	0.0000594	0.0000937	0.000214	....
(7)	e_1	$e_1 = e_0 + \frac{e_1 - e_2}{h}h_1$	0.00112	0.00117	0.00123	0.00129	0.00138	0.00153	....
(8)	e_2	$e_2 = e_0 + \frac{e_1 - e_2}{h}h_2$	0.00108	0.00113	0.00119	0.00123	0.00129	0.00132	....
(9)	$E_{t_1}/10^6$	from Fig. 2	2.17	2.17	2.06	1.90	1.70	1.40	....
(10)	$E_{t_2}/10^6$	from Fig. 2	2.17	2.17	2.17	2.06	1.88	1.85	....
(11)	x_0/h	Eccentricity of modified Section, Fig. 3	0	0	0.005	0.007	0.009	0.0465	....
(12)	A_1'/A	Fig. 3	1	1	0.974	0.911	0.8267	0.818	....
(13)	I'/I	Fig. 3	1	1	0.972	0.909	0.816	0.808	....
(14)	E_{t_0}/E	$\frac{(4)}{2{,}170{,}000}$	1	1	0.982	0.920	0.843	0.737	....
(15)	$\frac{E_{t_0}I}{EI_1'}$	$\frac{(14)}{(13)}$	1	1	1.01	1.01	1.02	0.912	....
(16)	$\sigma_{cr.}'$, kg. per sq.cm.	$\frac{\pi^2 EI'}{AL^2}$	3,810	3,810	3,700	3,460	3,150	3,078	....
(17)	$\Delta\sigma'$	$(1)_{n+1} - (1)_n$	100	100	100	100	100	10	....
(18)	$\sigma_{cr.}' - \sigma' - \Delta\sigma'$	(16) − (1) − (17)	1,310	1,210	1,000	660	250	168	....
(19)	$\frac{\delta' + \bar{\delta} + x_0}{h}$	(5) + (11) + 0.001	0.0026	0.0028	0.00803	0.01083	0.01446	0.05774	....
(20)	$\frac{\Delta\delta'/h}{\Delta\sigma'} \times 10^6$	$\frac{(19)}{(18)}$	1.985	2.32	8.03	16.40	57.8	344	....
(21)	$\Delta\delta'/h$	(17) (20)	0.000199	0.000232	0.000803	0.00163	0.00578	0.00344	0.00336†
(22)	$\Delta(e_1 - e_2)$	(21)/47.6	0.00000418	0.00000486	0.0000169	0.0000344	0.000121	....	....
(23)	$\frac{h_2 - \eta_1}{h}$	Fig. 3	....	....	....	....	....	0.37	....
(24)	e_{η_1}	$e = e_0 + \frac{e_1 - e_2}{h}\eta_1$	....	....	....	....	....	0.00140	....
(25)	$E_{t\eta_1}/10^6$	from Fig. 2	....	....	....	....	....	1.68	....
(26)	$E_{t\eta_1}/E$	$\frac{(25)}{2{,}170{,}000}$	....	....	....	....	....	0.774	....
Modified section			3a	3a	3b	3c	3d	3e	....

* From test curve, Fig. 9, reference 7.

† δ'/h, $\Delta\delta'/h$ of first approximation.

TABLE 2

Calculation of Section Properties of Modified Sections—at $\sigma' = 2{,}900$ Kg. per Sq.Cm., at Different Values of x Based on the First Approximate Curve $\Delta y = \Delta\delta \sin(\pi x/L)$

x/L		1/2	1/3	1/6	1/10	1/20	0
σ'	Kg. per sq.cm.	2,900	2,900	2,900	2,900	2,900	2,900
e_0	Fig. 2	0.00142	0.00142	0.00142	0.00142	0.00142	0.00142
y'/h	$0.01024 \sin(\pi x/L)$	0.01024	0.00888	0.00512	0.00317	0.0025	0
$e_1 - e_2$	$\frac{\pi^2 h^2}{L^2}\frac{y'}{h}$	0.000215	0.000186	0.000107	0.000066	0.000052	0
e_1	$e_0 + \frac{e_1 - e_2}{h} h_1$	0.00153	0.00151	0.00147	0.00146	0.00145	0.00142
e_2	$e_0 + \frac{e_1 - e_2}{h} h_2$	0.00132	0.00133	0.00137	0.00139	0.00140	0.00142
$E_{t_1}/10^6$	Kg. per sq.cm., from Fig. 2	1.40	1.45	1.55	1.55	1.60	1.62
$E_{t_2}/10^6$	Kg. per sq.cm., from Fig. 2	1.85	1.80	1.75	1.70	1.67	1.62
E_{t1}/E		0.645	0.668	0.714	0.718	0.737	0.746
E_{t2}/E		....	....	....	0.783	0.770	0.746
x_0/h	Fig. 4	0.0465	0.0439	0.0354	0.0282	0.003	0
A'/A	Fig. 4	0.81	0.82	0.821	0.796	0.750	0.746
I'/bh^3	Fig. 4	0.0674	0.0685	0.0702	0.0686	0.0625	0.0622
$\frac{h_2 - \eta_1}{h}$	Fig. 4	0.37	0.36	0.30	0.20	....	....
e_{η_1}	$e_0 + \frac{e_1 - e_2}{h}\eta_1$	0.00140	0.00140	0.00141	0.00141	....	....
$E_{t\eta_1}/10^6$	Fig. 2	1.68	1.67	1.675	1.675	....	....
$\frac{E_{t\eta_1}}{E}$		0.774	0.770	0.772	0.772	....	....
η_1/h	Fig. 4	0.0835	0.096	0.165	....	....	....
$P\frac{dy}{dP}$ *		0.941	0.815	0.471	0.291	0.147	....
y/h†		0.01124	0.00975	0.00562	0.00348	0.00175	0
Modified section		Fig. 3e	Fig. 4a	Fig. 4b	Fig. 4c	Fig. 4d	Fig. 4e

* $P\frac{d\delta}{dP} = P\frac{\delta + x_0}{P_{cr.} - P} = \frac{0.01124 + 0.0465}{(3{,}078 - 2{,}900)/2{,}900} = 0.941$; $P(dy/dP) = 0.941 \sin(\pi x/L)$.

† $y = \delta \sin(\pi x/L) = 0.01124 \sin(\pi x/L)$.

per sq.cm. would be very close to the first harmonic curve.

$$y = \delta \sin\frac{\pi x}{L}, \qquad \frac{d^2y}{dx^2} = -\frac{\pi^2}{L^2}\delta \sin\frac{\pi x}{L}$$

From Eq. (14),

$$e = e_0 + K\eta, \qquad e_1 - e_2 = Kh, \qquad \Delta(e_1 - e_2) = h\Delta K$$

Then consider a segment of beam of uniform curvature with radius R and extending an angle θ. Equate the difference in length of the extreme fibers of this segment to the difference in strain at the extreme fibers times the length of the neutral axis of the segment.

$$(R + h_1)\theta - (R - h_2)\theta = R\theta(e_1 - e_2)$$

$$h = R(e_1 - e_2)$$

$$e_1 - e_2 = h/R = Kh$$

$$K = 1/R = d^2y/dx^2$$

$$(e_1 - e_2)/h = d^2y/dx^2 = -\delta(\pi^2/L^2)\sin(\pi x/L) \quad (47)$$

At $x = L/2$

$$(e_1 - e_2)/h = -\delta\pi^2/L^2$$

$$\Delta(e_1 - e_2)/h = -\Delta\delta'\pi^2/L^2 \quad (48)$$

Dividing the denominators of Eq. (40) by A on both sides,

$$\frac{\Delta\delta}{\Delta\sigma'} = \frac{\delta + x_0}{\sigma_{cr.1}' - \sigma' - \Delta\sigma'} \quad (49)$$

From Eq. (42), with $P_{cr.1} = A\sigma_{cr.1}'$ and $P = A\sigma'$,

$$\eta_1 = \frac{-\rho'^2}{(\delta + x_0)(\sigma_{cr.1}'/\sigma_{cr.1}' - \sigma')} \quad (50)$$

Eqs. (49) and (50) are based on the assumption that EI' is constant throughout the length of the column, so these equations are only justified when the variation of EI' is shown to be negligible. Eq. (50) is used for first approximate calculation of η_1 in Table 1, row 23, but this value is to be revised if later successive approximation shows necessary revision.

Eq. (49) is used to calculate the deflection curve of the steel column until the reversal of strain occurs.

TABLE 3

Calculation of the Increment of Deflection Δy by Moment Area Method Based on the First Approximate Curve $\Delta y_1 = \Delta\delta \sin(\pi x/L)$, $\Delta\delta = 0.00336h$ (from Table 2)

(1)	$x/(L/2)$	1	0.9	0.8	0.7	0.6	0.5	0.4	0.3	0.2	0.1	0	Σ
(2)	$1 - x/(L/2)$	0	0.1	0.2	0.3	0.4	0.5	0.6	0.7	0.8	0.9	1	....
(3)	I'/bh^{3*}	0.0674	0.0675	0.0676	0.0680	0.0690	0.0692	0.0700	0.0702	0.0686	0.0625	0.0622	....
(4)	$\alpha = \frac{I'}{I'_1}$	1.00	1.002	1.004	1.009	1.024	1.028	1.038	1.042	1.018	0.927	0.924	....
(5)	$\frac{y + x_0}{h}$*	0.0575	0.0573	0.0562	0.0542	0.0517	0.0482	0.0440	0.0390	0.0320	0.005	0	....
(6)	$\frac{y + x_0}{\alpha h}$	0.0575	0.0572	0.0560	0.0537	0.0505	0.0469	0.0424	0.0374	0.0314	0.0054	0	....
(7)	$\frac{\Delta P(y + x_0)}{\alpha h}$	0.575	0.572	0.560	0.537	0.505	0.469	0.424	0.374	0.314	0.054	0	$\Delta P = 10$
(8)	Δy	0.00336	0.00331	0.00320	0.00300	0.00272	0.00238	0.00198	0.00153	0.00106	0.00052	0	$\Delta y = \Delta\delta \sin(\pi x/L)$ $\Delta\delta = 0.00336h$
(9)	$\frac{\Delta y}{\alpha}$	0.00336	0.00330	0.00319	0.00297	0.00266	0.00232	0.00191	0.00147	0.00104	0.00056	0	....
(10)	$P\frac{\Delta y}{\alpha}$	9.75	9.57	9.25	8.62	7.72	6.73	5.54	4.26	3.02	1.62	0	....
(11)	(7) + (10)	10.33	10.14	9.81	9.16	8.23	7.20	5.96	4.63	3.33	1.67	0	....
(12)	(11)Δx†	5.59	10.97	10.62	9.92	8.91	7.79	6.45	5.01	3.60	1.81	0	....
(13)	Center of Δx in terms of $L/20$	0.975	0.9	0.8	0.7	0.6	0.5	0.4	0.3	0.2	0.1	0.025	....
		0	....	....	....	....	....	....	....	....	....	....	0
(14)	(12)[(13) − 0.9]	4.53	0	....	....	....	....	....	....	....	....	....	4.53
(15)	(12)[(13) − 0.8]	10.58	11.86	0	....	....	....	....	....	....	....	....	22.44
(16)	(12)[(13) − 0.7]	16.62	23.75	11.50	0	....	....	....	....	....	....	....	51.87
(17)	(12)[(13) − 0.6]	22.68	35.60	23.00	10.74	0	....	....	....	....	....	....	92.02
(18)	(12)[(13) − 0.5]	28.7	47.5	34.5	21.5	9.65	0	....	....	....	....	....	141.85
(19)	(12)[(13) − 0.4]	34.7	59.3	46.0	32.2	19.30	8.43	0	....	....	....	....	199.93
(20)	(12)[(13) − 0.3]	40.8	71.2	57.5	43.0	29.0	16.86	6.98	0	....	....	....	265.34
(21)	(12)[(13) − 0.2]	46.9	83.1	69.0	53.7	38.6	25.3	13.96	5.42	0	....	....	335.98
(22)	(12)[(13) − 0.1]	52.9	95.0	80.5	64.4	48.2	33.7	21.0	10.83	3.9	0	....	410.43
(23)	(12)(13)	59.0	106.90	92.0	75.2	58.0	42.1	27.9	16.3	7.8	1.96	0	487.16
(24)	$EI_1'(\Delta\delta - \Delta y)$‡	0	4.53	22.44	51.87	92.02	141.85	199.9	265.3	336.0	410.4	487.2	....
(25)	$\Delta\delta - \Delta y$	0	0.000031	0.00015	0.000355	0.00063	0.00097	0.00137	0.00182	0.00230	0.00281	0.00334	....
(26)	Δy‡**	0.00334	0.00331	0.00319	0.00299	0.00271	0.00237	0.00197	0.00152	0.00104	0.00053	0	....

* Values of I' and $(y + x_0)$ from Fig. 5.

† $\Delta x = L/40$ of two ends, and $L/20$ for the rest.

‡ Values taken from summation column.

** y are plotted on Fig. 6.

Before the occurrence of the reversal of strain, the value of EI′ along the length deviates very little from its value at the center section. This is shown in the closeness of the ratio $E_{t0}I/EI'$ to unity as listed in Table 1, row 15.

So calculation of the deflection curve up to $\sigma' = 2{,}900$ kg. per sq.cm. in Table 1 based on the assumption of constant EI' along the length of the column at each load is justified, and the deflection curve at $\sigma' = 2{,}900$ kg. per sq.cm. is very near to first harmonic. After the occurrence of the reversal of strain at $\sigma' = 2{,}900$ kg. per sq.cm., the ratio $E_{t0}I/EI'$ is 0.912. Its deviation from unity would suggest the use of moment area method by considering the variation of EI' along the length as shown in Tables 2 and 3.

As mentioned above, the deflection curve at $\sigma' = 2{,}900$ kg. per sq.cm. is very near to first harmonic, so

$$y = \delta \sin (\pi x/L)$$

and

$$(d^2y/dx^2) = -(\pi^2/L^2)\delta \sin (\pi x/L)$$

From Eq. (48), $\Delta(e_1 - e_2)/h$ and then $(e_1 - e_2)/h$ for different sections can be found. With e_0 obtained from the stress-strain curve corresponding to σ', the values of e_1 and e_2 can be obtained by Eq. (14) with assumed eccentricity and later checked with the eccentricity found from the modified section. Then E_{t_1} and E_{t_2} are read from Fig. 2 corresponding to e_1 and e_2.

In order to compute η_1, dy/dP is required. So, for the first approximation, assume the column to be of constant EI' equal to that at the center section and assume the first harmonic amplitude of the $(y + x_0)$ curve at this load equal to its value at center section $(\delta + x_0)$. Assume η_1 and draw the modified section. Check the value of η_1 with Eq. (50). Revise η_1, if it does not agree with Eq. (50).

With I_1' and ρ'^2 known, calculate σ_{cr_1}' by the equation $\sigma_{cr_1}' = \pi^2 EI'/L^2A$. Apply Eq. (49) to find $\Delta\delta$. The increment deflection curve, based on the above assumptions, is a sine curve, $\Delta y = \Delta\delta \sin (\pi x/L)$, so dy/dP can be readily found by multiplying the value of $d\delta/dP$ by $\sin (\pi x/L)$. With dy/dP inserted in Eq. (37), the value of η_1 for other sections where reversal of strain exists can be found in the same way. The values of I' and x_0 at different sections are computed in Table 2 and plotted in Fig. 5.

With arbitrary $\Delta\sigma'$, the first approximate value of $\Delta\delta$ can be obtained from Eq. (49) and the first approximate increment deflection curve would be $\Delta y = \Delta\delta \sin (\pi x/L)$. Use this curve as first approximate Δy curve, calculate the deflection at various sections because of the increment of bending moment $P\Delta y + \Delta P(y + x_0)$ as shown in Table 3. If the new curve does not agree with the assumed Δy curve, the new curve should be used and dy/dP obtained by assuming it equal to $\Delta y/\Delta P$ from the new curve and η_1 recomputed and x_0, I' revised. Then compute the deflection curve caused by the increment of bending moment $P\Delta y + \Delta P(y + x_0)$ as before. This increment deflection curve would be the second approximation. But as shown in Fig. 6 the computed curve agrees extremely well with the assumed sine curve, so no further step is necessary. From Fig. 7, the curve is quite flat at this load, so this load may be taken as the maximum load. In general, this method of successive approximation converges rapidly to the final Δy curve. The convergence of this method is shown in Appendix (II).

Appendix (II)

The above method of successive approximation is shown to be convergent as follows. From Eq. (33),

$$\Delta y = \Delta\delta - \int_{L/2}^{x}\int_{L/2}^{x} \frac{P + \Delta P}{EI'} \Delta y\, dx\, dx - \int_{L/2}^{x}\int_{L/2}^{x} \frac{\Delta P}{EI'} (y + x_0)dx\, dx$$

$$\Delta\delta = \int_{L/2}^{L}\int_{L/2}^{x} \frac{1}{EI'}[(P + \Delta P)\Delta y + \Delta P(y + x_0)]dx\, dx \quad (51)$$

E is constant. P and y, which is a function of x, are known. The column is divided into n equal segments and they are numbered from the center of the column from 1 to n on each side. Let f, F, G, ψ, and ϕ denote functions. ΔP is given. From Eq. (33),

$$\Delta y_1 = f_1(\Delta\delta, I_1', x_{0_1})$$

$$\Delta y_2 = f_2(\Delta\delta, I_1', I_2', x_{0_1}, x_{0_2})$$

$$\Delta y_i = f_i(\Delta\delta, I_1', I_2', \ldots, I_i', x_{0_1}, x_{0_2}, \ldots, x_{0i})$$

I_i' and x_{0i} are functions of Δy_i.

$$I_i' = \psi(\Delta y_i)$$

$$x_{0i} = \phi_i(\Delta y_i)$$

So

$$\Delta y_1 = f_1[\Delta\delta, \psi_1(\Delta y_1), \phi_1(\Delta y_1)] = G_1(\Delta\delta)$$

$$\Delta y_2 = f_2\{\Delta\delta, \psi_1[G_1(\Delta\delta)], \psi_2(\Delta y_2), \phi_1[G_1(\Delta\delta)], \phi_2(\Delta y_2)\} = G_2(\Delta\delta)$$

Hence

$$\Delta y_i = G_i(\Delta\delta)$$

$$\frac{dI_i'}{d\Delta\delta} = \frac{dI_i'}{d\Delta y_i}\frac{d\Delta y_i}{d\Delta\delta} = \frac{dI_i'}{d\Delta\delta}$$

From Eq. (51)

$$\Delta\delta = F(I_1', I_2', \ldots, I_n', \Delta y_1, \Delta y_2, \ldots, \Delta y_n, x_{0_1}, x_{0_2}, \ldots, x_{0_n})$$

$$d\Delta\delta = \sum_{i=1}^{i=n}\left(\frac{\partial F}{\partial I_i'}\frac{dI_1'}{d\Delta\delta} + \frac{\partial F}{\partial \Delta y_i}\frac{d\Delta y_i}{d\Delta\delta} + \frac{\partial F}{\partial x_{0i}}\frac{dx_{0i}}{d\Delta\delta}\right)d\Delta\delta \quad (52)$$

If the above condition is satisfied, increment of deflection may increase without the increase of ΔP. Since $P + \Delta P$ is less than the critical load, the moment due to the increase of deflection alone is not sufficient to produce that deflection. Therefore

$$\sum_{i=1}^{i=n}\left(\frac{\partial F}{\partial I_i'}\frac{dI_i'}{d\Delta\delta} + \frac{\partial F}{\partial \Delta y_i}\frac{d\Delta y_i}{d\Delta\delta} + \frac{\partial F}{\partial x_{0i}}\frac{dx_{0i}}{d\Delta\delta}\right) < 1 \quad (53)$$

In the parentheses, the second and the third terms are positive because of the fact that the moment area increases as the deflection and eccentricity increase and that the eccentricity increases with deflection and $d\Delta y/dP$. But the first term may be negative when I' increases at the sections where reversal of strain occurs. Considering the extreme case with reversal of strain throughout the length of the column, from Eqs. (36) and (51),

$$\Delta\delta = \int_{L/2}^{L}\int_{L/2}^{x}\frac{\Delta P}{EI'}\left[(P + \Delta P)\frac{\Delta y}{\Delta P} + (y + x_0)\right]dx\,dx$$

$$-\eta_1 = \frac{\rho'^2}{(P + \Delta P)(\Delta y/\Delta P) + y + x_0}$$

$$I' = A'\rho'^2 = -A'\eta_1[(P + \Delta P)(\Delta y/\Delta P) + y + x_0]$$

$$\Delta\delta = \int_{L/2}^{L}\int_{L/2}^{x}\frac{\Delta P}{-EA'\eta_1}\,dx\,dx \quad (54)$$

$$d\Delta\delta = \left(\sum_{i=1}^{i=n}\frac{\partial\Delta\delta}{\partial(-A'\eta_1)_i}\frac{d(-A'\eta_1)_i}{d\Delta\delta}\right)d\Delta\delta \quad (55)$$

Let z in the following be the distance from the extreme fiber on the convex side, $z_1 = h_2 - (-\eta_1)$, $m = E/E_t$, and $bE_t'/E = f(z)$, where E_t' is the tangent modulus without considering the reversal of strain. Let

$$Q = \int_0^h zf(z)dz$$

and Q' be the moment of the modified section area about $z = 0$.

$$A' = \int_0^{z_1} mf(z)dz + \int_{z_1}^h f(z)dz$$

$$Q' = \int_0^{z_1} mf(z)zdz + \int_{z_1}^h f(z)z\,dz$$

$$h_2 = z_1 + (-\eta_1) = Q'/A'$$

$$-A'\eta_1 = Q' - A'z_1$$

$$= \int_0^{z_1}(m - 1)zf(z)dz + \int_0^h zf(z)dz - z_1\int_0^{z_1}(m - 1)f(z)dz - z_1\int_0^h f(z)dz$$

$$-A'\eta_1 = z_1\int_0^{z_1}(m - 1)f(z)dz - \int_0^{z_1}\int_0^{z_1}(m - 1)\times f(z)dz\,dz + Q - z_1\int_0^{z_1}(m - 1)f(z)dz - z_1\int_0^h f(z)dz$$

$$= Q - z_1\int_0^h f(z)dz - \int_0^{z_1}\int_0^z (m - 1)f(z)dz\,dz \quad (56)$$

From the above equation, $[d(-A'\eta_1)/dz_1] < 0$, reversal of strain increases with the increment of deflection, so $(d\Delta\delta/dz_1) > 0$.

$$\frac{d(-A'\eta_1)}{d\Delta\delta} = \frac{d(A'\eta_1)}{dz_1}\frac{dz_1}{d\Delta\delta} < 0 \quad (57)$$

From Eq. (54)

$$[\partial\Delta\delta/\partial(-A'\eta_1)_i] < 0 \quad (58)$$

$$\frac{\partial\Delta\delta}{\partial(-A'\eta)_i}\frac{d(-A'\eta)_i}{d\Delta\delta} > 0 \quad (59)$$

$$\sum_{i=1}^{i=n}\frac{\partial\Delta\delta}{\partial(A'\eta_1)_i}\frac{d(A'\eta_1)_i}{d\Delta\delta} > 0 \quad (60)$$

Equate the right side of Eq. (52) to that of Eq. (55). From Eqs. (53) and (60)

$$0 < \sum_{i=1}^{i=n}\left(\frac{\partial F}{\partial I_i'}\frac{dI_i'}{d\Delta\delta} + \frac{\partial F}{\partial \Delta y_i}\frac{d\Delta y_i}{d\Delta\delta} + \frac{\partial F}{\partial x_{0i}}\frac{dx_{0i}}{d\Delta\delta}\right) < 1 \quad (61)$$

Let the subscript I, II, III, IV, ..., N denote the order of approximation. In the successive approximation method shown in this paper, the first increment deflection curve is obtained by assuming it to be first harmonic,

$$\Delta y_{\mathrm{I}} = \Delta\delta_{\mathrm{I}}\sin(\pi x/L)$$

Then from $\Delta y_{\mathrm{I}}/\Delta P$, get η_1, x_0 and then with Δy_{I} curve, calculate $\Delta M/EI'$ with the new η_1 and x_0. Then

$$\Delta\delta_{\mathrm{II}} = \int_{L/2}^{L}\int_{L/2}^{x}\frac{\Delta M}{EI'}\,dx\,dx$$

$$\Delta y_{\mathrm{II}} = \Delta\,\delta_{\mathrm{II}} - \int_{L/2}^{x}\int_{L/2}^{x}\frac{M}{EI'}\,dx\,dx$$

Then from $\Delta y_{\mathrm{II}}/\Delta P$, get η_1, x_0. Based on Δy_{II}, calculate Δy_{III} and $\Delta\delta_{\mathrm{III}}$ by the moment area method. This process is repeated until $\Delta\delta_N$ is close enough to $\Delta\delta_{N+1}$. The above can be expressed as follows:

$$\Delta\delta_{\mathrm{II}} = \Delta\delta_{\mathrm{I}} + \sum_{i=1}^{i=n}\left[\frac{\partial F}{\partial I_i'}(I_{i_{\mathrm{II}}}' - I_{i_{\mathrm{I}}}') + \frac{\partial F}{\partial x_{0i}}\left(x_{0i_{\mathrm{II}}} - x_{0_{\mathrm{I}}}\sin\frac{\pi x}{L}\right)\right] \quad (62)$$

where $x_{0_{\mathrm{I}}}$ is the eccentricity at the center section in the

first approximation. In computing $\Delta\delta_{III}$, the moment curve based on Δy_{II} is used, while in computing $\Delta\delta_{II}$ the moment curve based on Δy_I is used.

$$\Delta\delta_{III} = \Delta\delta_{II} + \sum_{i=1}^{i=n}\left(\frac{\partial F}{\partial I_i'}\frac{dI_i'}{d\Delta\delta} + \frac{\partial F}{\partial x_{0i}}\frac{dx_{0i}}{d\Delta\delta}\right)\times (\Delta\delta_{II} - \Delta\delta_I) + \sum_{i=1}^{i=n}\left(\frac{\partial F}{\partial \Delta y_i}\frac{d\Delta y_i}{d\Delta\delta}\right)(\Delta\delta_{II} - \Delta\delta_I)$$

$$\Delta\delta_{III} - \Delta\delta_{II} = \sum_{i=1}^{i=n}\left(\frac{\partial F}{\partial I_i'}\frac{dI_i'}{d\Delta\delta} + \frac{\partial F}{\partial \Delta y_i}\frac{d\Delta y_i}{d\Delta\delta} + \frac{\partial F}{\partial x_{0i}}\frac{dx_{0i}}{d\Delta\delta}\right)(\Delta\delta_{II} - \Delta\delta_I) \quad (63)$$

Here $\Delta\delta$ is the final value to be found.

$$\Delta\delta = \Delta\delta_I + \sum_{i=1}^{i=n}\left[\frac{\partial F}{\partial I_i'}(I_i' - I_1') + \frac{\partial F}{\partial x_{0i}}\left(x_{0i} - x_{0_1}\sin\frac{\pi x}{L}\right)\right] + \sum_{i=1}^{i=n}\frac{\partial F}{\partial \Delta y_i}\frac{d\Delta y_i}{d\Delta\delta}(\Delta\delta - \Delta\delta_I) \quad (64)$$

From Eqs. (62) and (64)

$$\Delta\delta - \Delta\delta_{II} = \sum_{i=1}^{i=n}\left(\frac{\partial F}{\partial I_i'}\frac{dI_i'}{d\Delta\delta} + \frac{\partial F}{\partial \Delta y_i}\frac{d\Delta y_i}{d\Delta\delta} + \frac{\partial F}{\partial x_{0i}}\frac{dx_{0i}}{d\Delta\delta}\right)(\Delta\delta - \Delta\delta_I) \quad (65)$$

From Eqs. (63) and (65),

$$\Delta\delta - \Delta\delta_{III} = \sum_{i=1}^{i=n}\left(\frac{\partial F}{\partial I_i'}\frac{dI_i'}{d\Delta\delta} + \frac{\partial F}{\partial \Delta y_i}\frac{d\Delta y_i}{\partial\Delta\delta} + \frac{\partial F}{\partial x_{0i}}\frac{dx_{0i}}{d\Delta\delta}\right)(\Delta\delta - \Delta\delta_{II}) \quad (66)$$

$$\Delta\delta - \Delta\delta_N = \sum_{i=1}^{i=n}\left(\frac{\partial F}{\partial I_i'}\frac{dI_i'}{d\Delta\delta} + \frac{\partial F}{\partial \Delta y_i}\frac{d\Delta y_i}{d\Delta\delta} + \frac{\partial F}{\partial x_{0i}}\frac{dx_{0i}}{d\Delta\delta}\right)\times (\Delta\delta - \Delta\delta_{N-1}) \quad (67)$$

So

$$0 < \frac{\Delta\delta - \Delta\delta_N}{\Delta\delta - \Delta\delta_{N-1}} < 1 \quad (68)$$

$$0 < \frac{\Delta\delta_N - \Delta\delta_{N-1}}{\Delta\delta_{N-1} - \Delta\delta_{N-2}} < 1 \quad (69)$$

As N increases, $\Delta\delta_N$ approaches $\Delta\delta$, so this method is convergent.

References

[1] Shanley, F. R., *Inelastic Column Theory*, Journal of the Aeronautical Sciences, Vol. 14, No. 5, pp. 261–267, May, 1947.

[2] Von Kármán, Th., discussion on the previous paper.

[3] Southwell, R. V., *On the Analysis of Experimental Observations in Problems of Elastic Stability*, Proceedings of the Royal Society of London, Series A, Vol. 135, pp. 601–616, April, 1932.

[4] Southwell, R. V., *Theory of Elasticity*, pp. 424–439; Oxford Engineering Science Series.

[5] Von Kármán, Th., *Untersuchungen über Knickfestigkeit, Mitteilungen über Forschungsarbeiten*, Verein deutscher Ingenieure, Heft 81; Julius Springer, Berlin, 1910.

[6] Timoshenko, S., *Theory of Elastic Stability*, pp. 178; McGraw-Hill Book Company, Inc., New York, 1936.

[7] Chi-teh Wang, *Inelastic Column Theories and an Analysis of Experimental Observations*, Journal of the Aeronautical Sciences, Vol. 15, No. 5, pp. 283–292, May, 1948.

[8] Shanley, F. R., *The Column Paradox*, Journal of the Aeronautical Sciences, Vol. 13, No. 12, p. 678, December, 1946.

[9] Martin, G. H., *A Procedure for Determining the Critical Load for a Column of Varying Section*, Journal of the Aeronautical Sciences, Vol. 13, p. 135, March, 1946.

Steady Flow of Nonviscous Elastic Fluids in Axially Symmetric Channels

(*Continued from page 156*)

and inlet ducts of turbomachinery. For instance, it is possible to determine the flow conditions in channels that are subdivided into several flow paths by means of surfaces of revolution with respect to the axis of symmetry. With proper modifications, it is possible to use this calculating principle for the determination of three-dimensional flow patterns in rotating wheels, either of compressors or turbines, where energy is added to or taken away from the fluid.

References

[1] Weatherburn, C. E., *Advanced Vector Analysis*, G. Bell and Sons, Ltd., London, 1943.

[2] Traupel, W., *Neue Allgemeine Theorie der Mehrstufigen Axialen Turbomaschine*, p. 114; Gebr. Leemann and Co., Zürich, 1942.

[3] Stodola-Loewenstein, *Steam and Gas Turbines*, Vol. II, Eq. (20), p. 996; Petter Smith, New York, 1945.

[4] von Kármán, Th., and Biot, M. A., *Mathematical Methods in Engineering*, 1st Ed., Eq. (4.7), p. 12; McGraw-Hill Book Company, Inc., New York, 1940.

[5] Liepmann, H. W., and Puckett, A. E., *Aerodynamics of a Compressible Fluid*, Eq. (3.12), p. 26; John Wiley and Sons, New York, 1947.

[6] Wislicenus, G. F., *Fluid Mechanics of Turbomachinery*, McGraw-Hill Book Company, Inc., New York, 1947.

[7] Woodhouse, H., *Inlet Conditions of Centrifugal Compressors for Aircraft-Engine Superchargers and Gas Turbines*, Journal of the Aeronautical Sciences, Vol. 15, No. 7, pp. 403–406, July, 1948.

The Pressure on a Slender Body of Nonuniform Cross-Sectional Shape in Axial Supersonic Flow

ERNEST W. GRAHAM*

Douglas Aircraft Company, Inc.

ABSTRACT

The linearized theory for slender bodies is used to determine the pressure on an object that does not have rotational symmetry. The body extends infinitely far upstream as a circular cylinder, and in the region of interest (the distorted element) the cross section is gradually altered, without change of area, to a two-lobed shape at the downstream end of the element. The series of shapes passed through in the transition from circular to two-lobed is fixed. However, the rate at which this transition occurs (as a function of displacement in the downstream direction) may be varied.

The formula for pressure coefficient shows the dependency on rate of change of shape and also indicates that the pressure coefficient is proportional to the square of the thickness ratio of the distorted element. The thickness ratio of the distorted element is defined as the diameter of the initial circular cylinder divided by the length of the distorted element.

Since the expressions used for the perturbation velocities are independent of Mach Number, the analysis applies to transonic and subsonic flows, as well as to the supersonic case. From this fact it can be shown that, within its limits of accuracy, the linearized theory for slender bodies predicts zero wave drag for distorted elements ending in cylinders. From reference 1 (and probably from reference 2) more general conclusions may be obtained to the effect that altering only the cross-sectional shape of a body of revolution (and not the area) does not change the drag if the body ends in a cylinder or a point. From reference 1 it can also be concluded that the dependency of pure shape distortion pressures on thickness ratio squared is general.

The pressure coefficients are calculated for a particular example and appear to be of reasonable magnitude.

NOTATION

x = displacement along the x-axis (in the flow direction)
l = length of the distorted element (in the flow direction)
ξ = (x/l)
y = displacement along the y-axis
z = displacement along the z-axis
r = radius from the x-axis, $= \sqrt{y^2 + z^2}$
r_0 = radius of the initial circular cylinder
R = (r/r_0)
θ = angle of rotation about the x-axis
U_∞ = velocity at infinity (free stream)
M_∞ = Mach Number at infinity (free stream)
λ = $\sqrt{M_\infty^2 - 1}$
Φ = perturbation velocity potential
$V_{(r)}$ = radial velocity (from x-axis)
$V_{(\theta)}$ = tangential velocity (about the x-axis)
$V_{(x)}$ = axial velocity (along the x-axis)
$V_{(y)}$ = axial velocity (along the y-axis)
$V_{(z)}$ = axial velocity (along the z-axis)
$f(x)$ = a function representing the distribution of quadripole strength along the x-axis
L = $(4/U_\infty)\int_0^x f(x)\,dx$
L^* = (L/r_0^4)
$F(x, y, z)$ = a function determining body shape
G = an arbitrary function arising in the determination of the body shape
ΔW = perturbation of the absolute magnitude of the resultant velocity
Δp = increment of static pressure from free-stream value
q = dynamic pressure in free stream
C_p = pressure coefficient = $(\Delta p/q)$

Primes denote ordinary derivatives. Subscripts, unless otherwise indicated, denote partial derivatives.

Received August 9, 1949.

* Consultant in Aerodynamics, Santa Monica Plant.

INTRODUCTION

THE PURPOSE OF THIS STUDY is to determine, for slender bodies in axial flow, the order of magnitude of the pressure and drag arising from lack of rotational symmetry. Two simple classes of bodies are suggested for investigation. The first consists of bodies that have the same cross-sectional areas at every station but not the same cross-sectional shape.[3] The second class consists of bodies having similar cross-sectional shapes at every station but varying cross-sectional areas.[4] The first class is the subject of the present study.

For convenience, the type of distortion investigated is that produced by a simple quadripole distribution along the flow axis (a quadripole being produced from two dipoles as a dipole is produced from a source and sink). It is considered that a circular cylinder extends to infinity in the upstream direction. The distribution of quadripoles placed on the flow axis behind this cylinder then gradually distorts the cylinder, producing, at some distance downstream, a two-lobed cross section. The cross-sectional area is not altered at any station.

THE PERTURBATION VELOCITIES DUE TO A QUADRIPOLE DISTRIBUTION ON THE x-AXIS

The linearized equation for perturbation velocity potential in Cartesian coordinates is

$$[\Phi_{yy} + \Phi_{zz}] - \lambda^2\Phi_{xx} = 0 \qquad (1)$$

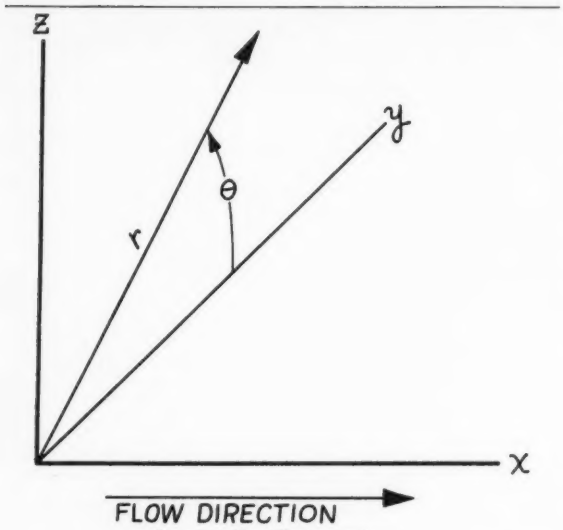

FIG. 1. Coordinate system.

or in cylindrical coordinates

$$\left[\Phi_{rr} + \frac{\Phi_r}{r} + \frac{\Phi_{\theta\theta}}{r^2}\right] - \lambda^2\Phi_{xx} = 0 \qquad (2)$$

where the expression in brackets is the Laplacian taken in a plane perpendicular to the flow direction and $\lambda = \sqrt{M_\infty{}^2 - 1}$.

It has been indicated in reference 1 that slender body theory may be obtained by using solutions of the Laplace equation in planes perpendicular to the flow. Certain restrictions are imposed on these solutions which correspond physically to a requirement that the body be smooth as well as slender.

The expression

$$\Phi = -f(x) \cos 2\theta/r^2 \qquad (3)$$

is a solution of the Laplace equation corresponding to a quadripole distribution on the x-axis, and a sufficient restriction is that $f(0) = f'(0) = f''(0) = 0$ and that $x^2f''(x)$ is not too large compared to $f(x)$. [The meaning of these restrictions is made clear by substituting the expression for Φ from Eq. (3) into Eq. (2) and noting that $\lambda^2\Phi_{xx}$ in Eq. (2) should be small by comparison with other individual terms in the equation.]

The corresponding perturbation velocities are

$$\left.\begin{aligned} \Phi_r &= 2f(x) \cos 2\theta/r^3 = V_{(r)} = \text{radial velocity} \\ \Phi_\theta/r &= 2f(x) \sin 2\theta/r^3 = V_{(\theta)} = \text{tangential velocity} \\ \Phi_x &= -f'(x) \cos 2\theta/r^2 = V_{(x)} - U_\infty = \text{axial velocity} \end{aligned}\right\} \qquad (4)$$

Determination of Body Shape from Boundary Conditions

In general, if $F(x, y, z) = 0$ is the equation determining the body shape and $V_{(x)}$, $V_{(y)}$, $V_{(z)}$, etc., are the velocities in the indicated directions, then, since the velocity component perpendicular to the surface of the body must be zero, the following equation holds:

$$V_{(x)}\frac{\partial F}{\partial x} + V_{(y)}\frac{\partial F}{\partial y} + V_{(z)}\frac{\partial F}{\partial z} = 0 \qquad (5)$$

For the present problem, it is more convenient to use cylindrical coordinates and define the body shape by $x = x(r, \theta)$, giving

$$V_{(x)} - V_{(r)}\frac{\partial x}{\partial r} - \frac{V_{(\theta)}\partial x}{r\ \partial\theta} = 0 \qquad (6)$$

Letting $V_{(x)} = U_\infty$, since the velocity perturbations are assumed small, and introducing the values of $V_{(r)}$ and $V_{(\theta)}$ from Eqs. (4) gives

$$\frac{2f(x) \cos 2\theta}{r^3}\frac{\partial x}{\partial r} + \frac{2f(x) \sin 2\theta}{r^4}\frac{\partial x}{\partial\theta} - U_\infty = 0 \qquad (7)$$

This equation may be linearized by the substitution

$$L = (4/U_\infty) \int_0^x f(x)\, dx$$

to give

$$(2 \cos 2\theta/r^3)L_r + (2 \sin 2\theta/r^4)L_\theta - 4 = 0 \qquad (8)$$

The solution is obtained by solving the following equations:

$$r^3\, dr/2 \cos 2\theta = r^4\, d\theta/2 \sin 2\theta = dL/4 \qquad (9)$$

The complete solution is

$$L + (r^4 \cos 2\theta/\sin^2 2\theta) = G(\sin 2\theta/r^2) \qquad (10)$$

where G is an arbitrary function. Assuming that the distortion is started from a circular cylinder of radius r_0, then G can be determined from the condition that $r = r_0$ when $L = 0$. It is convenient to let $L^* = (L/r_0{}^4)$ and $R = (r/r_0)$. Then, substituting into Eq. (10) and solving for R,

$$R = \left[\frac{1 + 2L^* \cos 2\theta + \sqrt{1 + 4L^* \cos 2\theta + 4L^{*2}}}{2}\right]^{1/4} \qquad (11)$$

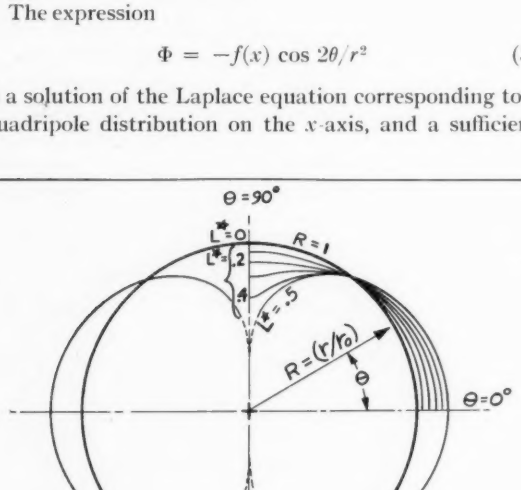

FIG. 2. Cross sections of the distorted element.

This equation describes a particular cross-sectional shape for each value of L^*, as shown in Fig. 2. If L^* is chosen to be some function of x, a particular cross-sectional shape is produced at each station along the flow axis.

Determination of the Pressure Coefficient

If ΔW (the perturbation of the absolute magnitude of the resultant velocity) is small by comparison with the free stream velocity, U_∞, then

$$C_p = -(2\Delta W/U_\infty) \tag{12}$$

Retaining the radial and tangential velocities affecting ΔW gives, with sufficient accuracy,

$$C_p = -\left[\frac{2\Phi_x}{U_\infty} + \left(\frac{\Phi_r}{U_\infty}\right)^2 + \left(\frac{\Phi_\theta}{rU_\infty}\right)^2\right] \tag{13}$$

Substituting into Eq. (13) the perturbation velocities corresponding to a quadripole distribution along the x-axis [see Eqs. (4)],

$$C_p = \frac{2f'(x)\cos 2\theta}{r^2 U_\infty} - \left(\frac{2f(x)}{r^3 U_\infty}\right)^2 \tag{14}$$

For convenience, let l be the length of the distorted element and let $\xi = (x/l)$. Since $f(x) = (U_\infty/4)(dL/dx)$ with $L = L^* r_0^4$ and since $R = r/r_0$, the following equation is obtained from Eq. (14):

$$C_p = \left(\frac{r_0}{l}\right)^2\left[\frac{d^2L^*}{d\xi^2}\frac{\cos 2\theta}{2R^2} - \left(\frac{dL^*}{d\xi}\right)^2\frac{1}{4R^6}\right] \tag{15}$$

If $(2r_0/l)$ is defined as the thickness ratio of the distorted element, then the pressure coefficient is proportional to the square of the thickness ratio. Although Eq. (15) applies only to the specific type of cross-sectional shape distortion considered here, the dependency of pressures due to shape distortion on the square of the thickness ratio is actually general, as can be demonstrated from the equations in reference 1.

From Eq. (15) it is possible to show in some specific cases that the distorted elements have zero wave drag. However, from Eqs. (4) it is seen that the perturbation velocities are independent of Mach Number, and the analysis therefore applies to transonic and subsonic flows, as well as to the supersonic case. It is known that a body ending in a cylinder has no pressure drag in an incompressible flow. Then, since the present method predicts the same pressure drag for supersonic as for incompressible flow, it cannot accurately predict any pressure drag supersonically for bodies ending in a cylinder. Reference 1 shows that, for a body of revolution ending in a cylinder or a point, the drag is not altered by changing only the cross-sectional shape. This is true within the limits of accuracy of the linearized theory for slender bodies. An equation for drag obtained by Ward[2] suggests a similar result.

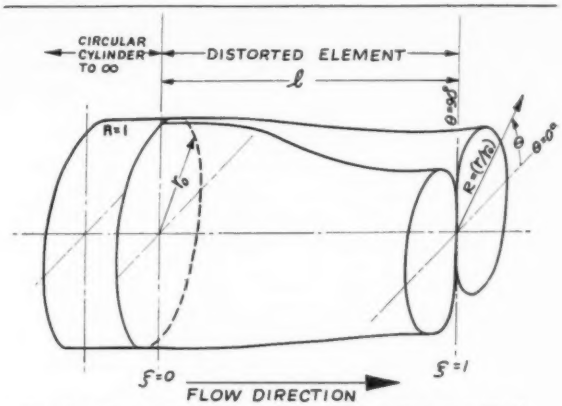

Fig. 3. Shape of element (example with radius magnified).

Example

As an example, consider a body that starts as a circular cylinder and undergoes a gradual transition to a two-lobed cylinder, as defined by Eq. (16):

$$L^* = (1/4)\{1 - \cos[\pi\xi^2(2\xi - 3)]\} \tag{16}$$

The distorted element extends from $\xi = 0$ to $\xi = 1$, since $L^* = 0$ at $\xi = 0$ and $L^* = 1/2$ at $\xi = 1$. It can be checked by differentiation that

$$L^{*\prime}(0) = L^{*\prime\prime}(0) = L^{*\prime\prime\prime}(0) = 0$$

which was specified as a requirement for smoothness.

(*Continued on page 192*)

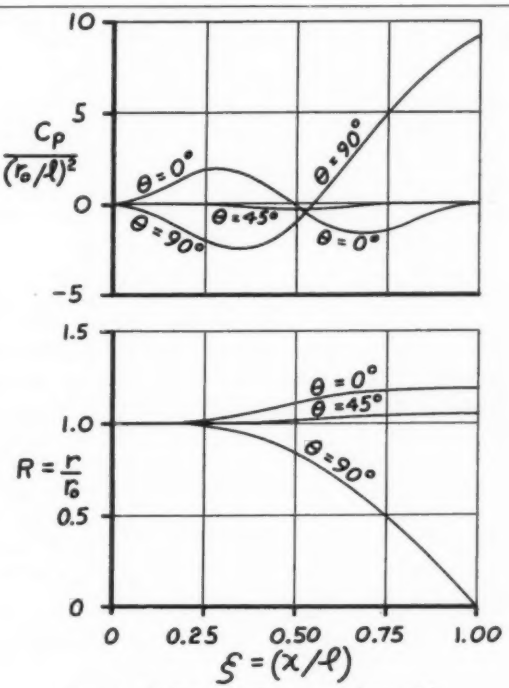

Fig. 4. Ordinates and pressures (example).

Reply to Discussions of the Wright Brothers Lecture*

A. E. RUSSELL†

The Bristol Aeroplane Company, Ltd.

A NUMBER OF THE POINTS raised in the discussion are concerned with the inherent restrictions on the operation of turbine-powered aircraft. As Mr. Kelly comments, if for any reason it becomes necessary to depart from the flight plan, there is, by comparison with piston-engined aeroplanes, much reduced flexibility of choice of operating speed and altitude. Mr. Hazen points out that some alleviation of this handicap is possible on a multiengined aeroplane by shutting down engines and, that with a coupled installation, this can be done without stopping propellers; so the need for an apology to the passengers would not arise.

For an aeroplane with eight engines, for each engine shut down the best altitude falls by about 4,000 ft. at the expense of about 25 m.p.h. in cruising speed and an increase of about 4 per cent of fuel consumed. In any case, reserves must be carried to provide for the possibility of inadvertent engine failure. Whereas at first sight the procedure of selecting the best combination may appear to place an added burden on the flight crew, if ambient conditions are known, there is no ambiguity as to the right course of action.

The argument Mr. Kelly used in his comparison of the net performance of aeroplanes powered with piston, turboprop, and turbojet engines is appropriate and can be extended to the case of greater ranges. It emphasises the danger of too general a conclusion and the increasing need for tailoring an aeroplane for specific routes. For example, if intermediate stops are compulsory for refuelling, then, in addition to the effect on block speed, time is lost on the ground and the cruising speed at altitude is a quite unreliable measure for journey time.

Also, the daily and seasonal variation of wind speeds, known to increase in velocity with altitude, may in some cases disproportionately penalise turbine aircraft with fuel reserves. The less flexible aeroplane suffers by its reduced ability to overcome adverse atmospheric conditions.

In making a case for the use of turboprops for short-range medium-altitude operation, Mr. Fink calls for a low-compression engine. It appears likely that, in selecting the best engine characteristics, the value of the compression ratio should bear some direct relationship to the take-off power. As it is convenient to couple units in pairs, a relatively small range of basic engine types will cover a large range of aeroplane requirements.

Mr. Hazen suggests that aircraft development may not be able to keep pace with the rapid rate of development of turbine engines. Firstly, it will never be difficult to persuade an aircraft man to accept a lower fuel consumption. If improved consumption is also accompanied by greater power, then, if there is a temporary limit on gross weight, the mean cruising altitude is raised. A general idea of the changed conditions can be had by inspection of the curves given for the engine inoperative case, but here, of course, the changes are of opposite sign. Higher power, besides increasing the altitude, raises the cruising speed and slightly improves fuel consumption. If toward the end of the flight the altitude must be limited for structural reasons, the cost in fuel can be estimated from the cruising chart.

It is unlikely that power-plant development would so outstrip aircraft development that even with a multi-engined arrangement it would be feasible or desirable to eliminate a power section.

On another point, I am sorry if I have misled anyone into supposing that the effect of flexibility of large aeroplanes at high speed will have any major effect on passenger comfort. The effect is restricted to the relative reduction of the amplitude of wing flexure due to aerodynamic damping which has a much larger influence on wing bending moment than on vertical acceleration at the centre of gravity.

Mr. Silverstein suggests that it is difficult to justify the application of turboprops for long range with the modest engine characteristics quoted in the lecture. However, starting with power-plant performance immediately available enables a general picture to be drawn, in which it is possible to place into some perspective the various related but individual problems. With so much acknowledged scope ahead for the development of turboprops, we can gain confidence that this form of power plant will produce a good balance between high performance, comfort, and operating economy over a wide range of stage distances. While a strong case can be made for other forms of power plants for the same and/or other operations, it is disturbing to reflect that, with a finite capacity for development effort, a dispersal of efforts retards development in each direction.

* "Some Factors Affecting Large Transport Aeroplanes with Turboprop Engines," by A. E. Russell, JOURNAL, Vol. 17, No. 2, pp. 67–106, February, 1950.

† Chief Designer, Aircraft Division.

The problem of gusts is in a different category, for here our concern is confined to refinement in marginal circumstances. At this stage we must question the validity of both premise and form of analysis. I agree with Mr. Silverstein that detectors on the fuselage will recognise rogue, as well as formalised, gusts. In the end, as with other aspects of safety, we must fall back on probabilities, but as yet we lack authentic statistics.

The use of the gust alleviator is not so critical as Professor Hoff suggests. Under the standard maximum gust for the aeroplane in question, the factor of safety exceeds unity at all speeds. The maximum potential alleviation greatly exceeds the needs of nominal strength requirements, so that a result that shows about 30 per cent effectiveness is adequate. The task of simplifying the signalling system is not discouraging; one might add that here there is plenty of scope.

On the question of fuselage shell stability, we are indebted to the work of Professor Hoff. If the frames appear to him to be too close, their position was dictated by window and door locations. The ultimate strength was finally established by a test to destruction on a half-scale model.

I believe that, since the example mentioned by Professor Hoff, much has been done to direct the transmission of scientific information between our two countries into accessible channels. Hitherto, it was frequently filed in obscure archives. The most effective contact is always personal, and the now established Joint Conferences should do much to reinforce the official procedure.

I find myself in accord with Mr. Wells' remarks, for, when it is necessary to introduce time as an additional parameter into structural analysis, we are ill prepared to assess the appropriate loading history. We are merely aware of the phenomenon but without means of assessing an empiricism. It is not essential for a set of design calculations to assume a close approach to precision, but it is important that departures from convention, in aircraft size or shape and in operating circumstances, shall have proper consideration on a logical basis. I share Mr. Wells' concern for the need to establish design data for gust loading for both symmetric and asymmetric application.

It is certainly fortunate that sweptback wings have built-in gust alleviation. It is also unusual for any arrangement dictated essentially by aerodynamic causes to have beneficial structural effects. These are outlined concisely in the discussion. The magnitude of such alleviation permits more than local refinement, for it plays a part in the initial selection of the design variables.

I am very encouraged to hear that the testing of scale flutter models is an effective design aid. Clearly, any form of calculation is limited by the validity of basic data; hence, if it can be argued that an experimental method reasonably simulates actual conditions or even if it merely indicates qualitative effects of changes, then the advantage of visual illustration and speed of assessment is obvious. The examples given by Mr. Wells not only justify scale flutter models but place them in the top priority of design methods.

I wish to thank all those who have contributed to this discussion, for their personal comments, and for the way in which they have amplified the subject matter. If I have succeeded in promoting a basis for further understanding, then I am proud of a small share in the unceasing flow of information, eastwards and westwards, across the Atlantic.

Readers' Forum

BRIEF REPORTS of investigations in the aeronautical sciences and discussions of papers published in the JOURNAL will be presented in this special department. The publication will be completed approximately 8 weeks after receipt of the material. No proof will be sent to the authors. The Editorial Committee does not hold itself responsible for the opinions expressed by the correspondents. Contributions should not exceed 800 words in length.

Station Functions in Flutter Analysis

J. H. Greidanus and A. I. van de Vooren
National Aeronautical Research Institute, Amsterdam
October 15, 1949

IN THE FIRST PART of the paper "Station Functions and Air Density Variations in Flutter Analysis" (JOURNAL OF THE AERONAUTICAL SCIENCES, Vol. 16, pp. 345–353, June, 1949), Manfred Rauscher has presented a method of calculating frequencies and modes of continuous systems of which the essential features are:

(i) The determination of an interpolation function $f(y)$ to the deflections $z_i (i = 1, 2, \ldots, n)$ at a series of reference stations y_i, representable by

$$f(y) = \sum_{i=1}^{n} z_i f_i(y), \qquad 0 \leq y \leq 1 \tag{1}$$

where the $f_i(y)$ are *station functions*—i.e., functions which vanish at all reference stations except one, this station being different for every function of the set.

(ii) The identification of assumed and calculated deflections *at the reference stations*, the calculated deflections being obtained from inertia loads based on the assumption (1) by means of influence functions.

It is suggested, though not stated explicitly, that the reference stations should divide the interval in equal parts. It is recommended to identify the station functions with continuous functions, having continuous derivatives up to the second order (in the case of bending), satisfying the geometrical and one of the dynamic boundary conditions, and representable *within each subinterval* by polynomials in y of lowest possible degree.

Now the polynomial approximation of modes is a classical procedure of vibration analysis.[1,2] Using one polynomial in the full interval, imposing the full set of geometrical and dynamic boundary conditions as usual, and restricting the degree (again for bending vibrations) to the fourth, fifth, etc., for subsequent exemplars from the required set, the following well-known three-term polynomials result:[1]

$$1/6(n+2)(n+3)y^{n+1} - 1/3n(n+3)y^{n+2} + 1/6n(n+1)y^{n+3}; \qquad n = 1, 2, \text{etc.} \tag{2}$$

Comparing this method with Rauschers', it is not clear what kind of advantages should result from the neglect of one dynamic boundary condition and the introduction of discontinuities, at the reference stations, in the third-order derivative. The classical polynomials do not have the station-function characteristic, but could easily be made to do so by suitable linear recombination. There is, in general, no advantage in this reduction, but Rauscher states that gains in convenience result, connected with the representation of unspecified aerodynamic finite span corrections in flutter calculations. Now, since these corrections, to be applied to the aerodynamic loading, will doubtlessly be linear, and since they are stated to vanish with tip deflection, they are evidently proportional to tip deflection, the probably complex ratio depending on y (giving the spanwise distribution of the correction) and perhaps on reduced frequency and aspect ratio. If so, no labor saving of any importance seems imaginable.

The proposition to improve station functions by application of the transformation

$$f_i^{(1)}(n) = \int_0^1 K(n, y) m(y) f_i^{(0)}(y) dy$$

where $K(\eta, y)$ = influence function, $m(y)$ = mass distribution, agrees again with a well-known procedure of vibration analysis,[1] applicable with equivalent success to all "zero-order" approximations of modes. The transformation reduces the components of disturbing modes and leads, when iterated, to the fundamental mode. When not only the fundamental but also overtones must be calculated, its application in combination with collocation or Rayleigh type analysis should be handled with some care, since otherwise even desired modes may disappear. To prevent this, computations should be made with an increased number of figures.

Concerning recommendation (ii), it is not clear why the collocation method has been preferred to the Rayleigh-Ritz-Galerkin method, which has the beneficial property of second-order errors in the frequencies, when the errors in the modes are considered to be of the first order, at least if the differential equation (*s*) of the system is (are) self-adjoint. The recommended method generally leads to first-order frequency errors.

When for some reason or other, use of collocation method is preferred, it can be shown to yield the best results when the collocation points coincide with the nodes of the first disturbing mode. In the example of the uniform beam of which the lowest two bending frequencies and modes have been calculated, the collocation points should be taken at the nodes of the third mode—i.e., at $y \sim 0.50$ and $y \sim 0.87$. Though one should be very careful in checking the theoretical considerations developed above by one *single* example, it may be of interest to compare results for the calculation of the lowest two bending frequencies ν_1, ν_2 of the uniform beam.

	ν_1	ν_2
I	3.52197	22.2789
II	3.51600	22.1780
III	3.51721	22.1440
IV	3.51604	22.7127
V	3.51602	22.0345

I = station functions, collocation at $y = 0.5$ and $y = 1$ (Rauscher); II = same station functions, collocation at $y = 0.5$ and $y = 0.87$; III = same station functions, Rayleigh; IV = polynomials (2) for $n = 1$ and $n = 2$, Rayleigh; V = exact.

All results are as expected, except that the continuous polynomials appear to be less suitable for an accurate representation of the overtone. This feature should, however, be considered as purely incidental and the same polynomials will doubtlessly be particularly efficient for certain beams of different stiffness or mass distribution. Finally, it may be remarked that, though an analysis on concentrated-mass basis requires a far greater number of reference sections, useless roots never are calculated when applying a matrix iteration method instead of solving a characteristic equation. Performed in this way, a concentrated-mass analysis remains a possible alternative to the Rayleigh analysis with simple polynomials.

REFERENCES

[1] Duncan, W. J., *Galerkin's Method in Mechanics and Differential Equations*, R. and M. 1798, 1937.

[1] Biezeno, C. B., and Grammel, R., *Technische Dynamik*, p. 747; J. Springer, Berlin, 1939.
[2] Biezeno, C. B., and Grammel, R., loc. cit., p. 169.

Author's Reply

In Part I of my paper on "Station Functions and Air Density Variations in Flutter Analysis," to which the preceding note refers, a relatively large amount of space is given to the development of the interpolation idea from elementary beginnings. The example of a uniform cantilever beam is used to show how the idea works out under simple conditions and how the accuracy of the outcome depends on the care of the interpolation. It is then observed that the use of standard polynomials, while satisfactory with the continuous beam, will prove unsatisfactory when there are discontinuities both in the elastic and in the inertial properties of a system—hence, the suggestion that the interpolation functions be adapted to the peculiarities of the system. This adaptation proposal, not the passing glance at the familiar polynomials, is the cardinal feature of the discussion.

A careful reader of the original paper might have noted that the polynomials chosen for illustration were of third degree, instead of fourth or higher, because they were intended to be intermediate between the straight-line functions on the one hand (which did obvious and serious violence to the boundary conditions) and the functions based on triangular loadings on the other hand (which took the boundary conditions into meticulous account). There was no expectation, implied or expressed, that any advantages, beyond a simplification of the interpolation functions, should result from the neglect of one of the dynamic boundary conditions in this case. As the condition violated was that of continuity of shear, the inaccuracies resulting from the violation are traceable to fictitious concentrations of loads at the points concerned. The quality of the results thus permits a judging of the possible satisfactoriness of an experimental determination of interpolation functions by means of concentrated loadings on a structure. Such a determination has been used with success in a Station Function analysis of the vibrations of a sweptback plate.[1]

With regard to the recommended procedure of adapting the Station Functions to the nature of a system, Greidanus and van de Vooren take the view that the scheme is simply the one underlying the well-known transformation formula they quote. A more careful scrutiny of the proposed plan should make clear to them that this view is mistaken. The determination of the functions in the manner actually suggested in the paper involves neither collocation nor any other type of explicit comparison between a first and a second set of deflections. The *subsequent* use of the functions in a collocation operation according to the formula quoted does *not* serve to supply or improve the Station Functions. Iterations and other processes of successive refinement, with all their familiar troubles of mode suppression, etc., are deliberately avoided through the painstaking initial choice of the functions.

The reduction of interpolation functions of any sort to the form of Station Functions was admitted to be a matter of preference, not necessity. The Station Function form of the expressions does, however, have the advantages of maximum physical clarity and of allowing the most convenient tie-in between the motions of the distributed masses and of masses concentrated at the reference stations. This tie-in makes it natural to choose the stations at points of mass concentration. It is emphatically not suggested, as Greidanus and van de Vooren take it to be, that the reference stations should always have uniform intervals between them—though equal spacings will usually be chosen when there are no reasons for another preference.

The methods of Rayleigh-Ritz, Galerkin, and Least Squares were not overlooked by me. Twenty years ago,[2] I suggested a simple Rayleigh-type procedure that does not seem too hopelessly out of date today. Concrete experience, not abstract speculation, has led to the belief that the Station Function method offers an especially favorable combination of convenience and accuracy for the unified handling of the still-air and moving-air phases of the problem. As the interpolation curves adjusted to a system's properties already are close to the exact deflection curves, there would actually be little gain from an averaging out of the differences by an integration process instead of the proposed method of simple collocation. The table of comparative results in the preceding note makes this clear even with the crude Station Functions that are taken for illustration.

It is recognized, of course, that the determination of the suggested interpolation curves by integration of static load-deflection curves requires a substantial advance investment of labor. This investment is, however, smaller than that commonly made to determine interpolation curves in the form of natural mode lines; it is believed to result in a gain in economy, as well as a gain of transparency, through the unification of method it permits in the handling of the flutter problem as one whole.

Admittedly, the discrete-point method offers an alternative way of treating the still-air and the moving-air phases of the problem according to a single general plan. This alternative may remain appealing to someone so accustomed to it that he no longer notices its tediousness. But the fact is that the numerous useless roots, even though they need not be calculated, do impede the solution for the useful roots. Also, the matrix iteration process frequently is held up by the proximity of two roots, especially those corresponding to the second and third coupled modes of a typical wing, and the whole iteration plan bogs down discouragingly when the analysis advances from the still-air to the moving-air phase of the problem. Still, in spite of these shortcomings, there certainly is no denying of the method's record of great utility.

Corrections of the aerodynamic effects for the influences of finite span have been proposed by various authors, notably Reissner, Biot, Jones, Küssner, and Cicala. My research group has been in closest touch with Reissner and is most familiar with his method of correction.[3] The finite span effects are being considered with increasing seriousness in advanced American practice. Because their incorporation into the analysis involves considerable extra labor, a careful planning of the procedure is of some importance. The desirability of having all but one of the deflection functions go to zero at the tip, which Greidanus and van de Vooren question, comes from the fact that the Fourier series for all but one of the component circulation or load distributions will then be rapidly convergent. It is true, of course, that the aerodynamic loading must come to the same total, no matter how it is built up of component loadings. The benefit of the plan advocated in the original paper is that it does simplify the computation work.

As far as the overall worth of the Station Function method is concerned, a fair judgment can naturally not be formed on the scant basis of an outline description. For this reason, the original paper made clear reference to the fuller reports submitted to the Bureau of Aeronautics, which also contain a fuller bibliography. A consultation of the reports in question and direct communication with me and my associates at M.I.T. are suggested as the best ways of clearing up points that may still remain obscure to anyone desirous of getting all the known facts about the method.

References

[1] Mollø-Christensen, E., *The Method of Station Functions and Its Application to Problems in Two Variables*, S.M. Thesis in Aeronautical Engineering, M.I.T., June, 1949.
[2] Rauscher, M., *Ueber die Schwingungen freitragender Fluegel*, "Luftfahrtforschung," Vol. IV, pp. 94–106, 1929.
[3] Reissner, E., and Stevens, J., *Effect of Finite Span on the Air Load Distributions for Oscillating Wings*, N.A.C.A. T.N. Nos. 1194 and 1195, October, 1947.

A Note on the Velocity of Sound

M. V. Morkovin
University of Michigan, Ann Arbor, Mich.
October 17, 1949

REFERENCE 1 called attention to a certain lack of rigor found in most of the elementary derivations of the formula for the speed of sound. The main point of the criticism was that the ratio $dp/d\rho$ was indeterminate in the sound wave and should not be treated as a derivative. While agreeing about the lack of rigor in the customary derivations, the present note concludes that the key to the confusion is not the alleged indeterminateness of $dp/d\rho$ but the lack of clarity in specifying the variables involved, especially the independent variables. In his counterexample, the author of reference 1 unfortunately forgets which quantities are variable and which are constant under the original assumptions of his problem.

(1) The assumptions of the problem are those of steady, continuous, adiabatic flow, without viscosity, in a duct of constant area. Then and only then Eqs. (1), (2), and (3) of reference 1—namely, $\rho\, du + u\, d\rho = 0$, $\rho u\, du + dp = 0$, and $u\, du + C_p\, dT = 0$—are valid simultaneously. These assumptions imply a flow at constant entropy, s, as the elimination of the term $C_p\, dT$ [which equals $T\, ds + (dp/\rho)$] between Eqs. (2) and (3) demonstrates. As the author of reference 1 remarks, these equations admit only the "trivial" solution u = constant, p = constant, ρ = constant; in an isentropic flow through a one-dimensional duct, there is simply no agency that could cause a change in these quantities.

The counterexample of reference 1 considers the particular solution of these equations, $u^2 = \gamma p/\rho$. This is one of the family of the constant solutions above, for which the constant values of the quantities u, p, and ρ are numerically related. Under the assumptions of the duct problem $du = 0$, $dp = 0$, and $d\rho = 0$, Eqs. (1), (2), and (3) are satisfied *without any contradiction*.

In order to allow a continuous change of u, p, and ρ, in steady flow through a constant area duct, as reference 1 assumes without explicit statement, one of the other assumptions must yield. The usage of Eq. (2) in the counterexample implies that the flow is still assumed nonviscous but that heat may be added steadily. This and the usage of $u^2 \equiv \gamma p/\rho$ *as an identity* for all flows in the given duct of necessity leads to nonisentropic processes characterized by Eq. (7) of reference 1. There is no contradiction, merely a misunderstanding.

(2) When more complicated flows are considered, such as viscous and diabatic flows, a more careful specification of the thermodynamic process corresponding to the phenomenon of propagation of sound is in order. The properties of a homogenous medium that is in thermodynamic equilibrium depend upon two independent variables, say ρ and s. In particular, $p = f(\rho, s)$. Following reference 2, a complete and rigorous definition of the speed of sound is obtained through the identity

$$a^2 \equiv \left(\frac{\partial p}{\partial \rho}\right)_s \equiv f_\rho(\rho, s) \tag{4}$$

It is immediately recognized that the use of the ratio $dp/d\rho$ from Eqs. (1), (2), and (3) is covered by definition (4).

(3) In order to dispose of the question of indeterminateness of the ratio $dp/d\rho$, it is merely necessary to use exactly the same reasoning as reference 1 did in its derivation of the limit $u_1^2 \to \gamma p_1/\rho_1$ as a shock wave approaches a sound wave. A somewhat tedious manipulation of the three conservation laws valid across a shock wave[3] leads to

$$\frac{p_2 - p_1}{\rho_2 - \rho_1} = \gamma\, \frac{p_1 + [(p_2 - p_1)/2]}{\rho_1 + [(\rho_2 - \rho_1)/2]} \tag{5}$$

As the strength of the shock wave vanishes, the ratio in question approaches not only a determinate value but also the "correct" one, $\gamma p_1/\rho_1$. Since, furthermore, $(s_2 - s_1)$ approaches zero, the concept of a sound wave as a limit of a shock wave checks with definition (4). Incidentally, Eq. (5) is valid for unsteady flows, and our deductions are general.

(4) Finally, it is proper to remark that Lamb's "rigorous" derivation of the equation for the speed of sound, recommended by reference 1, is subject to exactly the same criticism as the elementary derivations originally criticized. Lamb[4] assumes the determinateness of $dp/d\rho$ and a specific thermodynamic process with ρ as independent variable when he replaces $\partial p/\partial x$ by $(dp/d\rho)(\partial\rho/\partial x)$. The further assumption of infinitesimal pressure and density changes identifies the process as isentropic.

References

[1] Morduchow, M., *A Note on the Velocity of Sound*, Readers' Forum, Journal of the Aeronautical Sciences, Vol. 16, No. 10, p. 635, October, 1949.

[2] Courant, R., and Friedrichs, K. O., *Supersonic Flow and Shock Waves*, p. 5; Interscience Publishers, New York, 1948.

[3] Sauer, R., *Introduction to Theoretical Gas Dynamics*, English Ed., pp. 99–101; Edwards Bros., Ann Arbor, Mich., 1947.

[4] Lamb, H., *Hydrodynamics*, 6th Rev. Ed., pp. 476–477; London, 1932; reprinted by Dover Publications, New York, 1945.

Further Remarks on the Velocity of Sound

Morris Morduchow
Department of Aeronautical Engineering and Applied Mechanics, Polytechnic Institute of Brooklyn, Brooklyn, N.Y.
November, 1949

I SHOULD LIKE, if possible, to eliminate any confusion that may arise from a comparison of references 1 and 2.

In reference 1, item (1), it is at first agreed that Eqs. (1), (2), and (3) of reference 2 imply u, p, ρ, and T to be constants (with the space variable x). This, however, appears to be forgotten in the second part of item (1), reference 1, where it is attempted to explain the contradiction pointed out by Eqs. (4)–(7) in reference 2 with the statement that, if the equation

$$u^2 = \gamma(p/\rho) \tag{a}$$

is treated as an identity, then this merely replaces Eq. (3) of reference 1 and implies a "nonisentropic process." The fact that is overlooked in reference 1 is that the set of Eqs. (1) and (2) of reference 2, and Eq. (a) will also imply only the "trivial" type of solution: p, ρ, u constant. Consequently, these equations cannot imply any "process" at all in which p may be considered as varying as a function of ρ. It is implied in reference 1 that Eq. (7) of reference 2 represents such a "process." However, a different and contradictory "process" could have been mathematically arrived at by substituting $u\, du = (1/2)\gamma d(p/\rho)$ into Eq. (1), instead of Eq. (2), of reference 2. Then one would obtain $p = k/\rho$, contradicting Eq. (7). Moreover, contrary to the belief in reference 1, even an "isentropic process" could be mathematically arrived at by substituting Eq. (a) into Eq. (4) [which was obtained from Eqs. (1) and (2)] of reference 2. As implied in reference 2, such apparent contradictions are bound to occur when equations like Eqs. (1), (2), and (3) of reference 2—or Eqs. (1), (2), and (a)—are incorrectly treated as if the quantities p and u could be considered as dependent variables with ρ as independent variable, instead of remembering that all of the quantities u, p, T, and ρ are really constants in these equations, with the space variable x as the independent variable. (If there does exist any confusion with respect to dependent and independent variables, it is thus in reference 1.)

In reference 1, it is agreed that "elementary derivations" often lack rigor, but the author is fairly vague with respect to just where the rigor is lacking. Perhaps the entire discussion can be clarified and all apparent inconsistencies avoided if it is realized that a set of equations like Eqs. (1), (2), and (3) of reference 2 can be readily transformed into a set of algebraic equations in which all quantities are simply constants. This can be done (e.g., reference 2) by establishing the shock-wave equations and then considering a sound wave as the limit of a weak shock wave. Reference 1 [item (3)] is in agreement with reference 2 in this regard. However, since all quantities are identically constants, it is doubtful that differential expressions such as $a^2 = dp/d\rho$ can be properly derived and interpreted by such means.

With respect to item (4) of reference 1, it may be remarked that the only assumption in the derivation of the sound velocity in reference 3 is that p is a function of ρ and of ρ only. Although such an assumption, as shown in reference 2 and in the present note, leads to mathematical inconsistencies in the steady one-dimensional differential equations of nonviscous flow without heat addition, it does not lead to such inconsistencies in the unsteady-flow equations, since the latter equations admit of general solutions other than the "trivial" type.

References

[1] Morkovin, M. V., *A Note on the Velocity of Sound*, Readers' Forum, Journal of the Aeronautical Sciences, Vol. 17, No. 3, p. 180, March, 1950. (See preceding item.)

[2] Morduchow, M., *A Note on the Velocity of Sound*, Readers' Forum, Journal of the Aeronautical Sciences, Vol. 16, No. 10, p. 635, October, 1949.

[3] Lamb, H., *Hydrodynamics*, 6th Rev. Ed., pp. 476–477, London, 1932; reprinted by Dover Publications, New York, 1945.

On the Compressibility Correction for Subsonic Unsteady Flow

John W. Miles

Department of Engineering, University of California at Los Angeles

September 26, 1949

In a previous item in this column,[1] we set forth a transformation that reduced the problem of low-frequency harmonic motion of a supersonic airfoil to an equivalent problem in steady flow. A general study of low-frequency unsteady-flow effects at all speeds was recently (Summer, 1949) undertaken at the Aerophysics Laboratory of North American Aviation, Inc., and, as a part of this study, a similar transformation has been applied to reduce low-frequency unsteady-flow problems in subsonic compressible flow to equivalent problems in incompressible flow.

The linearized boundary value problem for the oscillating wing may be posed as

$$\left[\nabla^2 - M^2\left(\frac{\partial}{\partial x} + ik\right)^2\right]\phi(x,y,z) = 0 \tag{1}$$

$$\phi_z(x,y,0\pm) = w(x,y), \quad \underline{(x,y) \text{ in } S_1} \tag{2}$$

$$\phi(x,y,0\pm) = \pm\phi(x_1,y,0+)\exp[-ik(x-x_1)], \quad \underline{(x,y) \text{ in } S_2} \tag{3}$$

$$\phi(x,y,0) = 0, \quad \underline{(x,y) \text{ in } S_3} \tag{4}$$

$$k = (\omega b/U) \tag{5}$$

where a flow of velocity U and Mach Number M is directed along the x axis over an airfoil for which the projection on $z = 0$ is S_1 and which has the prescribed normal velocity $w(x,y)\exp(i\omega t)$. The regions S_2 and S_3 represent the wake [including the trailing edge, $x = x_1(y)$] aft of the wing (S_1) and the remainder of the plane $z = 0$, respectively; k is the reduced frequency; and b is the unit of length. Eq. (3) states that the potential is discontinuous across the vortex sheet constituting the wake, while the pressure is continuous there. If we introduce the transformation

$$x' = x, \quad y' = \beta y, \quad z' = \beta z, \quad b' = \beta^{-1} b \tag{6}$$

$$\phi'(x',y',z') = \exp(-i\lambda x)\phi(x,y,z) \tag{7}$$

$$w'(x',y') = \beta^{-1}\exp(-i\lambda x)w(x,y) \tag{8}$$

$$k' = (k/\beta^2) \tag{9}$$

$$\beta = (1 - M^2)^{1/2} \tag{10}$$

we find that Eq. (1) transforms to

$$[\nabla^2 + (k'M)^2]\phi'(x',y',z') = 0 \tag{11}$$

while the boundary conditions (2), (3), and (4) remain invariant, except for the scale transformation of S_1, S_2, and S_3. Hence, if we neglect terms of order $(k'M)^2$ (and possibly, order $k^2 \ln k$), our problem is reduced to one in incompressible flow. The transformation law for the potential follows as

$$\phi\left\{\frac{x}{b}, \frac{y}{sb}, \frac{z}{\delta b}, \frac{w}{U}, k, M\right\} = \beta^{-1}[1 + i\lambda(x/b)] \times \phi\left\{\frac{x}{b}, \frac{y}{\beta sb}, \frac{z}{\beta\delta b}, [1 - i\lambda(x/b)]\frac{w}{U}, (k/\beta^2), 0\right\} + 0[(kM/\beta)^2] \tag{12}$$

s and δ are aspect and fineness ratios, respectively. In general, the dependence of ϕ on (w/U) is linear and homogeneous, the notation being operational. The transformation law for the pressure on the wing is found to be

$$p\left\{\frac{x}{b}, \frac{y}{sb}, \frac{w}{U}, k, M\right\} = \beta^{-1} p\left\{\frac{x}{b}, \frac{y}{\beta sb}, \frac{w}{U}, (k/\beta^2), 0\right\} + i(kM^2/\beta^3)\left[(x/b)p\left\{\frac{x}{b}, \frac{y}{\beta sb}, \frac{w}{U}, 0, 0\right\} - p\left\{\frac{x}{b}, \frac{y}{\beta sb}, \left(\frac{x}{b}\cdot\frac{w}{U}\right), 0, 0\right\}\right] + 0[(kM/\beta)^2] \tag{13}$$

Our extension of the Prandtl-Glauert rule, as represented by Eq. (13), may now be stated as follows: To find the pressure distribution on an airfoil of aspect ratio s executing harmonic motion at reduced frequency k in a subsonic compressible flow, we calculate the pressure distribution on a second airfoil of aspect ratio βs and reduced frequency k/β^2 executing the same motion, add to this the distribution on the same airfoil multiplied by $i\lambda(x/b)$, subtract the distribution for the second airfoil with a new downwash $i\lambda(x/b)w$, neglect unsteady flow effects in the last two distributions, and divide the overall result by β. In carrying out these operations, it should be specifically remarked that any frequency dependence exhibited by w is not to be modified throughout the transformation, except insofar as parts of it may be neglected in conformance with the previous approximations.

It should be understood that these above results are not applicable to two-dimensional problems, since the solution for ϕ would involve integration over the infinite span, and this integration generally would not be commutative with the assumed expansion in powers of the frequency. The solution for low-frequency compressible flow has been given earlier,[2] and the compressibility correction obtained therein is rather more complex than that outlined above. Moreover, it is of particular interest that the logarithmic frequency term entering the two-dimensional solution is anomalous, and an examination of the low-frequency limit of the three-dimensional results[3] shows this logarithmic term to be important only for very large aspect ratios (say, $s > 10$).

Finally, we remark that the foregoing results are valid only for planar (wing) problems because of the assumed form of the boundary conditions.

REFERENCES

[1] Miles, J. W., *On Harmonic Motion at Supersonic Speeds*, Readers' Forum, Journal of Aeronautical Science, Vol. 16, No. 6, pp. 378–379, June, 1949.

[2] Miles, J. W., *Quasi-stationary Thin Airfoil Theory in Compressible Flow*, Readers' Forum, Journal of Aeronautical Science, Vol. 16, No. 7, p. 440, July, 1949.

[3] Reissner, E., and Stevens, J. E., *Effect of Finite Span on the Airload Distributions for Oscillating Wings—II*, N.A.C.A. T.N. No. 1195, 1947.

Upper and Lower Bounds on Variational Integral in Compressible Flow

G. V. R. Rao
New York University, New York, N.Y.

November 1, 1949

BECAUSE OF THE INHERENT DIFFICULTIES in obtaining solutions for compressible flow equations, we have no way of estimating the error in the solution. By variational methods,[3] an approximate solution can be obtained. Braun[1] formulated an integral, the first variation of which leads to a linear differential equation for the perturbation potential. When the domain extends to infinity, the integral has to be properly corrected by the addition of a boundary integral as indicated by Wang.[3] The correct form of the variational integral would then be as given below. A value of $\gamma = 2$ is used for simplicity in representation.

$$I_L = \int\int \left\{ 2\phi_2 \left(\frac{\partial F}{\partial x}\frac{\partial \phi_i}{\partial x} + \frac{\partial F}{\partial y}\frac{\partial \phi_i}{\partial y} \right) - F\left[\left(\frac{\partial \phi_2}{\partial x}\right)^2 + \left(\frac{\partial \phi_2}{\partial y}\right)^2 \right] + 2\left(\frac{\partial \phi_i}{\partial x}\frac{\partial \phi_2}{\partial x} + \frac{\partial \phi_i}{\partial y}\frac{\partial \phi_2}{\partial y} \right)^2 \right\} dx\, dy \quad (1)$$

where

ϕ_i = velocity potential for incompressible flow
ϕ_2 = perturbation potential
$F = q_m^2 - (\partial\phi_i/\partial x) - (\partial\phi_i/\partial y)^2$
q_m = maximum velocity that could be obtained by expansion into vacuum

The approximation involved in using $\gamma = 2$ was investigated by Wang.[3] Because the present problem is linear in its nature, a value of $\gamma = 1.5$ or $1^1/_2$ could be used without involving elaborate computations.

By the application of Friedrichs' method[2] to the above integral, an adjoint minimum problem is formulated. The integrand of the above variational integral is denoted by G, and we set

$$\partial G/\partial u_2 = a; \quad \partial G/\partial v_2 = b \quad (2)$$

where $u_2 = \partial\phi_2/\partial x$ and $v_2 = \partial\phi_2/\partial y$.

It can be easily verified that the first variation of the integral leads to the differential equation

$$(\partial a/\partial x) + (\partial b/\partial y) - f = 0 \quad (3)$$

where

$$f = 2\left(\frac{\partial F}{\partial x}\frac{\partial \phi_i}{\partial x} + \frac{\partial F}{\partial y}\frac{\partial \phi_i}{\partial y} \right)$$

The natural boundary condition $\partial\phi_2/\partial n = 0$ on the body can be expressed as

$$a(\partial x/\partial n) + b(\partial y/\partial n) = 0 \quad (4)$$

The relations (2) can be solved explicitly for u_2 and v_2

$$u_2 = \frac{-aF + 2a\left(\frac{\partial \phi_i}{\partial y}\right)^2 - 2b\,\frac{\partial \phi_i}{\partial x}\frac{\partial \phi_i}{\partial y}}{2F^2 - 4F\left[\left(\frac{\partial \phi_i}{\partial x}\right)^2 + \left(\frac{\partial \phi_i}{\partial y}\right)^2\right]} \quad (5)$$

and

$$v_2 = \frac{-bF + 2b\left(\frac{\partial \phi_i}{\partial x}\right)^2 - 2a\,\frac{\partial \phi_i}{\partial x}\frac{\partial \phi_i}{\partial y}}{2F^2 - 4F\left[\left(\frac{\partial \phi_i}{\partial x}\right)^2 + \left(\frac{\partial \phi_i}{\partial y}\right)^2\right]}$$

The conjugate functional can be written as

$$J_L = \int\int (1/2)(u_2 a + v_2 b)\,dx\,dy \quad (6)$$

with u_2 and v_2 expressed explicitly in terms of a and b. We will choose

$$\left.\begin{aligned} a &= 2F\,(\partial\phi_i/\partial x) + \psi_y \\ b &= 2F\,(\partial\phi_i/\partial y) - \psi_x \end{aligned}\right\} \quad (7)$$

satisfying Eq. (3), a priori. By this artifice the integral (6) can be expressed in terms of derivatives of ψ. For the function ψ, we can choose any function of order less than $1/r$, and satisfying the boundary condition $\partial\psi/\partial s = 0$ on the body.

Thus we have a new variational integral (6) which, together with the integral (1), gives us bounds on the value of the integral. From a solution obtained by minimizing integral (6), we can, with the aid of Eqs. (5) and (7), gather information on the approximations involved in the velocities.

REFERENCES

[1] Braun, G., *Die ebene Kompressible Potentialstromung als Variations—und Eigenwert Problem*, *Ann. d. Phys.*, Vol. 15, No. 6, pp. 645–676, December, 1932.

[2] Friedrichs, K. O., *Ein Verfahren der Variationsrechnung das Minimum eines Integral als das Maximum eines anderen Ausdruckes darzustellen*, Nachrichten von der Gesellschaft der Wissenschaften zu Gottingen, Mathematisch-physikalische Klasse, pp. 13–20, 1929.

[3] Wang, C. T., *Variational Method in the Theory of Compressible Fluid*, Journal of the Aeronautical Sciences, Vol. 15, No. 11, p. 675, November, 1948; Readers' Forum, Errata, Vol. 16, No. 2, p. 125, February, 1949.

Heat Addition to a Flowing Gas

Roger Weatherston
Cornell Aeronautical Laboratory, Inc., Buffalo, N.Y.

November 28, 1949

THE FOLLOWING RESULTS of experiments that have been conducted at Cornell Aeronautical Laboratory may be of interest in connection with recent discussions[1–6] of the problem of heat addition to a flowing gas.

A 6-in. diameter, 6-ft. long tube was placed axially in a free jet of air. Heat was added to the internal flow by means of Picatinny Arsenal 13-B flares that discharged transversally into the flow through flush wall openings at a short distance (about 18 in.) from the tube inlet. Inlet and outlet Mach Numbers and stagnation temperatures were measured by means of static pressure and stagnation pressure and temperature probes. The flares provided a steady source of heat for approximately 45 sec., which was ample time to establish a steady régime of heat addition and to record instrument readings.

The experimental results are plotted in Fig. 1, together with the theoretical curves calculated by the procedure of reference 1

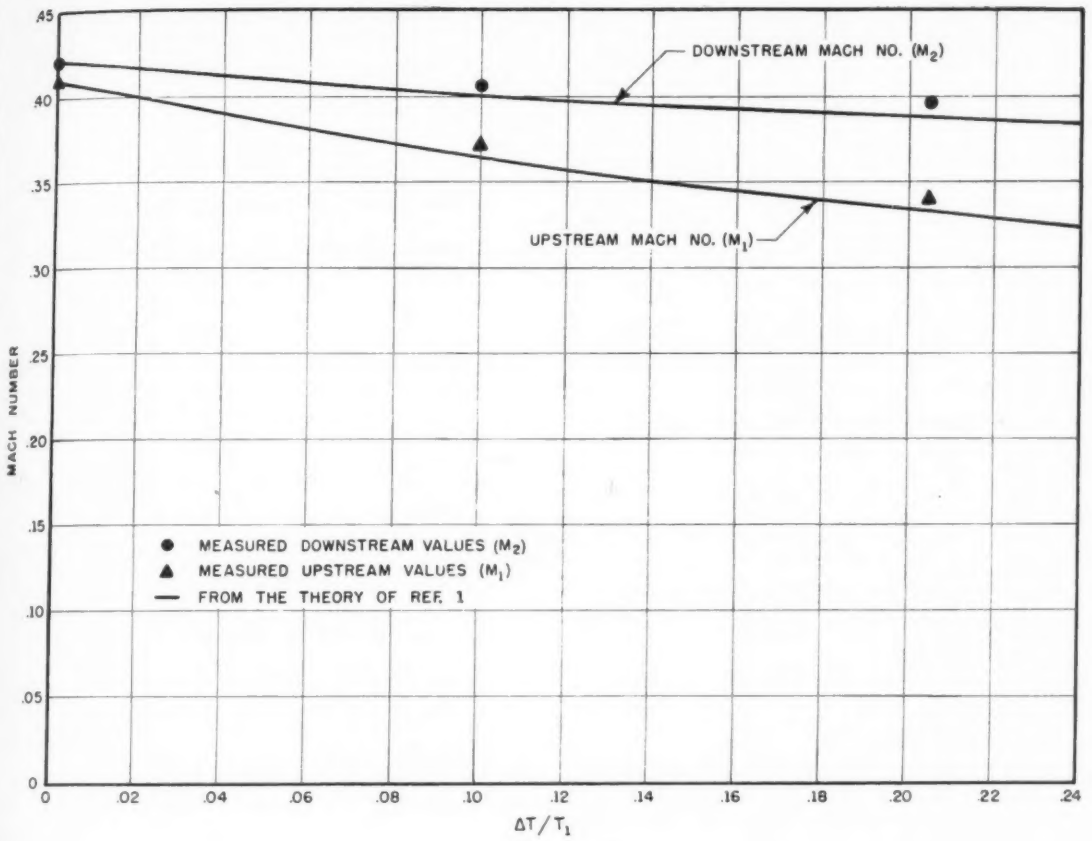

FIG. 1.

with consideration of wall-friction forces. These forces, measured in cold flow, were introduced as an additional impulse term in Eq. (8) of reference 1 and were assumed to be constant in the computation of the effects of heat addition. The additional impulse caused the initial values of M_1 and M_2 to be different.

The system tested was that of Case II of reference 1 (constant stagnation temperature and pressure upstream and constant static pressure downstream of the heating region).

The experimental results were in good agreement with the theoretical prediction and proved that important modifications of the upstream flow conditions are produced by changes in heating rate even when choking does not occur anywhere in the flow.

This work was sponsored by the U.S. Office of Naval Research.

REFERENCES

[1] Foa, J. V., and Rudinger, G., *On the Addition of Heat to a Gas Flowing in a Pipe at Subsonic Speed*, Journal of the Aeronautical Sciences, Vol. 16, No. 2, pp. 84–94 and 119, February, 1949.

[2] Hall, N. A., *Heat Addition to a Flowing Gas*, Readers' Forum, Journal of the Aeronautical Sciences, Vol. 16, No. 5, pp. 317–318, May, 1949.

[3] Barry, F. W., and Fulton, D. C., *Gas Flow in Ducts*, Readers' Forum, Journal of the Aeronautical Sciences, Vol. 16, No. 6, pp. 379–380, June, 1949.

[4] Roy, M., *Addition of Heat to a Gas Flowing in a Pipe at Sonic and Subsonic Speeds*, Readers' Forum, Journal of the Aeronautical Sciences, Vol. 16, No. 9, p. 566, September, 1949.

[5] Foa, J. V., and Rudinger, G., *Heat Addition of a Flowing Gas*, Readers' Forum, Journal of the Aeronautical Sciences, Vol. 16, No. 9, pp. 566–567, September, 1949.

[6] Samaras, D. G., *Heat Addition in a Pipe*, Readers' Forum, Journal of the Aeronautical Sciences, Vol. 16, No. 11, pp. 699–700, November, 1949.

Potential Flow Around a Rotating Cylindrical Blade

W. R. Sears
Cornell University, Ithaca, N.Y.
December 2, 1949

CONSIDER THE PROBLEM of an infinitely long cylinder, of arbitrary section, rotating steadily about an axis normal to it, in a perfect incompressible fluid otherwise at rest. This may be thought of as an idealization of the case of a rotor of cylindrical or nearly cylindrical blades. Let $\boldsymbol{q}$ denote the velocity vector; $\boldsymbol{\omega}$, the angular velocity; and p and ρ, the pressure and density. In addition, since it is convenient to use axes rotating with the blade, let us define a Cartesian set x, y, z, wherein y is measured outward along the blade from the center of rotation, z is measured along the axis of rotation, and x forms the third member of a right-hand system—i.e., for $y > 0$ the cylinder moves in the $-x$ direction. We also define the radius vector $\boldsymbol{r} = (x, y, 0)$, the unit vector $\boldsymbol{k}$ in the z direction, and the relative velocity $\boldsymbol{q}' = \boldsymbol{q} - \boldsymbol{\omega} \times \boldsymbol{r}$.

We have, then,

$$\text{curl } \boldsymbol{q}' = -2\omega\boldsymbol{k}, \qquad \text{div } \boldsymbol{q}' = 0 \tag{1}$$

and by integration of the Euler equations for this case[1]

$$(p/\rho) + (q'^2/2) = (1/2)\omega^2 r^2 + \text{constant} \tag{2}$$

As usual, the solutions of Eqs. (1) are found by combining a particular integral with solutions of the homogeneous problem. We write

$$\left.\begin{aligned} u' &= \phi_x + \psi_y \\ v' &= \phi_y - \psi_x \\ w' &= \phi_z \end{aligned}\right\} \quad \text{where} \quad \left\{\begin{aligned} &\phi_{xx} + \phi_{yy} + \phi_{zz} = 0 \\ &\psi_{xx} + \psi_{yy} = 2\omega \end{aligned}\right\} \tag{3}$$

That is, we assume that the particular integral will be expressible by means of a two-dimensional stream function, and we propose to find the irrotational part of the solution in the form of a three-dimensional velocity potential. Here u', v', w' denote the components of $\boldsymbol{q}'$, and it is easily verified that Eqs. (1) are satisfied.

The boundary conditions are:

(1) The normal component of $\boldsymbol{q}'$ vanishes at the cylinder—i.e.,

$$lu' + nw' = 0 \qquad \text{on } C \tag{4}$$

where C is the contour of the cylinder cross section and (l, m, n) is the normal to C.

(2) As $x \to \infty$ and/or $z \to \infty$, $\boldsymbol{q}' \to -\boldsymbol{\omega} \times \mathbf{r}$—i.e.,

$$u' \to \omega y, \quad v' \to -\omega x, \quad w' \to 0 \tag{5}$$

A particular solution satisfying the differential equation for ψ is

$$\psi = (1/2)\omega r^2 \tag{6}$$

If this value is selected, the boundary conditions become

$$(1) \quad l(\phi_x + \omega y) + n\phi_z = 0 \qquad \text{on } C \tag{7}$$

$$(2) \quad \phi_x, \phi_y, \phi_z \to 0 \text{ as } x \to \infty \text{ and/or } z \to \infty \tag{8}$$

These are exactly the boundary conditions for the plane flow produced by motion of the infinite cylinder in the $-x$ direction with speed ωy, and the differential equation for the potential of that flow is the same as for ϕ if $\phi_{yy} = 0$. In other words, if $\varphi_1(x, z)$ denotes the potential for plane, steady flow past the cylinder placed in a parallel stream of unit speed, we can write

$$\phi = \omega y[\varphi_1(x, z) - x] \tag{9}$$

Consequently, combining our results, we now have

$$\left.\begin{aligned} u' &= \phi_x + \omega y = \omega y \varphi_{1x}(x, z) \\ v' &= \phi_y - \omega x = \omega[\varphi_1(x, z) - 2x] \\ w' &= \phi_z = \omega y \varphi_{1z}(x, z) \end{aligned}\right\} \tag{10}$$

This solution satisfies all the requirements of the problem.

Thus, the flow in a plane transverse to the cylinder at any y is the same as steady plane potential flow about the same cylinder, so far as the u' and w' components are concerned. The outward component v' is given by a simple formula, dependent upon the potential of such plane flow, and is independent of y.

It may be of interest to look at the special case of the circular cylinder.

Circular cylinder of radius 1: $\varphi_1 = (s + s^{-1}) \cos\theta$ where $\theta = \tan^{-1}(z/x)$ and $s = (x^2 + z^2)^{1/2}$. Here,

$$v' = \omega(s + s^{-1} - 2s) \cos\theta = \omega(s^{-1} - s) \cos\theta$$

Thus, on the circular cylinder itself, $v' = 0$. The flow immediately adjacent to the cylinder lies in a transverse plane.

It should be noted that we have implicitly assumed here that there is no circulation about the cylinder. If the circulation were not zero or at least constant along the length of the cylinder, the presence of trailing vortices would have to be considered. The results given here are being applied by L. E. Fogarty and the present author to calculate laminar boundary-layer flow on rotating blades. Subsequently, attention will be directed toward the problem of the blade with circulation.

Reference

[1] Lamb, H., *Hydrodynamics*, p. 20, Eq. (8); Cambridge, 1932.

A Note on the Evaluation of a Definite Integral

Henry E. Fettis
Mathematician, Dynamics Branch, Aircraft Laboratory, Air Materiel Command, Wright-Patterson Air Force, Dayton, Ohio
November 23, 1949

In the theory of the oscillating wing of finite span, it is required to evaluate the following integral:

$$F(iz) = \int_0^\infty \frac{e^{-il(z + t - \sqrt{z^2 + t^2})}}{zt}\, dt = \int_0^\infty \frac{e^{-iz \sinh\theta}(1 + \sinh\theta - \cosh\theta)\cosh\theta\, d\theta}{\sinh\theta} \tag{1}$$

Series expressions for this function are given by Cicala[1] and by Dingle and Küssner.[2] In the following development, the function is expressed in terms of known functions, with the exception of one part, which, however, may be expressed by a simple and rapidly converging power series.

It is convenient to consider first the function with the argument real—namely,

$$F(x) = \int_0^\infty \frac{e^{-x \sinh\theta}(1 + \sinh\theta - \cosh\theta)\cosh\theta\, d\theta}{\sinh\theta} \tag{2}$$

It is known that $F(x)$ has a logarithmic singularity at $x = 0$ and is regular elsewhere and, further, that[3]

$$\lim_{x \to 0} [F(x) + \log x] = 1 - \gamma - \log 2 \tag{3}$$

where $\gamma = 0.57732$ is Euler's constant. It is therefore sufficient to consider the function

$$f(x) = \log x + \int_0^\infty \frac{e^{-x \sinh\theta}(1 + \sinh\theta - \cosh\theta)\cosh\theta\, d\theta}{\sinh\theta} \tag{4}$$

which is regular at $x = 0$ and may therefore be developed in a Taylor Series about this point.

Differentiation of Eq. (4) with respect to x gives

$$f'(x) = \frac{1}{x} - \int_0^\infty e^{-x \sinh\theta}(1 - e^{-\theta}) \cosh\theta\, d\theta = \frac{1}{x} - \frac{1}{2}\int_0^\infty e^{-x \sinh\theta}(e^{\theta} - 1 + e^{-\theta} - e^{-2\theta}) d\theta \tag{5}$$

and since[4]

$$\left.\begin{aligned} &\int_0^\infty e^{-x \sinh\theta} d\theta = \frac{1}{2}[N_0(x) + E_0(x)] \\ &\int_0^\infty e^{-x \sinh\theta \mp k\theta} d\theta = \\ &\qquad \frac{(-)^k + 1}{2}[S_k(x) \mp N_k(x) \mp E_k(x)], \; k > 0 \end{aligned}\right\} \tag{6}$$

in which N_k is the Neumann function, E_k is the Lommel-Weber function, and S_k ($k > 0$) is a polynomial in $(1/x)$ determining the singularity of N_k, it is found that

$$f'(x) = \frac{1}{x} - \frac{1}{4}\{2S_1(x) + S_2(x) + \pi[E_0(x) + E_2(x)] + \pi[N_0(x) + N_2(x)]\} \tag{7}$$

Making use of the following known relations:

$$\left.\begin{aligned} &S_1(x) = \frac{2}{x}, \quad S_2(x) = \frac{4}{x^2}, \quad E_0(x) + E_2(x) = \frac{2}{x}E_1(x) - \frac{4}{x\pi} \\ &N_0(x) + N_2(x) = (2/\pi)N_1(x) \end{aligned}\right\} \tag{8}$$

gives, finally,

$$f'(x) = \left\{\frac{1}{x} - \frac{1}{x^2} - \frac{\pi}{2x}\left[E_1(x) + N_1(x)\right]\right\} \tag{9}$$

Therefore

$$\left.\begin{aligned} f(x) &= f(0) + \int_0^x \left\{\frac{1}{x} - \frac{\pi}{2}\left[\frac{E_1(x)}{x}\right]\right\} dx - \\ &\qquad \int_0^x \left\{\frac{1}{x^2} + \frac{\pi}{2}\left[\frac{N_1(x)}{x}\right]\right\} dx \\ &= f(0) + \int_0^x \left\{\frac{1}{x} - \frac{\pi}{2}\left[\frac{E_1(x)}{x}\right]\right\} dx + \\ &\qquad \left[\frac{\pi}{2} N_1(x) + \frac{1}{x}\right] - \frac{\pi}{2}\int_0^x N_0(x)\, dx \end{aligned}\right\} \tag{10}$$

and since

$$\int_0^x N_0(x)dx = \frac{\pi x}{2}\left[N_0(x)E_1(x) - N_1(x)E_0(x)\right] \tag{11}$$

$$F(x) = 1 - \gamma - \log 2x - \frac{\pi^2 x}{4}\left[N_0(x)E_1(x) - N_1(x)E_0(x)\right] + \left[\frac{\pi}{2} N_1(x) + \frac{1}{x}\right] + \int_0^x \left[\frac{1}{x} - \frac{\pi}{2}\frac{E_1(x)}{x}\right] dx \tag{12}$$

Thus, $F(x)$ is determined in terms of known functions with the exception of the term

$$u(x) = \int_0^x \left[\frac{1}{x} - \frac{\pi}{2}\frac{E_1(x)}{x}\right] dx \tag{13}$$

and this term presents no great difficulty since its Taylor expansion can be written down at once from the corresponding expansion of E_1:

$$\frac{\pi}{2} E_1(x) = 1 - \frac{x^2}{1\cdot 3} + \frac{x^4}{1^2\cdot 3^2\cdot 5} - \frac{x^6}{1^2\cdot 3^2\cdot 5^2\cdot 7} + \ldots \tag{14}$$

In the practical application, $x = iz$, and the following expressions result:

$$F_R(iz) = 1 - \gamma - \log 2z + \frac{\pi^2 z}{4}\left[I_0(z)L_1(z) - I_1(z)L_0(z)\right] - \frac{\pi}{2} I_1(z) + u(iz)$$

$$F_I(iz) = -\frac{\pi}{2} + \frac{\pi}{2} z\left[K_0(z)L_1(z) + K_1(z)L_0(z)\right] + \left[K_1(z) - \frac{1}{z}\right]$$

in which

$$L_0(z) = iE_0(iz) = \frac{2}{\pi}\left[z + \frac{z^3}{1^2\cdot 3^2} + \frac{z^5}{1^2\cdot 3^2\cdot 5^2} + \ldots\right]$$

$$L_1(z) = E_1(iz) = \frac{2}{\pi}\left[1 + \frac{z^2}{1^2\cdot 3} + \frac{z^4}{1^2\cdot 3^2\cdot 5} + \ldots\right]$$

$$u(iz) = -\left[\frac{z^2}{1^2\cdot 2\cdot 3} + \frac{z^4}{1\cdot 3^2\cdot 4\cdot 5} + \frac{z^6}{1\cdot 3^2\cdot 5^2\cdot 6\cdot 7} + \ldots\right]$$

These expansions are convergent for all values of z and are particularly useful when z is small.

A short table of the functions L_0 and L_1 has been compiled by Owen.[5]

References

[1] Cicala, P., *Comparison of Theory with Experiment in the Phenomenon of Wing Flutter*, N.A.C.A. T.M. No. 887, February, 1939.

[2] Dingle and Küssner, *The Vibrating Wing of Large Aspect Ratio*, A.A.F. Translation No. F-TS-935-RE, May, 1947. [The function $S(z)$ in this work is related to $F(z)$ by the equation $S(z) = 1 - izF(iz)$.]

[3] Reissner, Eric, and Stevens, John E., *Effect of Finite Span on the Airload Distributions for Oscillating Wings*, N.A.C.A. T.N. No. 1195 (Part II, App. A), October, 1947.

[4] Watson, G. N., *Theory of Bessel Functions*, p. 313, Eqs. (6), (7); Cambridge University Press 1944.

[5] Owen, S. P., *Tables of the Values of the Integral* $\int_0^x K_0(t)\, dt$, Philosophical Magazine, Vol. 47, No. 280, April, 1924.

Lift-Curve Slope for Swept and Unswept Wings

Innes Bouton
McDonnell Aircraft Corporation, St. Louis, Mo.

October 18, 1949

An expression has been developed by the Loads Group of McDonnell Aircraft Corporation for the low-speed lift-curve slope of swept and unswept wings. This expression seems to correlate with experimental results over a wider range of aspect ratios and sweep angles than any other known formula.

This expression is as follows:

$$C_{L_\alpha} = \frac{C_{l_\alpha}}{\frac{1}{\sqrt{\cos \Lambda}} + \frac{1}{A} + \frac{18.24 C_{l_\alpha}}{A}} \tag{1}$$

where C_{L_α} is the surface lift-curve slope per degree, C_{l_α} is the two-dimensional lift-curve slope per degree of the section perpendicular to the sweep axis, Λ is the angle of sweep at the quarter chord line, and A is the aspect ratio.

The idea for Eq. (1) resulted from a similar expression developed from the Jones edge-velocity correction by George, of the Bureau of Aeronautics, who presented the expression:

$$C_{L_\alpha} = \frac{C_{l_\alpha}}{1 + \frac{1}{A} + \frac{18.24 C_{l_\alpha}}{A}} \tag{2}$$

for unswept wings. The first two terms of the denominator represent the ratio of semiperimeter to span for an elliptic wing and are empirically applied to a wing of any plan form. The same reasoning for a swept wing results in the term $1/\cos \Lambda + 1/A$. The formula incorporating this term was compared with experimental data, and the correlation was found to be poor for swept surfaces. An empirical change of the term $1/\cos \Lambda$ to $1/\sqrt{\cos \Lambda}$, as is often done in dealing with the effects of sweep, results in Eq. (1), which correlates satisfactorily with over 90 surfaces ranging in aspect ratio from less than 1 to over 12 and with more than half of the surfaces having sweepback, some as much as 60°. The maximum departure between Eq. (1) and experimental data is no more than the experimental differences between similar surfaces or approximately 10 per cent. A value for C_{l_α} of 0.105 is suggested when the section lift-curve slope is not readily available.

Base Pressures at Supersonic Velocities

Freeman K. Hill
Physicist, Applied Physics Laboratory, The Johns Hopkins University, Silver Spring, Md.

November 21, 1949

In an earlier issue of the Journal of Aeronautical Sciences,[1] data were presented of pressure measured at the base of missiles in free flight in the range of Mach Numbers from 0.9 to 2.5. The reduced data in terms of base pressure coefficient indicated substantial differences with data obtained by other investigators and by other experimental techniques. However, since the time of this publication, the free-flight data have been substantiated by extensive wind-tunnel tests with

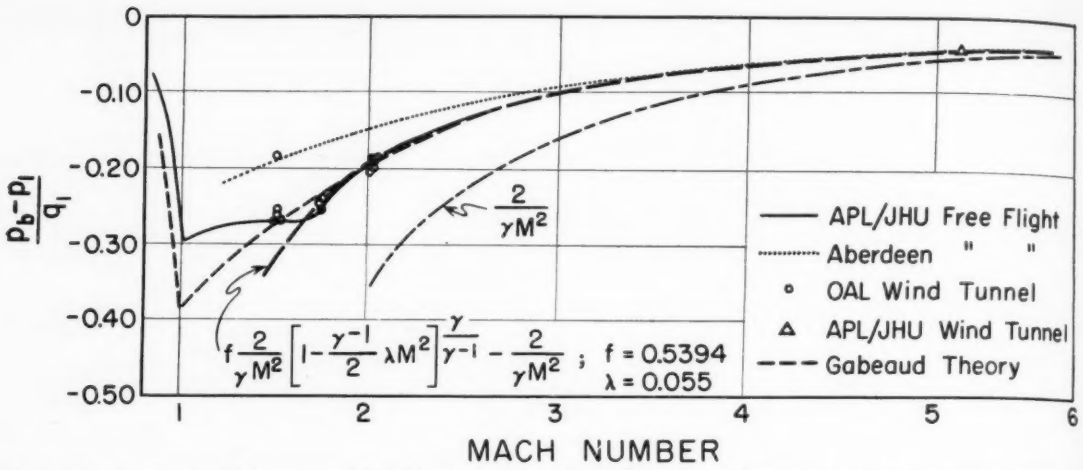

FIG. 1. Base pressure coefficient versus Mach Number. The APL/JHU free-flight data and all the wind-tunnel data shown were taken on a model having an ogival nose tangent to a cylindrical body, four biconvex tail fins, and a flat base. The length-to-diameter ratio was 6.1. The OAL wind-tunnel data were corrected where necessary to compensate for the effect of reflected shocks from the tunnel walls.

homologous models at relatively large Reynolds Numbers, approaching but not equaling those of free flight. In addition, a recent test at a Mach Number of 5.1 has provided data that enable a correlation to be made of nearly all results at Mach Numbers above 2 and also suggest the causes of the wide discrepancy that exists in many of the base pressure measurements at low supersonic Mach Numbers. It should also be mentioned that the recent letter of Gabeaud to the JOURNAL[2] further substantiates the general analysis presented below.

Measurements were made at $M = 5.1$ in the 5- by 8-in. test section of the APL/JHU blow-down wind tunnel. The test model was a 1/3.2-scale model of one of the free-flight models described earlier,[1] and the test Reynolds Numbers were 5.4 to 8.5 millions. The model was supported in the wind tunnel by extending two of the tail fins to the test section walls, and the pressure was measured at the center of the base. Numerically the base pressure coefficient, C_B, was found to be -0.0457 with a standard deviation of 0.0009. (Complete details given in reference 3.) C_B is defined by $C_B = (p_b - p_1)/q_1$, where p_b is the absolute pressure at the base of the missile, p_1 is the free-stream static pressure, and q_1 is the dynamic head.

Fig. 1 is a summary of base pressure coefficient data now available from both free-flight and wind-tunnel tests made with homologous models having tail fins. The free-flight data are reported in reference 1, and the wind-tunnel data were obtained in the APL/JHU tunnel at $M = 5.1$ and in the Ordnance Aerophysics Laboratory wind tunnel, Daingerfield, Tex., at $M = 1.5$, 1.75, and 2.00. Free-flight results obtained by ballistic firings[4] are also shown, where the model configurations and test conditions were different from those mentioned above; these results, however, illustrate the dispersion of data in the low supersonic range of Mach Numbers and the trend toward agreement above $M = 2$. The theoretical curve of Gabeaud is also shown. The agreement in the data above $M = 2$ is evident from this figure. In this connection it may be pointed out that as M increases, the value of the base pressure will approach but cannot exceed the perfect vacuum condition, which, according to the above definition of C_B, g ves a value of $-2/\gamma M^2$. It is clear, therefore, that at high Mach Numbers the base pressure becomes mainly a dynamical effect and will approach the perfect vacuum limit. This suggests that an expression may be derived similar to the one set forth by von Kármán and Moore[5] in 1932 and that the experimental data now available may be used to fix the boundary conditions. In the low Mach Number range, $1 < M < 2$, the effects of model shape, Reynolds Number, boundary layer, etc., however, are so predominant that the base pressure coefficient cannot be simply expressed in analytical form.

For relatively high Mach Numbers we have therefore considered[6] that a fraction, f, of the base pressure, p_b, is proportional to the dynamic head, $(1/2)\rho_1 V^2$. This yields the dynamical equation

$$\int_{(1/f)p_b}^{p_1} dp/\rho_1 = (1/2)\lambda V^2 \qquad (1)$$

When this equation is integrated and the results are written in terms of the base pressure coefficient C_B, one obtains

$$C_B = \frac{p_b - p_1}{q_1} = f\frac{2}{\gamma M^2}\left(1 - \frac{\gamma - 1}{2}\lambda M^2\right)^{\gamma/(\gamma-1)} - \frac{2}{\gamma M^2} \qquad (2)$$

where $q_1 = (1/2)\rho_1 V^2$, and M is the local Mach Number. Eq. (2) now presents two arbitrary constants, λ and f, which may be evaluated from the experimental data. The experimental values of C_B found at $M = 2.50$ and 5.10 were -0.132 and -0.0457, respectively, and substituting these in Eq. (2) gives $\lambda = 0.055$ and $f = 0.5394$. Eq. (2) is plotted in Fig. 1. Not only does this curve show the trend of base pressures at high Mach Numbers, but also in the Mach Number range near 2 its steep descent indicates where the effects of Reynolds Number, boundary layer, body shape, etc., play a predominant role. For example, at $M = 1.75$ the knee of the free-flight base pressure curve indicates the region where divergence from the dynamical curve occurs.

It may be noted from Eq. (2) that for values of $M > 9.5$, p_b becomes negative, and, hence, Eq. (2) is no longer physically tenable. However, at these high Mach Numbers the base pressure is going to be nearly zero, and there seems little point in deriving an analytical expression for it, especially in view of the fact that the usual isentropic laws are questionable in flows where such high Mach Numbers obtain. For the purpose of predicting base pressure on simple missiles in the range $0.9 < M < 1.8$, experimental data must be used, but in the range $2 < M < 6$ an expression such as Eq. (2) is useful.

REFERENCES

[1] Hill and Alpher, *Base Pressures at Supersonic Velocities*, Journal of the Aeronautical Sciences, Vol. 16, No. 3, p. 153, March, 1949.

[2] Gabeaud, *Base Pressures at Supersonic Velocities*, Readers' Forum, Journal of the Aeronautical Sciences, Vol. 16, No. 10, p. 638, October, 1949.

[3] Hill, *Base Pressures at a Mach Number of 5.1*, APL/JHU Internal Memorandum CF-1306, July, 1949.

[4] Charters and Turetsky, *Determination of Base Pressure from Free Flight Data*, BRL No. 653, Aberdeen Proving Ground, March, 1948.

[5] von Kármán and Moore, *Resistance of Slender Bodies Moving with Supersonic Velocities, with Special Reference to Projectiles*, A.S.M.E. Trans., pp. 302-310, 1932.

[6] Faro and Hill, *Base Pressures of High Mach Numbers*, APL/JHU Internal Memorandum CF-1322, August, 1949.

Erratum

William F. Savage
Assistant Professor of Mechanical Engineering, University of Kentucky, Lexington, Ky.
December 30, 1949

THE FOLLOWING ERROR appeared in my Readers' Forum item "Effect of Disposable Load on Range of Turbojet Airplanes" (JOURNAL OF THE AERONAUTICAL SCIENCES, Vol. 16, No. 10, p. 637, October, 1949).

The first equation at the top of the right-hand side of the page should be:

$$V_{avg.} = 4V_i \frac{[K_F/(1 + K^{1/2})]}{\ln\left[\frac{1}{K}\left(\frac{2K^{1/2} + 2K + K_F}{2K^{1/2} + 2 - K_F}\right)^2\right]}$$

On the Surface Effects of a Compressible Laminar Boundary Layer

Arthur N. Tifford
Associate Professor of Aeronautical Engineering, The Ohio State University, Columbus, Ohio
December 5, 1949

THE PAPER, "Temperature and Velocity Profiles in the Compressible Laminar Boundary Layer with Arbitrary Distribution of Surface Temperature," by D. R. Chapman and M. W. Rubesin (published in the September, 1949, issue of the JOURNAL OF THE AERONAUTICAL SCIENCES) is an excellent mathematical analysis of the problem. A notable contribution has been made to the analysis of the laminar boundary layer subjected to an imposed temperature gradient. I find myself in disagreement, however, with the emphasis given to the need for considering the change in the velocity profile due to temperature effects when dealing with most of the practical problems to which reference is made in the subject paper. Rather, it is to be expected on the basis of earlier works that the Blasius velocity profile persists *effectively* to relatively high Mach Numbers *if the fluid properties are taken as those at the plate's surface.* A brief review of the relevant literature follows:

Busemann in his original treatment[1] of the laminar boundary layer along an insulated flat plate exposed to the flow of a gas, whose viscosity and thermal conductivity vary with temperature directly as $\sqrt{T}$, noted that $c_{d_f}\sqrt{R_e}$ increases only 20 per cent as the Mach Number increases from 0 to ∞ *if* $c_{d_f}\sqrt{R_e}$ is expressed as

$$\mu_w(\partial u/\partial y)/(\rho_w U_\infty^2/2)\sqrt{U_\infty L/\nu_w}$$

rather than as

$$\mu_w(\partial u/\partial y)/(\rho_\infty U_\infty^2/2)\sqrt{U_\infty L/\nu_\infty}$$

von Kármán, in his famous Volta Congress paper,[2] suggested the application of this finding to the analysis of the effect of compressibility on the turbulent boundary layer. However, in the later paper[3] by von Kármán and Tsien reanalyzing Busemann's problem, assuming the coefficient of absolute viscosity and thermal conductivity of the gas to vary directly as $T^{0.76}$, no consideration was given to this remarkable simplification and its implications. Thus it remained for Eckert and Drewitz[4] to show that von Kármán and Tsien's results confirm Busemann's finding of only a slight dependence of $c_{d_f}\sqrt{R_e}$ (properly defined) on the Mach Number. In addition, they find that only a small deviation from the Blasius velocity profile occurs at Mach Numbers as high as those considered in the paper being discussed here—i.e., Mach Numbers up to 5—*when the nondimensional boundary-layer coordinate is based on the kinematic viscosity of the gas at the surface of the plate.* What are the independent findings of the present paper?

Eq. (58a),

$$c_{d_f} = \frac{\tau_w}{\rho_\infty U_\infty^2/2} = \frac{1.328}{\sqrt{R_e}}\sqrt{C}$$

was derived as applicable to a plate at a constant temperature. Direct substitution of the definition of C and R_e and simplification yields

$$(\tau_w\sqrt{U_\infty L/\nu_w})/(\rho_w U_\infty^2/2) = 1.328 \qquad (1)$$

exactly the result obtained by ignoring velocity profile and fluid property alterations due to the temperature field! Furthermore, it is the comparison in Fig. 6 between Eq. (58a) and Crocco's[5] more exact results that was used to establish the precision of the new analytical approach as within 5 or 6 per cent for Mach Numbers as high as 5. This identical precision therefore applies to an analytical approach neglecting fluid property variations.

Fig. I compares lines representing Chapman and Rubesin's approximation, $\mu^* = CT^*$, with plots of the actual variation of the absolute viscosity of air with temperature. It is seen that

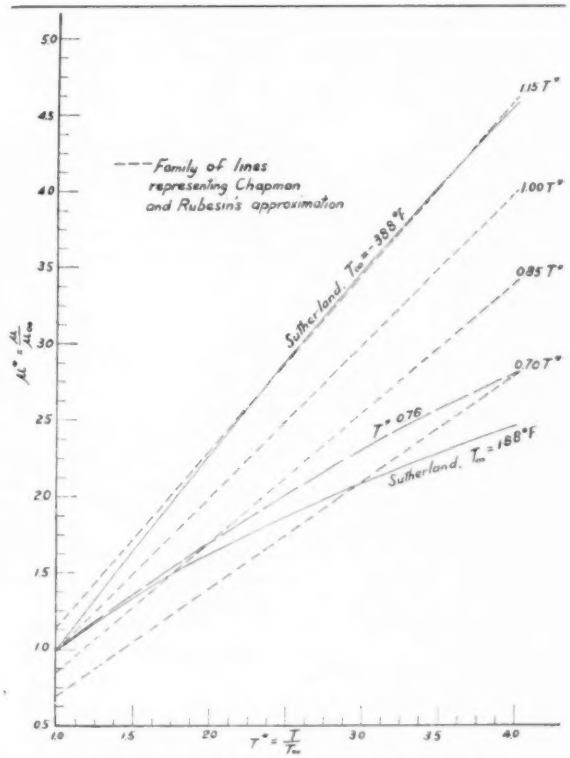

Figure I – Variation of viscosity with temperature

only at extremely low free-stream temperatures is the approximation reasonably good. Under these conditions, C_w is essentially the same as C. Eq. (58) for the total drag coefficient, c_{d_f},

$$c_{d_f} = \left[\frac{f''(0)}{\sqrt{R_e C}}\right]^{1/3} \int_0^1 \frac{C_w\, dx^*}{\sqrt{x^*}} \tag{58}$$

therefore reduces for extremely low free-stream temperatures to Eq. (I) above. *In other words, when a plate has a nonuniform surface temperature, an analysis based on constant fluid properties, properly interpreted, yields the same results as the analysis under discussion, whenever the latter's assumption, $\mu^* = CT^*$, is actually a good approximation.* The poorer the approximation becomes, the less the agreement between the two analyses. Which is the better approach can only be fully established after a more exact analysis of the boundary layer of a plate of nonuniform temperature has been made for atmospheric flight conditions.

The discussion up to this point has been primarily concerned with the surface friction. One may readily confirm, however, by an analogous study that the heat transfer rate determined by an analysis neglecting fluid property variations is identical with that derived in the paper under discussion, except when dealing with a plate of nonuniform temperature operating in a flow field having a free-stream static temperature of above approximately $-100°$F. Under the latter circumstance it is, as discussed above, indeterminate at the present time which type of analysis is the more precise.

It may be of interest to the reader to replot the boundary-layer velocity profiles of the typical example of the paper as a function of $(y/2)\sqrt{U_\infty/\nu_w x}$ instead of $(y/2)\sqrt{U_\infty/\nu_\infty x}$. The three distinct velocity profiles shown in Fig. 10 merge into a single one, the Blasius profile, except for an extremely small region near the outer edge of the boundary layer. This is not surprising in view of the discussion which has been given here.

In conclusion, (a) Chapman and Rubesin's paper is a major contribution in that it makes available for the first time the solution of the boundary-layer equations in the presence of a fairly general analytic distribution of surface temperature.

(b) The results of the analysis, properly interpreted, yield additional support for the assumption that the evaluation of local boundary-layer surface phenomena, such as friction and heat transfer in a compressible gas flow field, need not be complicated by the consideration of the fluid properties anywhere but at the surface if the Mach Number outside the boundary layer is less than about 5.

References

[1] Busemann, A., *Gasstroemung mit laminarer Grenzschicht entlang einer Platte*, ZAMM, Vol. 15, No. 23, pp. 22–25, 1935.

[2] von Kármán, Th., *The Problem of Resistance in Compressible Fluids*, Proc. 5th Volta Congress, Rome, pp. 255–264, 1935.

[3] von Kármán, Th., and Tsien, H. S., *Boundary Layer in Compressible Fluids*, Journal of the Aeronautical Sciences, Vol. 5, No. 6, p. 227, April, 1938.

[4] Eckert, E., and Drewitz, O., *The Heat Transfer to a Plate in Flow at High Speed*, Forschung a. d. Gebiete d. Ingenieurwesens, Vol. 11, No. 3, pp. 116–122, May–June, 1940; also N.A.C.A. T.M. No. 1045, May, 1943.

[5] Crocco, Luigi, *Lo strato limite laminare nei gas*, Monografie Scientifiche di Aeronautica, No. 3, May, 1946.

On the Vorticity of the Flow Behind Curved Shock

S. I. Pai

Institute for Fluid Dynamics and Applied Mathematics, University of Maryland, College Park, Md.

December 1, 1949

IT IS WELL KNOWN that vortices are generated suddenly by shock waves and that the strength of the vorticity is proportional to the rate of change of entropy with respect to stream function.[1] One of the assumptions usually made in calculation of flow involving shock wave is that the vorticity introduced into the flow by the shock wave is extremely small and negligible. This note will show that this assumption, in general, is not accurate and that, in most practical cases, the vorticity introduced by the shock should be considered, particularly when the flow behind detached shock is considered.

For simplicity, we consider only the practically important iso-energetic flow. The basic equations for the present analysis are:[2]

$$\text{vorticity} = \omega = \frac{p}{R}\, y^\epsilon \frac{dS}{d\psi} \tag{1}$$

and

$$\frac{S_2 - S_1}{C_v} = \log\left[\left(\frac{2\gamma}{\gamma+1} M_1^2 \sin^2\alpha - \frac{\gamma-1}{\gamma+1}\right) \times \left(\frac{\gamma-1}{\gamma+1} + \frac{2}{(\gamma+1)M_1^2 \sin^2\alpha}\right)^\gamma\right] \tag{2}$$

where p is the pressure, R is gas constant, y is radial distance, $\epsilon = 0$ for two-dimensional flow, $\epsilon = 1$ for axially symmetrical flow, S is entropy, ψ is stream function, C_v is specific heat at constant volume, γ is ratio of specific heats (C_p/C_v), M is Mach Number, α is shock angle with respect to velocity in front of shock, sub 1 refers to the value in front of the shock, and sub 2 refers to the value behind the shock.

In order to show the order of magnitude of vorticity introduced by the shock, we consider the small perturbation from those irrotational flow involved shock wave, such as a uniform supersonic flow over two-dimensional wedge or over unyawed cone. There are two possible kinds of perturbation from the original irrotational flow:

(A) Disturbance comes from the front of the shock, which affects both M_1 and α. For instance, Adams studied a special case of such a problem.[3]

(B) Disturbance comes from the rear of the shock, which affects only α. This corresponds to the case that the shape of the body is slightly different from that of the wedge or cone.

Since case (A) involves both the change of M_1 and α, we need to consider it only. The change of entropy behind the shock with respect to stream function due to the small perturbation is

$$\frac{dS_2}{d\psi} = \frac{1}{\rho_2 q_2 y^\epsilon \sin\delta}\left[\frac{\partial S_2}{\partial\alpha}\frac{\partial\alpha}{\partial\sigma} + \frac{\partial S_2}{\partial M_1}\frac{\partial M_1}{\partial\sigma}\right] \tag{3}$$

where ρ is the density, q is the resultant velocity, δ is the shock angle with respect to q_2, and σ is arc length along the shock curve, S_1 = constant.

The first order value of vorticity behind the shock introduced by the perturbation is

$$\omega = \frac{p_2}{\rho_2 q_2 R \sin\delta}\left[\frac{\partial S_2}{\partial\alpha}\frac{\partial\alpha'}{\partial\sigma} + \frac{\partial S_2}{\partial M_1}\frac{\partial M_1'}{\partial\sigma}\right] \tag{4}$$

where prime refers to the value of perturbation quantity.

$$\frac{1}{C_v}\frac{\partial S_2}{\partial\alpha} = \frac{2\gamma M_1^2 \sin 2\alpha[(\gamma-1)M_1^2\sin^2\alpha + 2] - 4\gamma\cot\alpha[2\gamma M_1^2\sin^2\alpha - (\gamma-1)]}{[(\gamma-1)M_1^2\sin^2\alpha + 2][2\gamma M_1^2\sin^2\alpha - (\gamma-1)]} \tag{5}$$

and

$$\frac{1}{C_v}\frac{\partial S_2}{\partial M_1} = \frac{4\gamma(\gamma-1)(M_1^2\sin^2\alpha - 1)^2}{M_1[(\gamma-1)M_1^2\sin^2\alpha + 2][2\gamma M_1^2\sin^2\alpha - (\gamma-1)]} \tag{6}$$

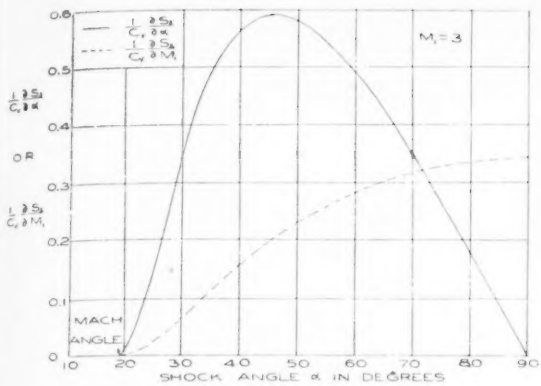

FIG 1 ENTROPY VARIATION BEHIND SHOCK

The typical curves of $(1/C_v)(\partial S_2/\partial\alpha)$ and $(1/C_v)(\partial S_2/\partial M_1)$ at $M_1 = 3$ against the shock angle α are plotted in Fig. 1, which shows that these quantities are of the order of magnitude of unity over practically the entire range of shock strength. The first term of Eq. (4)—i.e., $(\partial S_2/\partial\alpha)(\partial\alpha'/\partial\sigma)$—shows the variation of vorticity along a given shock polar (M_1 = constant), and it is small only near α = Mach angle and $\alpha = 90°$. The second term of Eq. (4)—i.e., $(\partial S_2/\partial M_1)(\partial M_1'/\partial\alpha)$—shows the variation of vorticity from one shock polar to another, which is only negligible when α is near Mach angle.

In general, the vorticity introduced by the shock wave is of the same order of magnitude as the perturbation terms $\partial\alpha'/\partial\sigma$ and $\partial M_1'/\partial\sigma$, and it cannot be neglected. In case of detached shock, the shock angle varies from normal shock $\alpha = 90°$ to Mach angle $\alpha = \sin^{-1}(1/M_1)$; it is clear that the vorticity introduced by the shock should be considered there.

References

[1] Vazsonyi, A., *On Rotational Gas Flow*, Quarterly of Applied Mathematics, Vol. III, No. 1, pp. 29–37, April, 1945.

[2] Lin, C. C., and Rubinov, S. I., *On the Flow behind Curved Shock*, Journal of Mathematics and Physics, Vol. XXVII, No. 2, pp. 105–129, July, 1948.

[3] Adams, Mac C., *On Shock Waves in Inhomogeneous Flow*, Journal of the Aeronautical Sciences, Vol. 16, No. 11, pp. 685–690, November, 1949.

Formulation of the Flutter Problem for Solution on an Electronic Analog Computer

Eugene F. Baird and Henry J. Kelley
Grumman Aircraft Engineering Corporation, Bethpage, L.I., N.Y.

November 23, 1949

THE PRESENT NOTE deals with the formulation of an initial value problem in the stability of airfoil oscillations and its solution by means of an electronic analog computer. The advantages of this approach lie mainly in speed and ease of analysis.

Wagner[1] first obtained the lift response as a function of time for an airfoil whose quasi-steady circulation Γ experiences a sudden unit increment. In terms of lift deficiency ϕ:

$$L = \rho V\left\{(\Gamma(t) - \int_0^t \frac{d\Gamma}{d\tau}\phi\left[\frac{V}{b}(t-\tau)\right]d\tau\right\} \qquad (1)$$

Using the notation of Theodorsen,[2] the circulatory lift may be written:

$$L = 2\pi\rho Vb\int_0^t\left\{1 - \phi\left[\frac{V}{b}(t-\tau)\right]\right\}\times \frac{d}{d\tau}[\dot h + V\alpha + b(1/2 - a)\dot\alpha]\,d\tau \qquad (2)$$

That the quasi-steady circulation depends on the downwash at the rear quarter chord in the above fashion has also been shown by Küssner.[3]

The equilibrium of forces and moments is expressed in the two following equations, which include virtual inertia terms:

$$M\ddot h + S_\alpha\ddot\alpha + C_h h + \pi\rho b^2(\ddot h + V\dot\alpha - ab\ddot\alpha) + 2b\pi\rho V\int_0^t\left\{1 - \phi\left[\frac{V}{b}(t-\tau)\right]\right\}\frac{d}{dt}\times [\dot h + V\alpha + b(1/2 - a)\dot\alpha]\,d\tau = 0 \qquad (3)$$

$$I_\alpha\ddot\alpha + S_\alpha\ddot h + C_\alpha\alpha + \pi\rho b^2[(1/2 - a)Vb\dot\alpha + b^2(1/8 + a^2)\ddot\alpha - ab\ddot h] - 2\pi\rho Vb^2(1/2 + a)\int_0^t\left\{1 - \phi\left[\frac{V}{b}(t-\tau)\right]\right\}\times \frac{d}{d\tau}\left[\dot h + V\alpha + b(1/2 - a)\dot\alpha\right]d\tau = 0 \qquad (4)$$

Since the function ϕ is not available in closed form, various approximate representations have been developed. A number of these may be listed:

$$\phi(\sigma) \cong 0.165e^{-0.0455\sigma} + 0.335e^{-0.30\sigma} \qquad (5a)[4]$$
$$\phi(\sigma) \cong 0.25e^{-0.5\sigma} + 0.25(1 + 0.185\sigma)e^{-0.185\sigma} \qquad (5b)[5]$$
$$\phi(\sigma) \cong 0.165e^{-0.041\sigma} + 0.335e^{-0.32\sigma} \qquad (5c)[6]$$

For comparison with Theodorsen's analytic result, the Fourier transforms of $1 - \phi$ in the approximate forms above have been plotted in Fig. 1. The scale is chosen for purpose of contrast.

Choosing the Jones approximation for ϕ, we rearrange as follows:

$$\phi(\sigma) \cong (1/2) - [0.165(1 - e^{-0.0455\sigma}) + 0.335(1 - e^{-0.30\sigma})]$$

The method for treating the integrals in Eqs. (3) and (4) is to introduce auxiliary variables ξ and η into the equations of motions, creating a set of four simultaneous linear differential equations in four dependent variables as follows:

$$(M + \pi\rho b^2)\ddot h + (S_\alpha - \pi\rho b^3 a)\ddot\alpha + C_h h + \pi\rho b^2 V(3/2 - a)\dot\alpha + \pi\rho bV\dot h + \pi\rho bV^2\alpha + \xi + \eta = 0 \qquad (6)$$

$$[I_\alpha + \pi\rho b^4(1/8 + a^2)]\ddot\alpha + (S_\alpha - \pi\rho b^3 a)\ddot h + C_\alpha\alpha + \pi\rho b^2(1/2 - a)^2V\dot\alpha - \pi\rho b^2V(1/2 + a)\dot h - \pi\rho b^2(1/2 + a)\times V^2\alpha - b(1/2 + a)(\xi + \eta) = 0 \qquad (7)$$

$$\dot\xi + \left(\frac{b}{0.0455V}\right)\xi = (2\pi\rho Vb)(0.165)[\dot h + V\alpha + b(1/2 - a)\dot\alpha] \qquad (8)$$

$$\dot\eta + \left(\frac{b}{0.30V}\right)\eta = (2\pi\rho Vb)(0.335)[\dot h + V\alpha + b(1/2 - a)\dot\alpha] \qquad (9)$$

It is easily shown by Laplace transformation that ξ and η represent the integrals:

$$\xi = (2\pi\rho Vb)(0.165)\int_0^t [1 - e^{-0.0455(V/b)(t-\tau)}]\times \frac{d}{d\tau}[\dot h + V\alpha + b(1/2 - a)\dot\alpha]d\tau + (2\pi\rho Vb)(0.165)\times [1 - e^{-0.0455(Vt/b)}][\dot h + V\alpha + b(1/2 - a)\dot\alpha]_{t=0}$$

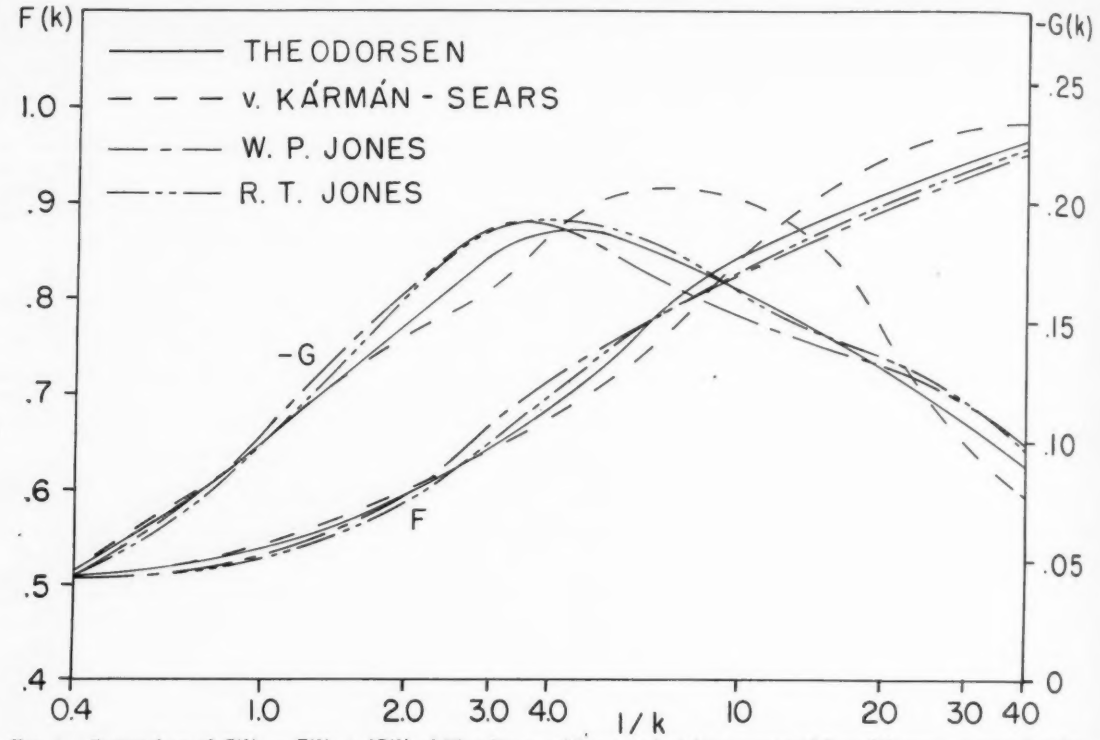

FIG. 1. Comparison of $C(k) = F(k) + iG(k)$ of Theodorsen with approximations computed from Wagner response function.

$$\eta = (2\pi\rho Vb)(0.335)\int_0^t [1 - e^{-0.30(V/b)(t-\tau)}] \times \frac{d}{d\tau}[h + V\alpha + b(1/2 - a)\dot{\alpha}]d\tau + (2\pi\rho Vb)(0.335) \times [1 - e^{-0.33(Vt/b)}][\dot{h} + V\alpha + b(1/2 - a)\dot{\alpha}]_t = 0$$

Solution of linear differential equations with constant coefficients is a routine task for most electronic analog computers. The aerodynamic forces and moments that arise from initial values of h, $\dot{h}$, α, $\dot{\alpha}$ are provided for in the representations ξ and η. The procedure consists of solving the four equations at successive values of forward velocity for sets of initial conditions chosen with the purpose of exciting pure modes in each of the degrees of freedom. For values of V greater than a flutter speed, however, arbitrary initial conditions suffice to excite flutter. In practice it has been found that use of Vt/b as independent time variable facilitates the analysis in that only a few coefficients depend on V.

Results of a two-dimensional two-degree numerical example will be shown for comparison with results of a conventional analysis (A.M.C. Method). The following parameters were used: $b = 0.969$ ft.; $a = 0$; natural frequencies $\omega_h = 147$ rad. per sec. and $\omega_\alpha = 305$ rad. per sec.; $M = 15$ lbs. per ft.; $S_\alpha = 0$; $I_\alpha = 675.7$ lbs. ft.^{2} per ft.; ρ at 10,000 ft. altitude. A plot of damping coefficient g as obtained by the A.M.C. method appears in Fig. 2, together with rates of decay observed on the R.E.A.C.* in the form of logarithmic decrements. Although flutter speeds are identical, the steady state assumptions of the A.M.C. method preclude comparison for other V.[7]

The method affords facility in the study of gust response and in the inclusion of the effects of servo units in control surface analysis. Extension to the supersonic case does not follow directly, however, since the response functions involved are not easily represented as solutions of linear differential equations (discontinuous derivatives).

* Reeves Electronic Analogue Computer.

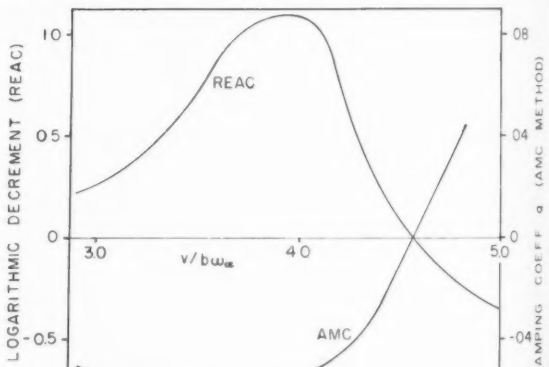

FIG. 2. Comparison of stability curves from A.M.C. method and from R.E.A.C.

REFERENCES

1 Wagner, Herbert, *Über die Entstehung des Dynamischer Auftriebes von Tragflügeln*, Zeitschr. f. Math. und Mech., Bd. 5, p. 17, 1925.

2 Theodorsen, Theodore, *General Theory of Aerodynamic Instability and the Mechanism of Flutter*, N.A.C.A. T.R. No. 496, 1935.

3 Küssner, H. G., *Zusammenfassender Bericht über den instationären Auftrieb von Flügeln*, Luftfahrtforschung, Bd. 13, p. 410, 1936.

4 Jones, R. T., *Operational Treatment of the Non-Uniform Lift Theory in Airplane Dynamics*, N.A.C.A. T.N. No. 667, 1938.

5 von Kármán, Th., and Sears, W. R., *Airfoil Theory for Non-Uniform Motion*, Journal of the Aeronautical Sciences, Vol. 5, No. 10, 1938.

6 Jones, W. P., *Aerodynamic Forces on Wings in Non-Uniform Motion*, A.R.C. Tech. Rept., R. & M. No. 2117, 1945.

7 Goland, M., and Luke, Y. L., *A Study of the Bending-Torsion Aeroelastic Modes for Aircraft Wings*, Journal of the Aeronautical Sciences, Vol. 16, No. 7, p. 389, July, 1949.

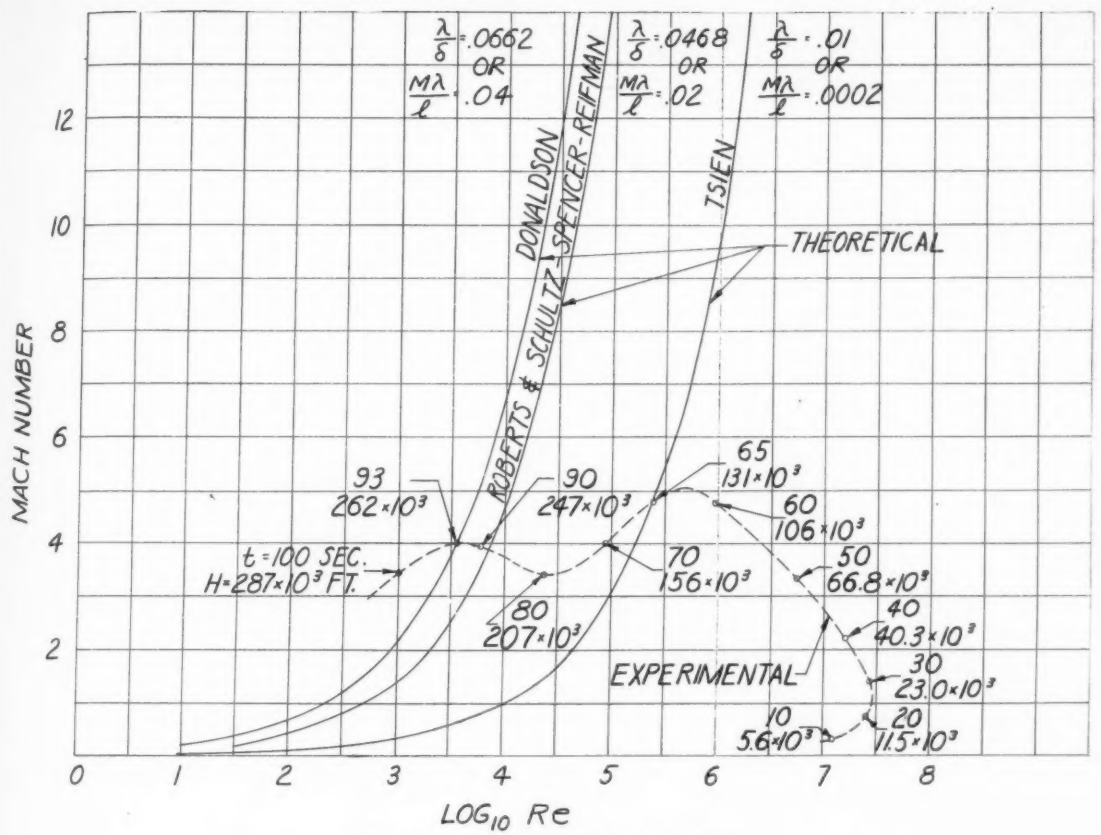

FIG. 1. Comparison of slip flow criteria.

Boundaries of Fluid Mechanics

Keeve M. Siegel
Research Associate, Aeronautical Research Center, University of Michigan, Ann Arbor, Mich.
November 14, 1949

IN OCTOBER'S AERONAUTICAL ENGINEERING REVIEW, Mr. Roberts points out a new criterion[1] suggested by H. W. Liepmann to distinguish the realms of fluid mechanics. In the literature there already are criteria that attempt to define the regions of fluid mechanics. This note compares these criteria.

BOUNDARY BETWEEN CONTINUUM ANALYSIS AND SLIP FLOW

M = Mach Number
δ = boundary layer thickness
l = effective length
R = Reynolds Number
λ = mean free path
v = velocity
ρ = density
μ = viscosity coefficient
c = mean molecular velocity for air
a = velocity of sound

Subscript 0 signifies sea-level conditions.

(1) Donaldson:[2]

$$M\lambda/l = 0.04$$

(2) Tsien:[3]

$$\lambda/\delta = M/\sqrt{R}, \quad R \gg 1$$
$$\lambda/\delta = M/R, \quad R \ll 1$$
$$\lambda/\delta = 0.01$$

(3) Schultz, Spencer, and Reifman:[4]

$$\lambda/\delta = 0.438(M/\sqrt{R}) \leqq M/2\sqrt{R}$$
$$\lambda/\delta = 0.05$$

(4) Roberts:[1]

$$R/M^2 = 100$$

We can compare these criteria in two ways: first,

$$\frac{M}{R} = \frac{M(v/a)}{\rho l v/\mu} = \frac{M}{l}\frac{\mu}{\rho a} = \frac{M\lambda}{l}\frac{\mu_0(T/T_0)^{0.75-0.5}}{\lambda_0 a_0}$$

In the region of the atmosphere under consideration T/T_0 can be considered unity in an order of magnitude analysis.

$$\frac{M^2}{R} = \frac{M\lambda}{l}(0.438)\left(\frac{T}{T_0}\right)^{0.25} \cong \frac{M\lambda}{l}\frac{1}{2}$$

Second, an extension of Donaldson's Appendix A,[2]

$$\frac{M^2}{R} = \frac{M^2}{\rho v l/\mu} = \frac{M^2}{(vl/\lambda)(\rho\lambda/\mu)}$$

but $\mu = 0.499\rho\, c\, \lambda$ and $c = 1.462a$; hence, $\mu = 0.73\rho a\lambda$ and

$$\frac{M^2}{R} = \frac{M^2}{vl/0.73\lambda a} = 0.73\frac{M\lambda}{l} \cong \frac{3}{4}\frac{M\lambda}{l}$$

Let us use $M^2/R = (M\lambda/l)(1/2)$ to compare the criteria.

(1) Donaldson:

$$M\lambda/l = 0.04$$

(2) Tsien:

$$M\lambda/l = 0.0002$$

(3) Schultz, Spencer, and Reifman:

$$M\lambda/l = 0.02$$

(4) Roberts:

$$M\lambda/l = 0.02$$

It thus appears that in any order of magnitude discussion that criteria (1), (3), and (4) are equivalent.

Lo[5] has superimposed Tsien's criteria on a graph of M versus log R for the flight of V-2 missile No. 21, fired on March 7, 1947. We have added the other criteria to this curve. We note in Fig. 1 that there is a spread of 131,000 ft. between application of these criteria.

DIFFERENT CRITERIA FOR THE LOWER BOUND OF FREE MOLECULE FLOW

(A) Roberts:

$$R/M^2 = 0.01$$
$$M/\sqrt{R} = 10$$

(B) Schultz, Spencer, and Reifman:

$$\lambda/\delta = 10$$
$$\lambda/\delta = 0.438(M/\sqrt{R})$$

(C) Tsien:

$$\lambda/\delta = \lambda/l = M/R = 10$$

One notes that, in the intended region of application of criterion (B), it was thought that $R \gg 1$, while criterion (C) implied that $R \ll 1$. Thus we can make no real comparison between these criteria.

Of course, we do not know which criteria are the best, since this answer must be determined by experiment.

REFERENCES

[1] Roberts, Howard E., *The Earth's Atmosphere*, Aeronautical Engineering Review, Vol. 8, No. 10, p. 19, October, 1949.

[2] Donaldson, Coleman duP., *An Approximate Method for Estimating the Incompressible Laminar Boundary-layer Characteristics on a Flat Plate in Slipping Flow*, N.A.C.A. R.M. No. L9C02, May 2, 1949.

[3] Tsien, Hsue-Shen, *Superaerodynamics*, Journal of the Aeronautical Sciences, Vol. 13, No. 12, pp. 653–664, December, 1946.

[4] Schultz, F. V., Spencer, N. W., and Reifman, A., *Atmospheric Pressure and Temperature Measurements between the Altitudes of 40 and 110 Kilometers*, Upper Air Research Program Report No. 2, Engineering Research Institute, University of Michigan, July 1, 1948.

[5] Lo, Hsu, *Determination of Transient Skin Temperature of Conical Bodies during Short-time, High-speed Flight*, N.A.C.A. T.N. No. 1725, p. 33, October, 1948.

The Pressure on a Slender Body of Nonuniform Cross-Sectional Shape in Axial Supersonic Flow

(*Continued from page 175*)

Fig. 3 shows a sketch of the distorted element, and Fig. 4 gives the ordinates and pressure coefficients for lines on the surface defined by various planes passing through the flow axis. The importance of the longitudinal shape of the element is indicated by the pressure reversals that occur for $\theta = 0°$ and $\theta = 90°$. The pressure reversals also indicate qualitatively that a drag force acts on the forward half of the element and that a negative drag force acts on the rear half. This tendency to eliminate the resultant drag is consistent with the conclusion previously stated—that no resultant drag could be predicted, within the limits of accuracy of the theory, for a body ending in a cylinder.

REFERENCES

[1] Graham, E. W., *Pressure and Drag on Smooth Slender Bodies in Linearized Flow*, Douglas Aircraft Company Report No. SM-13417, April, 1949.

[2] Ward, G. N., *Supersonic Flow Past Slender Pointed Bodies*, The Quarterly Journal of Mechanics and Applied Mathematics, Vol. II, Part I, p. 75, March, 1949.

[3] Graham, E. W., *The Pressure on a Slender Body of Non-Uniform Cross-Sectional Shape in Axial Supersonic Flow*, Douglas Aircraft Company Report No. SM-13346, August, 1948.

[4] Graham, E. W., *The Pressure on Slender Bodies of Uniform Cross-Sectional Shape in Axial Supersonic Flow*, Douglas Aircraft Company Report No. SM-13377, August, 1948.